

University of Louisville

ThinkIR: The University of Louisville's Institutional Repository

Electronic Theses and Dissertations

12-2023

The interplay between lung adenocarcinoma, nutrient availability, and the microbiome.

Alexis A. Vega
University of Louisville

Follow this and additional works at: <https://ir.library.louisville.edu/etd>



Part of the [Molecular Biology Commons](#)

Recommended Citation

Vega, Alexis A., "The interplay between lung adenocarcinoma, nutrient availability, and the microbiome." (2023). *Electronic Theses and Dissertations*. Paper 4191.
<https://doi.org/10.18297/etd/4191>

This Doctoral Dissertation is brought to you for free and open access by ThinkIR: The University of Louisville's Institutional Repository. It has been accepted for inclusion in Electronic Theses and Dissertations by an authorized administrator of ThinkIR: The University of Louisville's Institutional Repository. This title appears here courtesy of the author, who has retained all other copyrights. For more information, please contact thinkir@louisville.edu.

THE INTERPLAY BETWEEN LUNG ADENOCARCINOMA, NUTRIENT
AVAILABILITY, AND THE MICROBIOME

By: Alexis A. Vega

B.S., Florida Gulf Coast University, 2015

M.S., University of Louisville, 2018

A Dissertation

Submitted to the Faculty of the
School of Medicine of the University of Louisville

In Partial Fulfillment of the Requirements

For the Degree of

Doctor of Philosophy

In Biochemistry and Molecular Genetics

Department of Biochemistry and Molecular Genetics

University of Louisville

Louisville, Kentucky

December 2023

THE INTERPLAY BETWEEN LUNG ADENOCARCINOMA, NUTRIENT
AVAILABILITY, AND THE MICROBIOME

By

Alexis A. Vega

B.S. Florida Gulf Coast University 2015

M.S. University of Louisville 2018

A Dissertation Approved on

July 12, 2023

by the Following Dissertation Committee:

Levi Beverly, Ph.D.

Brian Clem, Ph.D.

Carolyn Klinge, Ph.D.

Leah Siskind, Ph.D.

Corey Watson, Ph.D.

ACKNOWLEDGEMENTS

I would like to thank Dr. Levi Beverly for his guidance and support over the past few years. I would also like to thank my committee members, Drs. Brian Clem, Alan Cheng, Carolyn Klinge, Leah Siskind, and Corey Watson. I would also like to thank the members of the ToTOL lab, both current and past, especially Parag P. Shah and Lavona Casson. Thank you to the University of Louisville Genomics Core and the Bioinformatics Core for their assistance in generating and analyzing the RNA-seq data. I would like to express my gratitude to Drs. Wan Lam, William Lockwood, and Erin Marshall for their expertise in the microbiome. I would like to also express a great appreciation to my undergrad advisors, Drs. Jan DeJarnette and Takashi Ueda, and my undergrad lab mate, Nicole Jensen, for believing in my potential even when I was unable to. I would like to express my appreciation to my dog, Betsy, for listening to my ramblings and reminding me to go outside, at least twice a day, even after a long day in the lab. Finally, I would like to thank my family and friends for their constant support and encouragement throughout my life.

ABSTRACT

THE INTERPLAY BETWEEN LUNG ADENOCARCINOMA, NUTRIENT
AVAILABILITY, AND THE MICROBIOME

Alexis Avidan Vega

July 12, 2023

Lung cancer is one of the most common forms of cancer diagnosed, and has the highest lethality rate across all other forms of cancer in the U.S. While current therapeutic options include chemo-, immuno-, and radio-therapy, the benefits of caloric or nutrient restriction on cancer cells has also been investigated. Due to the many biological functions associated with methionine, many have proposed a methionine restricted diet would lead to favorable outcomes when combating cancer. Although our cells are incapable of synthesizing methionine, the bacteria found in our microbiome can. Furthermore, recent discoveries suggest an independent microbiome found within tumors that portray increased methionine production. In this dissertation, I investigate: 1) the impact of nutrient restriction on cancer phenotypes, 2) the role of bacteria in this nutrient restricted environment, and 3) the direct impact of bacteria on cancer growth and survival. I show that low methionine availability lessens lung adenocarcinoma (LUAD) proliferation, which I rescued upon introduction of bacterial biomolecules. Additionally, our RNA-seq data revealed several altered pathways due to bacterially supplemented media, including glycolysis and Epithelial-to-Mesenchymal Transition (EMT). These

results were verified using western blot, measuring lactate production, glucose uptake, and invasive potential. I hypothesized the increased glycolysis and EMT was attributed to activation of Toll-Like Receptor 4 (TLR4), a receptor well known to recognize bacterial lipopolysaccharides (LPS). To test my hypothesis, I treated LUAD cell lines with 1-Methylethyl 2-(acetylamino)-2-deoxy- α -D-glucopyranoside 3,4,6-triacetate (C34), a potent TLR4 inhibitor. My results indicated C34 inhibition of TLR4 did not reduce lactate production or invasive potential. To gain a better understanding of which biomolecule was responsible for this altered phenotype, I treated bacterially supplemented media with RNase, charcoal stripping, or dialysis. From the results, I show bacterial RNA, lipids, and biomolecules greater than 3kDa influences HKII and Claudin in similar ways. However, bacteria RNA was shown to have opposite effects on cJUN expression compared to either bacterial lipids or biomolecules greater than 3kDa. Future work will be required to characterize these biomolecules and elucidate their role in tumor development. The characterization of the biomolecules will help in two-fold: 1) opening novel therapeutic options that targets and inhibits the bacteria's ability to synthesize these biomolecules; 2) allowing for the characterization of bacteria into tumor promoting microbes and tumor suppressive microbes by using the biomolecules produced as markers.

TABLE OF CONTENTS

ACKNOWLEDGEMENTS.....	iii
ABSTRACT.....	iv
LIST OF TABLES.....	viii
LIST OF FIGURES.....	ix
CHAPTER 1: INTRODUCTION.....	1
Lung Cancer.....	1
Nutrition.....	2
Methionine Pathway.....	4
SLC Transporters.....	9
Tumor Microenvironment.....	14
Microbiome.....	17
Interplay Between LUAD, The Microbiome, and Methionine.....	20
CHAPTER 2: LUNG ADENOCARCINOMA CELL LINES UNDERGO INCREASED MACROPINOCYTOSIS UNDER METHIONINE RESTRICTION.....	24
Introduction.....	24

Methods and Materials.....	26
Results.....	32
Discussion.....	56
CHAPTER 3: ESCHERCIA COLI BIOMOLECULES ENHANCE GLYCOLYSIS AND EMT IN LUNG ADENOCARCINOMA.....	61
Introduction.....	61
Methods and Materials.....	64
Results.....	70
Discussion.....	111
CHAPTER 4: OVERALL CONCLUSIONS AND FUTURE DIRECTIONS.....	116
REFERENCES.....	123
CURRICULUM VITA.....	133

LIST OF TABLES

Table 1. Tumor microbiome predicted upregulated pathways.....	23
Table 2. Top 20 upregulated genes in A549 incubated in <i>E. coli</i> biomolecules p≤0.05; q≤0.05; log2FC ≥0; counts ≥ 10 across samples).....	82
Table 3. Top 20 genes upregulated in H2009 incubated in <i>E. coli</i> biomolecules p≤0.05; q≤0.05; log2FC ≥0; counts ≥ 10 across samples).....	83
Table 4. Top 20 downregulated genes in A549 incubated in <i>E. coli</i> biomolecules p≤0.05; q≤0.05; log2FC ≥0; counts ≥ 10 across samples).....	84
Table 5. Top 20 downregulated genes in H2009 incubated in <i>E. coli</i> biomolecules p≤0.05; q≤0.05; log2FC ≥0; counts ≥ 10 across samples).....	85

LIST OF FIGURES

Figure 1. Methionine cycle in mammalian cells.....	5
Figure 2. Bacterial methionine biosynthetic pathway.....	8
Figure 3. LAT1 high RNA expression in LUAD demonstrates poorer patient survival.....	11
Figure 4. SLC7A5 import of methionine activates mTOR activity.....	13
Figure 5. The tumor microenvironment is composed of multiple cell types.....	16
Figure 6. Methionine restriction decreases cellular proliferation without impacting viability.....	33
Figure 7. Methionine restriction decreases cellular proliferation.....	36
Figure 8. Methionine restriction elicits cell cycle arrest at G2 phase.....	38
Figure 9. Slowed proliferation can be reversed following returning cells to high levels of methionine.....	39
Figure 10. LUAD motility is not affected under methionine restriction.....	40
Figure 11. LUAD tumor growth is lessened when animals are placed in low methionine diet.....	43

Figure 12. Methionine restriction leads to increased MYC and LC3b in LUAD cell lines.....	45
Figure 13. LAT1 localizes with LAMP1 under methionine restriction.....	48
Figure 14. GeCKO screening results indicate macropinocytosis crucial for survival under methionine restriction.....	51
Figure 15. LAT1 KO and BCH administration impacts genes related to macropinocytosis.....	53
Figure 16. LAT1 inhibition leads to increased macropinocytosis.....	55
Figure 17. Graphical representation of methionine restriction and BCH treatment effects.....	60
Figure 18. <i>E. coli</i> synthesized methionine can rescue cancer phenotypes.....	72
Figure 19. Altered signaling in LUAD in the presence of bacteria.....	73
Figure 20. LUAD can take up <i>E. coli</i> biomolecules.....	76
Figure 21. <i>E. coli</i> can take up LUAD biomolecules	78
Figure 22. KEGG analysis reveals multiple pathways impacted by <i>E. coli</i> biomolecules in LUAD.....	79
Figure 23. Differentially expressed genes of LUAD incubated with <i>E. coli</i> biomolecules.....	80
Figure 24. <i>E. coli</i> supplemented media enhances enzymes related to glycolysis in LUAD.....	88

Figure 25. LPS increases IL1β and cJUN mRNA transcription in LUAD cell lines.....	89
Figure 26. <i>E. coli</i> supplementation increases glucose uptake in LUAD cell lines.....	90
Figure 27. <i>E. coli</i> supplementation increases lactate production.....	92
Figure 28. <i>E. coli</i> can take up lactate released by LUAD cell lines.....	94
Figure 29. <i>E. coli</i> supplementation shows elevated EMT markers.....	96
Figure 30. LUAD cell lines do not use <i>E. coli</i> biomolecules as chemoattractant.....	97
Figure 31. LUAD invasion, but not motility, increases with <i>E. coli</i> biomolecules.....	99
Figure 32. Increased cJUN expression in LUAD cells incubated with <i>E. coli</i> biomolecules.....	102
Figure 33. Effects of C34 inhibition on cell viability.....	103
Figure 34. MAPK phosphorylation decreases on C34 administration.....	104
Figure 35. TLR4 inhibition does not lead to decreased glycolysis in LUAD cells treated with <i>E. coli</i> supplemented media.....	105
Figure 36. TLR4 inhibition does not lower invasive potential of LUAD incubated in <i>E. coli</i> supplemented media.....	108

Figure 37. <i>E. coli</i> RNA, lipids, and biomolecules over 3kDa impacts LUAD phenotype.....	110
Figure 38. Graphical summary of relationship between <i>E. coli</i> and LUAD.....	115

CHAPTER 1: INTRODUCTION

Lung Cancer

Lung cancer remains within the top 3 most diagnosed cancers of 2023 and continues to be the most lethal form of cancer in the United States. In fact, lung cancer is estimated to account for 127,000 deaths; about 20,000 less than the cumulative deaths of colorectal (52,500), pancreatic (50,550), and breast cancer (43,700) [1]. Some common risk factors of lung cancer include smoking (either active or second-hand), exposure to asbestos or radiation, and previous history with lung diseases such as Chronic Obstructive Pulmonary Disease (COPD) [2, 3]. Of these factors, smoking is the leading cause of lung cancer in the United States [2]. There are specific factors that must be accounted for when treating patients diagnosed with lung cancer, one of which is determining the stage at which the cancer has progressed.

Lung cancer is clinically staged using a Tumor/Node/Metastasis (TNM) classification system, wherein the primary tumor stage is denoted as T, the regional lymph node involvement as N, and distant metastasis as M [2, 4, 5]. The most preferred method for treating lung cancer remains surgical resection; however, this method is only available for patients in the early stages of lung cancer before it has metastasized. The most common sites for lung cancer metastasis have been observed to be the breast, brain, and bone [6]. Patients that are found in the M stage of cancer rely on other therapies, including targeted therapies [7] and immunotherapies [8-10], in attempts of regressing

tumors or, at the very least, slowing tumor growth. Unfortunately, diagnosing lung cancer at a particular stage is not enough to begin treatment, as lung cancer can be divided into either small cell carcinoma, accounting for 20% of lung cancer, or non-small cell carcinoma (NSCLC), which accounts for the remaining 80% [11]. Furthermore, NSCLC can be further subdivided into large cell carcinoma, squamous cell carcinoma, and adenocarcinoma (LUAD). Of these lung cancer subtypes, LUAD has proven to be the most challenging subtype to treat, garnering resistance against a multitude of therapies over time [7]. This dissertation will focus on LUAD, the most prevalent form of lung cancer diagnosed (around 40% of all lung cancers) [6, 11].

Nutrition

One of the hallmarks of cancer is the ability to proliferate at uncontrolled rates [12]. Cellular proliferation requires biomolecules and energy to allow cells to grow, synthesize new DNA, and undergo mitosis. Due to the uncontrolled proliferation that cancer cells exhibit, they require a larger amount of nutrients compared to their non-malignant counterparts. One such nutrient that cancer cells are known to consume higher concentrations of than healthy tissue is glucose.

Glucose is a 6-carbon ring sugar molecule that plays a vital role in cellular energy. Our cells metabolize glucose through glycolysis, wherein glucose is converted into pyruvate following multiple steps. While two of the steps in glycolysis require ATP, namely hexokinase II and phosphofructokinase, others produce ATP and a molecule known as NADH. In non-malignant cells, pyruvate is then further metabolized into acetyl CoA, where it enters the citric acid cycle. As the citric acid cycle is turned over, it produces more NADH, as well as produces FADH_2 . NADH and FADH_2 act as electron

donors during oxidative phosphorylation, where their electrons enter the electron transport chain and produce 3 ATP molecules for every 1 molecule of NADH and 2 molecules of ATP for every 1 molecule of FADH₂. During stages of low oxygen, cells can instead undergo anaerobic glycolysis where pyruvate is shuttled into lactate production, thus regenerating NADH back to NAD⁺. Unlike our healthy cells, cancer cells favor the production of lactate from pyruvate even in the presence of oxygen. This phenomenon of aerobic glycolysis is called the Warburg Effect, named after the discoverer, Otto Warburg. While much has gone into understanding the Warburg Effect, the driving force behind this phenomenon remains a topic of much debate.

With a larger dependency to glucose, others have investigated the therapeutic potential a caloric restrictive diet would have on cancers. Caloric restriction is defined as the decrease of calories without malnutrition. In as early as 1935, Clive et. al. had noted that caloric restricting rats greatly increased their life span [13]. Furthermore, Coleman et. al. investigated the benefits of a caloric restrictive diet on rhesus monkeys. They not only found that the caloric restrictive diet lengthened the lifespan of these animals, but also decreased the percentage of age-related diseases [14]. An early study in 2012 investigated the potential of lowering dietary restriction as a method for treating several cancer types, including breast, colorectal, and prostate cancer [15]. The results of these studies showed that short-term fasting resulted in decreased tumor sizes in breast cancer, glioma, and melanoma cells xenografted in their mouse models. Furthermore, short-term fasting *in vivo* or starvation *in-vitro* increased cancer cell sensitivity to doxorubicin treatment.

Restricting overall calories and glucose are not the only means by which we can modulate our diet to affect cancer development. Other nutritional sources are seen to be elevated in cancer cells compared to their non-malignant counterpart [16]. One such source are amino acids, which are the building blocks of protein. Elevated consumption of leucine, serine, glutamine, isoleucine, and even methionine has been observed in 60 cancer cell lines by metabolic profiling [17].

Methionine Pathway

Methionine

Methionine is a sulfur containing amino acid considered essential in humans, as there is no pathway in mammalian cells capable of synthesizing methionine *de novo*. Instead, we rely on our diets, such as meat and beans, for our source of methionine. Methionine plays a critical role in protein synthesis as it is the first amino acid incorporated and initiates translation of mRNA to protein. Methionine metabolism is key to multiple pathways including: transmethylation, transsulfuration, and polyamine synthesis. Metabolism of methionine begins with Methionine Adenosyltransferase to produce S-adenosylmethionine (SAM) (Figure 1).

S-adenosylmethionine

SAM serves as a major contributor to epigenetic and posttranslational modification. In both epigenetic and posttranslational modifications, SAM acts as a methyl donor, resulting in methylation of biomolecules including DNA, RNA, and protein. Methylation of a biomolecule is not permanent, specific enzymes are responsible

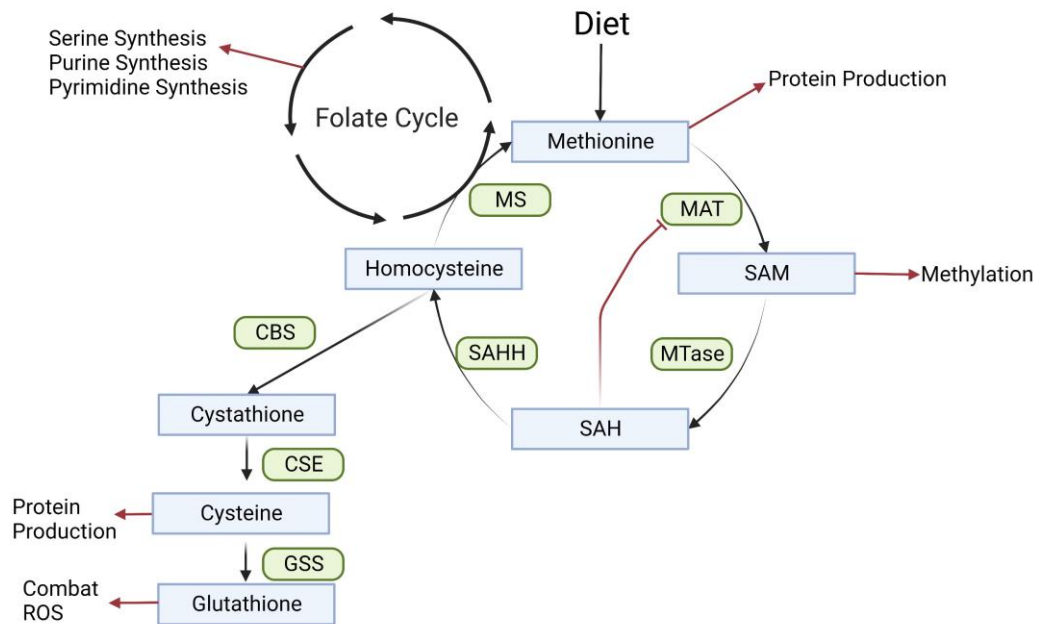


Figure 1. Methionine cycle in mammalian cells.

Methionine plays a key role in multiple cellular functions, including protein synthesis, methylation, and turning over the folate cycle. MAT = Methyladenosyl Transferase, MTase = Methyltransferase, SAHH = S-adenosylhomocysteine Hydrolase, MS = Methionine Synthase, CBS = Cystathionine Beta Synthase, CSE = Cystathionase, GSS = Glutathione Synthase.

for either adding a methyl group while others are responsible for the removal of the methyl group.

Enzymes known as DNA Methyltransferases catalyzes the reaction that adds the methyl group to cytosines within the DNA and regulates the gene expression without altering the DNA sequence. While methylation can occur at any cytosine residue, the most common DNA methylation site is called a CpG island, where the cytosine is followed immediately by a guanine. These CpG islands can silence gene expression by impairing the DNA binding transcription factors, recruiting repressive proteins to the site, and even impact the 3D genome structure [18].

As mentioned earlier, DNA is not the only biomolecule that can be methylated; proteins also undergo methylation and results in altered protein function. Methylation of a protein occurs at either the lysine or arginine residues. Methylation of proteins can impact the trafficking of a protein, function of the protein, and interaction with other molecules. For example, histones can be methylated by different enzymes, such as DOT1L. DOT1L is responsible for mono-, di-, and tri-methylation of the lysine residue at 79 of Histone H3. When this lysine residue is methylated, it changes the interaction between the histone and DNA, resulting in exposed DNA ready to be transcribed. However, the methylation of histones does not always lead to exposure of DNA. Other sites, such as lysine residue 9 of Histone 3, inhibit transcription of a gene by tightly packing the DNA onto the histone. Regardless of the methylation enzymes used, SAM is converted to S-adenosylhomocysteine (SAH) after its methyl group had been transferred to an acceptor.

S-adenosylhomocysteine and Homocysteine

While SAM's key function is to incorporate methyl groups onto biomolecules, SAH functions to inhibit methylation. The inhibitory function of SAH can be alleviated by further metabolizing SAH, through hydrolase activity, to generate homocysteine. Homocysteine can either be recycled back into methionine or further metabolized into cysteine (Figure 1). Recycling of homocysteine into methionine results in turning over of the folate cycle, a cycle important in nucleotide synthesis critical for DNA and RNA nucleotide synthesis. Alternatively, homocysteine can be metabolized into cystathionine and then cysteine by cystathionine beta synthase and cystathionase, respectively. Cysteine is further metabolized into glutathione, an antioxidant that is important in removing the reactive oxygen species formed during oxidative phosphorylation.

Synthesis of Methionine in Bacteria

Unlike mammalian cells, many bacteria cells have their own dedicated pathway in synthesizing methionine *de novo* (Figure 2). It begins by aspartate being metabolized into aspartate semialdehyde. Aspartate semialdehyde can go on to become Lysine (another essential amino acid) or homoserine. Homoserine can be further metabolized into either Threonine and then Leucine (essential amino acids) or can become O-acetylhomoserine or O-succinylhomoserine through an enzyme known as metA. metA is the first committed step of the methionine synthesis pathway. From here, the bacteria generate cystathionine using metB, followed by homocysteine using metC. Finally, metE or metH can metabolize homocysteine into methionine (Figure 2).

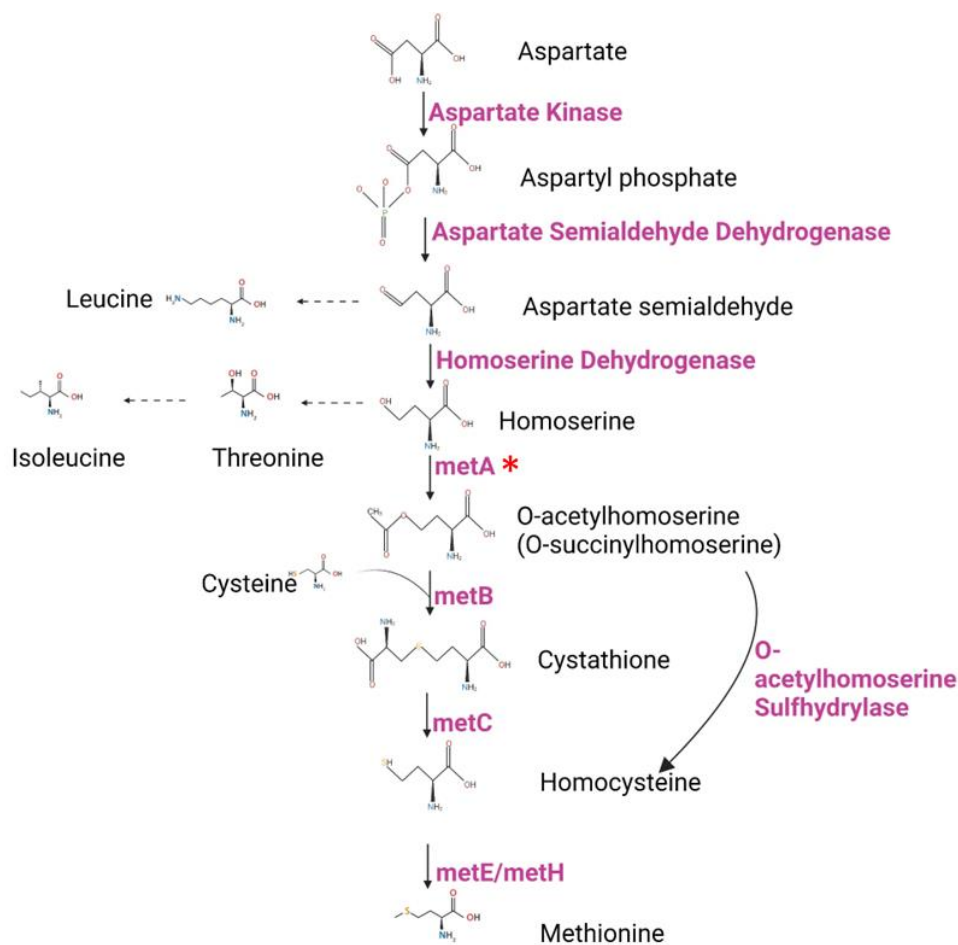


Figure 2. Bacterial methionine biosynthetic pathway.

Aspartate taken up by bacteria is metabolized by several enzymes leading to synthesis of methionine. This pathway can shuttle off to synthesize other amino acids such as leucine, threonine, and isoleucine. MetA, highlighted with a star, is considered the committed step into synthesizing methionine in bacteria. Created with BioRender.com

SLC Transporters

How do cells acquire nutrients from their environment and keep them where they are needed? Cells sustain homeostasis thanks in part to the plasma membrane, which acts as a barrier to keep cell contents in and other sources out. Even intracellularly, the cell relies on lipid membranes that compartmentalize the cell and keep each compartments content from being freely released. Specialized proteins, called transporters, help pass molecules through these membrane structure. Transporters can nclude water channels, ATP-driven pumps, and solute carriers (SLC) [19, 20]. Of these transporters, SLCs constitute the largest group, currently with over 400 members divided into 52 subfamilies [19, 21]. The nomenclature of SLC families consist of SLC as the base, followed by an integer expressing the family, a letter to denote subfamilies, and finally a second integer representing the individual member [19]. The upregulation or downregulation of specific SLCs has been shown to have an impact on cancer progression and metastasis [22-25].

SLC7A5

SLC7 transporters belong to the Amino Acid-Polyamine-Organocation superfamily, which is responsible for the transport of amino acids [26, 27]. The SLC7 family can be subdivided into 15 separate members, of which 2 are pseudogenes [26]. The remaining 13 members consists of either cationic amino acid transporters (CAT) or light subunit of amino acid transporters (LAT). *SLC7A5* encodes for LAT1 transporter, which requires the assistance of SLC3A2, or 4F2 heavy chain (4F2hc), to localize to the plasma membrane and function properly [28-30]. In addition to requiring SLC3A2 to function properly, LAT1 also requires SLC1A5 (ASCT2), a glutamine transporter [20].

LAT1 acts as an antiporter responsible for transporting several essential amino acids such as leucine, isoleucine, valine, and methionine [31]. By using the glutamine that enters through the ASCT2, LAT1 can exchange glutamine and allow for the influx of methionine. The expression of LAT1 is tissue specific, having high expression in the lung, brain, colon, and activated lymphocytes [32].

LAT1 and cancer

LAT1 has been observed to be upregulated in several different cancer types [33-37]. A previous study investigating the clinical significance of LAT1 on lung cancer found positive LAT1 staining in NSCLC by immunohistochemistry staining [38]. Additionally, LAT1 expression is further elevated in metastatic sites compared to the primary tumor site [34, 39]. Patients which exhibited increased expression of LAT1 exhibited dramatically poorer survival outcomes (Figure 3).

LAT1 expression is closely tied to the well-known proto-oncogene MYC [40]. MYC is a helix-loop-helix leucine zipper that interacts with a second helix-loop-helix leucine zipper, Max, and enhances transcription of specific genes by binding to E-boxes [41]. MYC expression can be enhanced by several mechanisms including chromosomal translocation, amplification, signaling pathways, and altering the protein stability. Hayashi, K. et. al. found that knockdown of MYC using siRNA resulted in decreased levels of LAT1 in both RNA expression and protein expression [40].

In addition to using siRNA to knockdown LAT1, drugs have been synthesized to inhibit the function of LAT1. 2-Aminobicyclo-(2,2,1)-heptane-2-carboxylic acid (BCH) is an amino acid analogue that competitively inhibits LAT [42]. BCH can inhibit LAT1

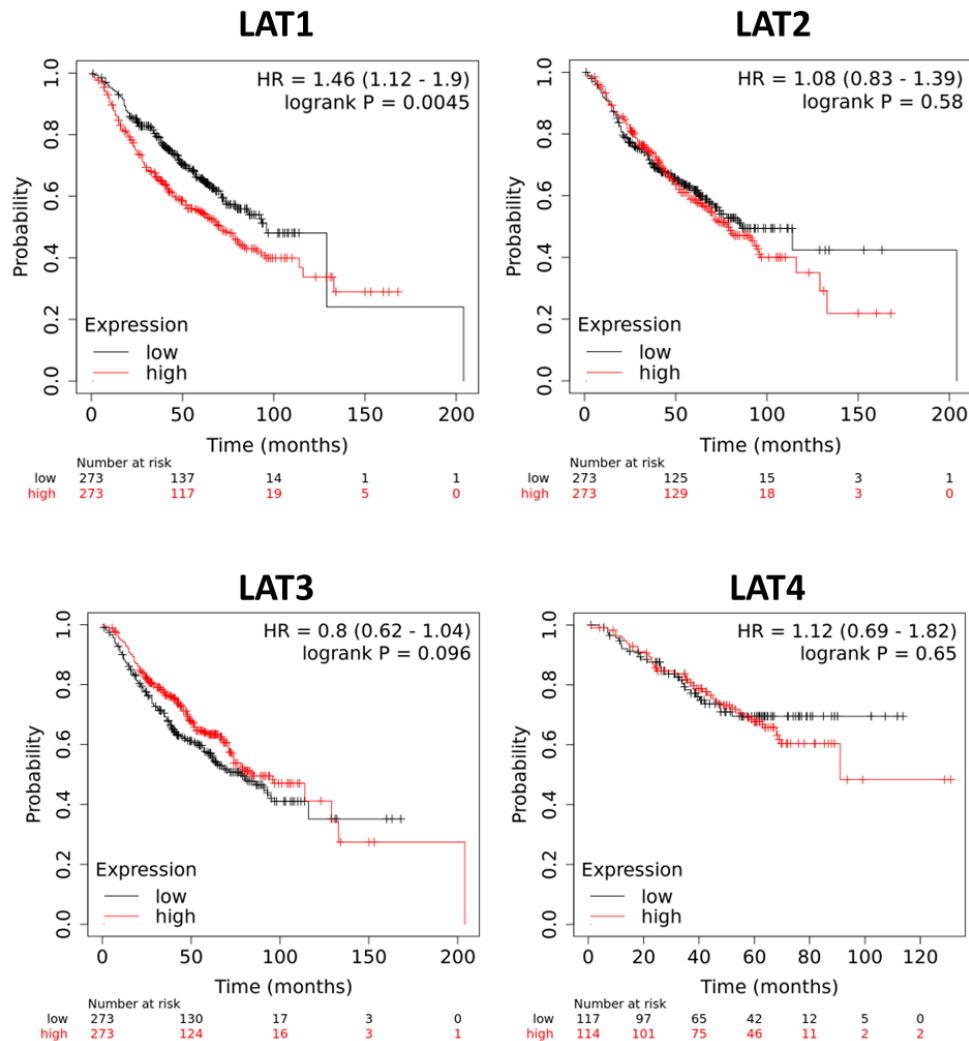


Figure 3. LAT1 high RNA expression in LUAD demonstrates poorer patient survival.

Kaplan Meier curve of mRNA expression of LAT1-4 for patients diagnosed with lung adenocarcinoma, excluding non-smokers, investigated the probability of overall survival.

Györfy B. Survival analysis across the entire transcriptome identifies biomarkers with the highest prognostic power in breast cancer, Computational and Structural

Biotechnology Journal, 2021;19:4101-4109,

<https://doi.org/10.1016/j.csbj.2021.07.014>

at concentrations of 131.5 μ M and LATs 1-4 at 10mM [32, 43-45]. Treatment with BCH has been shown to reduce proliferation and increased apoptosis across multiple cancer types [45, 46]. The mechanism by which BCH inhibition of LAT results in these phenotypes is through inhibition of mammalian target of rapamycin complex 1 (mTORC1) signaling [47, 48]. mTORC1 signaling is important in many cellular phenotypes, including proliferation and autophagy, and can be influenced by the availability of amino acids [49].

With respect to LAT inhibition, mTORC1 is dependent on the availability of leucine and methionine. Leucine binds to Sestrin2, a stress inducible metabolic protein, causing Sestrin2 to release GAP activity towards Rags 2 (GATOR2) [50]. GATOR2 is a complex of 5 proteins (WDR24, MIOX, WDR59, SEH1L, SEC13) that can inhibit GATOR1 through ubiquitination [51, 52]. GATOR1 is known to directly interact by acting as a GAP for the RabA/B complex of mTOR, thus inhibiting mTOR activity [53]. With leucine interacting with Sestrin2 to release GATOR2, GATOR2 can then lead to GATOR1 degradation, thus activating mTORC1. Methionine can also activate mTORC1 in a similar fashion. SAM, the immediate product of methionine metabolism, can bind to a protein called S-adenosylmethionine sensor upstream of mTORC1 (SAMTOR) [54]. Under low methionine levels, SAMTOR can bind to the GATOR1 complex and help inhibit mTORC1. The mechanism by which SAMTOR influences GATOR1 on mTORC1 inhibition remains unknown. However, it is seen that activation of mTORC1 can occur either through the addition of methionine or the knockdown of SAMTOR (Figure 4).

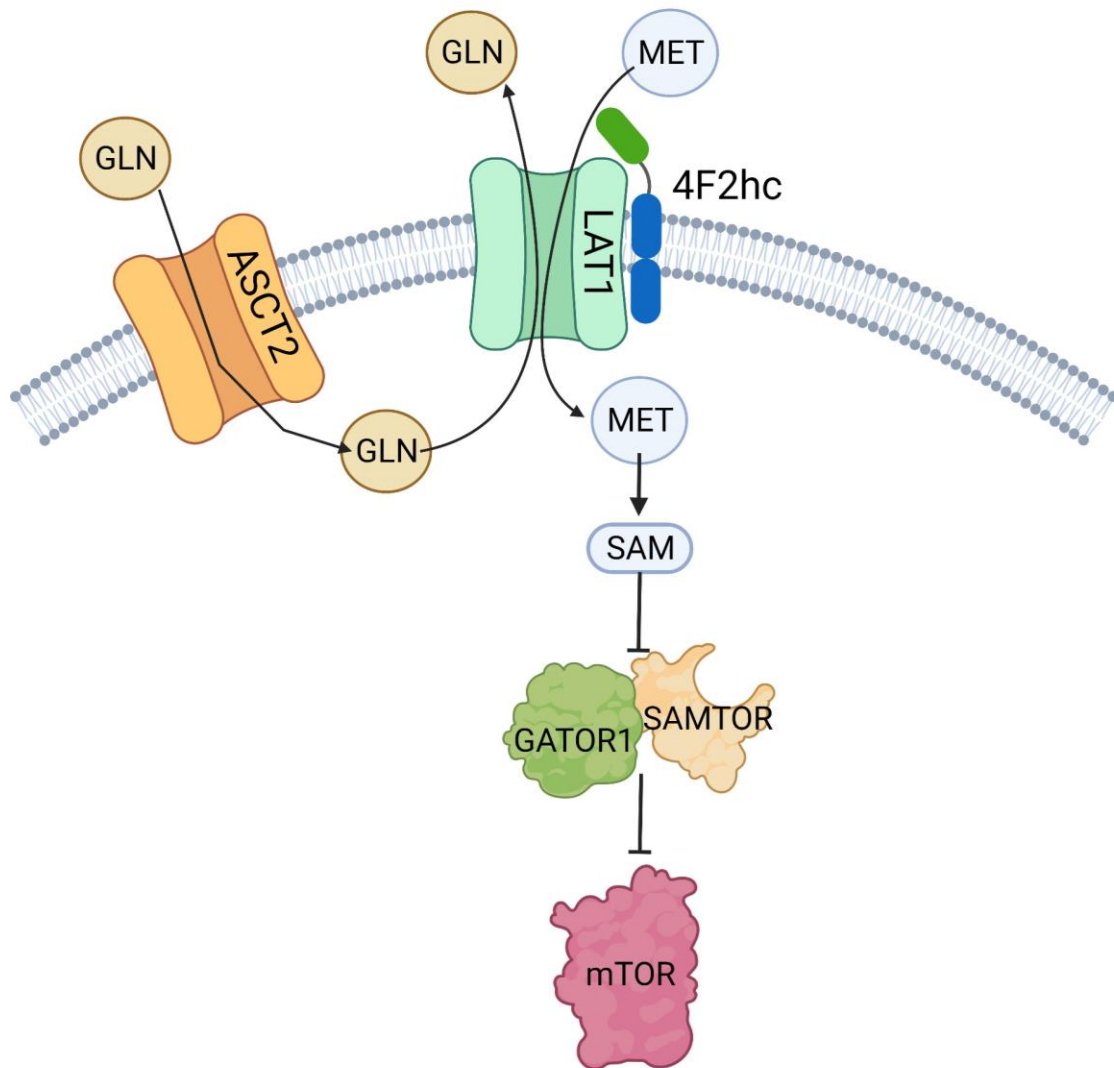


Figure 4. SLC7A5 import of methionine activates mTOR activity.

LAT1 localizes to the plasma membrane with the assistance of 4F2hc. LAT1 then shuttles methionine (MET) into the cell by exporting the glutamine (GLN) previously imported by ASCT2. MET is then metabolized into SAM, wherein it binds to SAMTOR and disrupts GATOR1: SAMTOR complex. Disruption of this complex leads to the activation of mTOR.

Created with BioRender.com

Tumor Microenvironment

LUAD, like many other types of cancers, is a complicated disease due its heterogenous cellular population. Due to the uncontrolled growth and high rates of mutation, individual cancer cells can differ greatly from one another within the larger tumor mass. Some cells, such as cancer stem cells, are less inclined to proliferate and undergo quiescence until activated, while others readily divide and can confer resistance against therapeutics such as chemotherapies or immunotherapies. However, cancer cells are not the only cell type to be involved in tumor progression. Cancer cells can develop their own niche environment, known as the tumor microenvironment (TME). In addition to the cancer cells, the TME includes infiltrating immune cells, fibroblasts, and extracellular matrix [55-57] (Figure 5).

Immune Cells in the TME

Normally, our immune cells assist us in battling against infection and diseases. Our immune cells can distinguish between healthy and cancerous tissues through neoantigen peptides. These neoantigens can arise from genomic mutations, transcriptomic variations, and even proteomic variation. Recognition of the neoantigens by the immune cells leads to a potent immune response, killing the cell expressing the neoantigen. With our immune system being critical for destroying harmful cells, why is it that we see them within the TME?

As mentioned earlier, the immune system plays both a pro-inflammatory and anti-inflammatory role. While the pro-inflammatory response will recruit immune cells to the tumor, thus eliminating the tumor, cancer cells can reprogram the immune cells to

become anti-inflammatory and regulate the immune system. T-cells are a great example of understanding how reprogramming can facilitate cancer survival. CD4 T-helper cells are T-cells that have limited cytotoxic effects but are designed to be pro-inflammatory and recruit cytotoxic cells to the diseased site. Once recruited, CD8 cytotoxic T-cells release cytokines that result in the elimination of the targeted cell. Once eliminated, T-regulatory cells come in, dampening the immune response at the site, and prevent CD8 T-cells from targeting healthy cells. Cancer cells can utilize the effects of T-regulatory cells, recruiting them to the TME and taking advantage of the immune suppressive role of the T-regulatory cells. This allows the tumor to evade the immune system and continue thriving. T-cells are not the only cells recruited from the immune system that can demonstrate immunosuppressive roles; dendritic cells, macrophages, and other immune cells have all been identified within the TME.

Macrophages are another well studied immune cell that have been found to facilitate tumor progression. Like T-cells, there are several different types of macrophages that are found in the immune system. M₁ macrophages, for example, are inflammatory macrophages, while M₂ macrophages are known to be immunosuppressive. In addition to their immunosuppressive role, macrophages have been seen to enhance tumor proliferation, motility, and even metastasis [58].

Extracellular Matrix and Fibroblast

The extracellular matrix (ECM) is the noncellular component of the TME that functions as a scaffold for the tumor [59]. The ECM is composed of hundreds of different proteins, such as collagen and glycoproteins [60], which are constantly being degraded and rebuilt. Not only is the dysregulation of ECM important for tumor

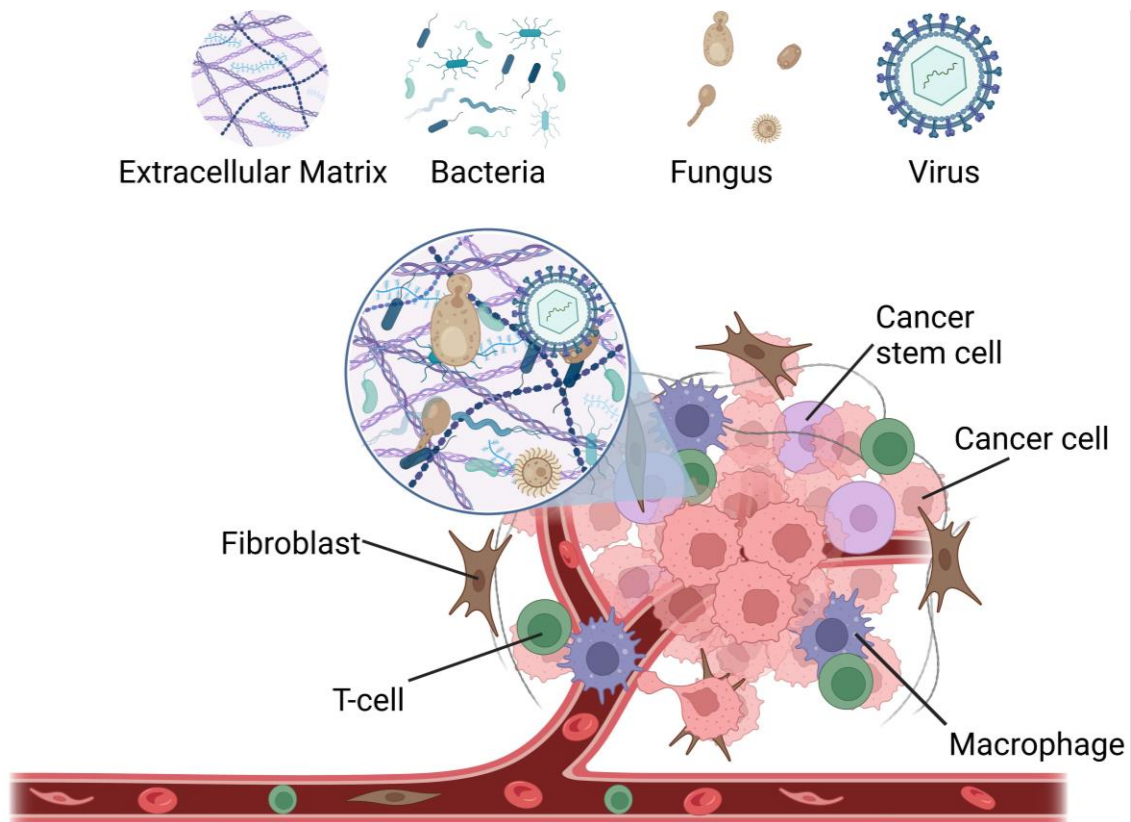


Figure 5. The tumor microenvironment is composed of multiple cell types.

The tumor microenvironment is known to house several key cell types. The main body consist of cancer cells at different stages of progression. Meanwhile, immune cells such as macrophages and T-cells help the progression and immune evasion of cancers.

Fibroblasts and extra-cellular matrix facilitate tumor anchorage and metastasis. The vasculature facilitates in nutrient transport, oxygen supply, and a route to distal organs. Bacteria, fungi, and viruses are also found within the tumor microenvironment and can also impact tumor progression. Created with BioRender.com

development, but it is also important in tumor growth and metastasis [60-62]. The fibroblasts are key to remodeling the ECM, and cancer cells can even reprogram these cells.

Cancer associated fibroblasts (CAF) can originate from a multitude of different locations. CAFs can be recruited from residential tissue fibroblasts, bone marrow derived mesenchymal stem cells, and even epithelial cells through a process called epithelial-to-mesenchymal transition (EMT), which will be discussed later [63]. Regardless of where they originate from, once they are reprogrammed into CAFs they begin expressing key genes for motility, various growth factors and cytokines to facilitate motility and invasion [64, 65]. CAFs have been shown to not only impact tumor progression, but also facilitate chemoresistance by either modulating the tumor stroma or the release of biomolecules such as glutathione, recruit the immune cells mentioned earlier to assist in immune evasion, and their remodeling of the ECM can further enhance metastasis [66, 67]. However, the current visual representation of the TME remains incomplete, as new studies are uncovering more cells and organisms contributing to the TME, such as bacteria.

Microbiome

Bacteria are single celled organisms that constitute a large majority of the prokaryotic microorganisms. These unicellular organisms can be ubiquitously found on living multicellular organisms. In fact, it has been proposed that of all cells that compromise humans, bacteria constitute over 50% [68, 69]! The range of bacterial families found within a community has been termed as the microbiome. Studies have characterized the diversity of the microbiome to better understand the role of bacteria on

human health and disease. The most well studied microbiome to date, our gut microbiome, houses between 150-400 different species of bacteria[70]. While the species of bacteria differ from host to host, the most dominant phylas found in humans are Bacteroidetes, Firmicutes, and Proteobacteria [70, 71].

Many of the bacteria found in the microbiome of an organism have a symbiotic relationship with their multicellular organism host. Studies have shown bacteria to be instrumental in helping express host genes key to intestinal physiology [72]. Others have gone on to investigate how bacteria can play a role in digestion. Fiber, for example, is well known to be a key player in a healthy diet for humans, but humans are unable to metabolize these macromolecules. Instead, we rely on the bacteria in our gut to metabolize and break down the fiber into short chained fatty acids that we can use as an energy source [73]. In fact, previous studies have found that germ-free mice require a larger amount of calories to maintain body weight [74]. The colonization of diverse, non-pathogenic bacteria also helps in keeping pathogenic bacteria from expanding. This protection becomes removed as we take antibiotics, removing the gut microbiome that keeps us healthy and allows for vacant spots for opportunistic pathogens to invade and begin proliferating. Finally, bacterial presence is also critical in developing a healthy immune system in the intestines. Umesaki et. al. has previously shown microbial introduction into germ free mice elevate $\alpha\beta$ CD4⁺ and CD8⁺ T-cells of the intestinal intraepithelial lymphocytes [75]. Bacteria also assists in the production of IgA antibodies from B-cells [76]. Our microbiome helps keep us healthy, but as mentioned earlier, an imbalance of the microbiome, or dysbiosis, has been known to lead to many health issues [77].

Originally, the relationship between lungs and the microbiome focused on the gut-lung axis. Certain lung disorders, such as asthma, are known to be influenced by the gut microbiome. As the gut microbiome is heavily influenced by our diets, researchers discovered that high fiber diets changed the gut microbiome in mice and resulted in an overall increase in short-chain fatty acids metabolized from the fiber. This would lead to altered maturation of dendritic cells that are incapable of activating T cells, thus decreasing lung inflammation. This interaction has been observed to be a crosstalk between both organs, with respiratory influenza having an impact on the gut microbiome by the lung derived T cells invading into the gut and modulating the microbiome through secretion of IFN- γ [78].

Microbiome and cancer

It is estimated that 13% of all cancers are related to infectious diseases, which includes bacteria such as *Helicobacter pylori* [79-81]. There are currently 11 microbes that can directly cause cancer, known as oncomicrobes [80], including viruses, bacteria, and platyhelminths [82]. Initiation of cancer by these oncomicrobes can occur due to their secretion of toxins resulting in double-stranded breaks in the mammalian DNA and alteration of tumorigenic pathways such as the E-cadherin signaling pathway [80, 83].

H. pylori cytotoxin-associated gene A (cagA) has been identified as an oncoprotein in relation to gastric cancer. CagA enters the epithelial cells and becomes phosphorylated by Src family kinases, wherein phosphor-CagA then activates signaling pathways involved in unregulated proliferation, such as the ERK signaling pathway [84]. Yin et. al. investigated the role of *Fusobacterium nucleatum* on colorectal cancer and found mice administered *F. nucleatum* exhibited an increase in metastasis towards the

liver [85]. They found mice administered *F. nucleatum* exhibited elevated levels of pro-inflammatory cytokines such as TNF- α and IFN- γ . Furthermore, it was shown that *F. nucleatum* surface adhesion protein, FadA, can induce EMT in oral epithelial cell lines and oral squamous cell carcinoma. FADA can upregulate lncRNA MIR4435-2HG, which inhibits miR-296-5p and leads to upregulation of EMT associated proteins such as SNAIL1 [86]. *Escherichia coli* are also believed to play a part in tumor progression. Many have reported the genotoxin, known as colibactin, secreted by *E. coli* are responsible for DNA damage that promotes colorectal cancer [87, 88].

The dysbiosis observed with LUAD in mice is believed to facilitate in the progression and metastasis of the tumor. Jin et. al. were among the first to investigate the effects of the microbiome on LUAD [78]. They had utilized a genetically modified mouse model containing the KRAS^{LSL-G12D}; p53^{flox/flox}, with Cre being under the control of lung specific promoter *Sftpc*. They observed both germ free animals and animals treated with an antibiotic cocktail showed in lower overall tumor burden. Moreover, germ free mice that were intratracheally inoculated with bacteria showed a drastic increase in tumor nodules. The cause of the increased tumor burden in bacterial bearing mice was a result of the lipopolysaccharides (LPS) found on the bacterial cell wall stimulating $\gamma\delta$ T cells and, ultimately, promoting tumor progression. While evident that bacteria play a role in tumor progression, how bacteria may directly influence the tumor remains largely unexplored.

Interplay Between LUAD, the Microbiome, and Methionine

Lung cancer is known to be influenced by its microenvironment [55, 57, 60, 67]. While it was previously believed that the lung was a sterile environment, we are now

beginning to appreciate how the lung microbiome may impact diseases [68, 78, 82]. Previous work has evaluated how the microbiome is modulated by the tumor and the impact this modulation has on the overall environment of tumors [78]. However, this work remains in its infant stage and our understanding of this novel interaction remains incomplete.

Marshall et. al. found a change in the microbiome predating the presence of lung cancer [89]. Interestingly, previous studies have observed the microbiome of LUAD cell lines to have an increase in alphaproteobacterial families and a decrease in gammaproteobacterial families in both mice and human patient samples [78]. Interestingly, analyzing the patient tumor samples using Phylogenetic Investigation of Communities by Reconstruction of Unobserved States (Picrust2), a software capable of predicting metabolic profiles, uncovered overexpression in glycine betaine degradation and a decrease in S-adenosyl-L-methionine cycle I pathways in the microbiome of LUAD tumors [90]. These pathways are involved in the methionine recycling pathway, where Glycine betaine degradation is responsible for the recycling of homocysteine to methionine, and S-adenosyl-L-methionine cycle I is involved in the metabolism of SAM to SAH. These findings would imply that the bacteria found in the microbiome are efficient at producing methionine (Table 1).

The importance of methionine availability for cancer progression is gaining traction [50, 54, 91-97]. This dissertation focuses on understanding the interplay between LUAD and the microbiome, using methionine as a tool to measure the impact of nutrient restriction. We hypothesized that bacteria play a role in nutrient supplementation, acting as a reserve for nutrients, such as methionine, when LUAD cells find themselves in a

state of inadequate nutrient availability. We sought to understand the multi-organismal interplay using the following aims.

Aim 1 focuses on investigating the importance of methionine restriction on LUAD. While it is evident that methionine restriction would lessen tumor progression in several cancer types, not much is known on the effects of methionine restriction on LUAD. Aim 2 centers around understanding the interaction between LUAD and bacteria, by using *E. coli* as our bacterial model organism.

Direction (tumours)	Pathway #	Fold change	BH p-value*
Up	Glycine betaine degradation ^{M1}	46.4	0.002
	Nylon-6 oligomer degradation ^{M2}	2.1	0.001
	Bifidobacterium shunt ^{A3}	1.9	<0.001
	Ketogluconate metabolism ⁴	1.8	<0.001
	Pyruvate fermentation to acetone ^{A5}	1.7	<0.001
	Acetyl-coA fermentation to butanoate II ^{A6}	1.6	0.003
	Photorespiration ⁷	1.5	0.003
Down	S-adenosyl-L-methionine cycle I ^{M-6}	0.7	0.002
	2-methylcitrate cycle I ^{A-5}	0.68	0.002
	L-Glutamate and L-glutamine biosynthesis ⁻⁴	0.65	<0.001
	NAD biosynthesis II ⁻³	0.63	0.002
	Pyridoxal 5'-phosphate biosynthesis I ^{M-2}	0.6	0.001
	GDP-D-glycero-alpha-D-manno-heptose biosynthesis ⁻¹	0.1	0.002

*All pathways differentially predicted to be involved in the metabolism of the tumour microbiome (|FC|>1.3, Benjamini-Hochberg corrected p-value <0.05). # Pathways associated with epigenetic modifiers are labelled as: methylation (M) or acetyl group donation (A).

Table 1. Tumor microbiome predicted upregulated pathways.

CHAPTER 2: METHIONINE RESTRICTION DECREASES CELLULAR PROLIFERATION OF LUNG ADENOCARCINOMA CELL LINES

Introduction

Lung cancer mortality remains the highest of all other cancer types, estimated to total about 127,000 deaths [1]. The most common form of lung cancer observed in the U.S. is LUAD, a branch of non-small cell lung cancers [98]. One common hallmark of cancer is its capacity to proliferate [99], which accounts for cancer's dependency for nutrient availability [100].

Previous work has investigated the therapeutic potential of starving cancer cells of calories and nutrients without leading to malnutrition in the individual. Caloric restriction, for example, has previously been shown to lengthen lifespan of organisms while also decreasing onset of age-related diseases [13, 14]. Due to the difficult nature of calorically restricting patients diagnosed with cancer, others have investigated the therapeutic potential of restricting specific macromolecules from the diet. This is of particular importance when considering the availability of essential amino acids, such as methionine, as mammalian cells are incapable of synthesizing de novo and must rely on an external source. Methionine is not only responsible for initiating protein synthesis, but is also responsible for: epigenetic methylation, purine and pyrimidine synthesis, serine and cysteine synthesis, recycling of the folate cycle, polyamine synthesis, and glutathione synthesis. Solute carrier (SLC) transporters facilitate the movement of molecules across

the plasma membrane [101-103]. SLC transporters function as either uniporters, symporters, or antiporters and can be either sodium-dependent or sodium-independent [101-104]. Certain SLC transporters are known to be upregulated in cancer cells [101, 103, 105, 106], such as SLC7A5 [105, 107, 108]. SLC7A5, also identified as light subunit of amino acid transporters (LAT1), is responsible for importing dopamine and essential amino acids, such as leucine and methionine, into the cell [103, 107-110]. LAT1 acts as a sodium-independent antiporter, importing its contents while exporting other amino acids such as glutamine, a non-essential amino acid [107, 111]. With cancer's dependency to nutrients, it becomes apparent why LAT1 is overexpressed in cancer cell lines including LUAD cells [105, 106, 108].

Our findings show that methionine restriction halts LUAD cell proliferation without impacting survival. We observed a halt in the cell cycle and, by returning cells to adequate levels of methionine, cellular proliferation can be rescued. Furthermore, we observed an elevation of LAT1 expression in our animal models, increase in autophagy, and observed an increase in macropinocytosis, a non-specific endocytic pathway. These results indicate that LUAD cells activate multiple pathways to try and sustain cytoplasmic methionine levels.

Methods and Materials

Cell culture

A549, H2009, PC9s, and H2030 cells were obtained from ATCC and cultured in RPMI-1640 media (Cytiva) and supplemented with 10% Fetal Bovine Serum (HyClone), 50mg Penicillin – Streptomycin solution (HyClone), and 146mg of L-Glutamine (HyClone). Cells were maintained in 5% CO₂ and in 36°C. RPMI 1640 Medium without L-methionine was purchased through Gibco. Concentrations of methionine in media was attained by combining the methionine-free RPMI-1640 with the methionine-complete RPMI-1640. 2-amino-bicyclo[2.2.1]heptane-2-carboxylic acid (BCH) was purchased through Cayman Chemicals and resuspended in 1x PBS.

Cell Proliferation and Viability

Cell lines were seeded in a 96-well dish (Corning) at 1,000 cells per well. For our methionine restriction study, we seeded the cells with decreasing concentration of methionine: 50, 20, 2, and 0μM. For our BCH study, we performed serial dilutions of BCH, and used 1x PBS as our vehicle control. Proliferation and viability were measured by alamarBlue over the course of 5 days.

Cellular Apoptosis

Cell lines were seeded in a 6-well dish (Corning) at a concentration of 100,000 cells per well. Cells were incubated in decreases concentrations of methionine, ranging from 50μM to 0μM methionine. Cells were collected over the course of 5 days. Apoptosis was measured using flow cytometry (Beckman), using APC anti-Annexin V (BD Pharmingen) and Propidium Iodide solution (Sigma-Aldrich).

Cell Cycle

Cell lines were seeded in media with increasing concentration of methionine for 3 days. During the final 6 hours, cells were incubated with BrdU at a final concentration of 10 μ M. Cell staining was performed using BD Bioscience APC BrdU Flow kit (#552598) and analyzed through flow cytometry.

Real Time PCR

Total RNA was isolated from cell pellets using E.Z.N.A Total RNA Kit I (OMEGA) according to the manufacture's protocol. 1 μ g isolated RNA was converted to cDNA using High-Capacity RNA-to-cDNA kit (Applied Biosystems). Gene expression was determined by qPCR using SYBR green and the following primers: LAT1 Forward: CTGGTCTTCGCCACCTACTT, LAT1 Reverse: GCCTTTACGCTGTAGCAGTTC, LAT2 Forward: AGGACTGGCTGGGTTCCTGAGG, LAT2 Reverse: GAGCGGCTGCAGCACGTAGTT, LAT3 Forward: GTCTCATCAACAACCTTACACCTCCAG, LAT3 Reverse: GAAGCAAGGCGAACACAGCAC, LAT4 Forward: TCTCTCCGTCGCTCATCTTCA, and LAT4 Reverse: ATTCCTGGAAAGGTGACTGC. GAPDH Forward: GTCTCCTCTGACTTCAACAGCG, GAPDH Reverse: ACCACCCTGTTGCTGTAGCCAA was used as our housekeeping genes. Fold change was normalized to our 50 μ M methionine control and transformed to log base 2 to delineate statistical significance.

CRISPR-cas9 screen

10x10⁶ cas9 expressing LUAD cell lines were plated in 150cm dish in RPMI-1640 (Hyclone) and infected with a gRNA-library for 2 days. Following infection, puromycin (Thermo Fisher) was added to LUAD cell lines for 14 days in RPMI-1640 containing either 50μM or 16μM methionine, with cells passaged every 4 days. Cells were then harvested, and DNA content was isolated using DNA Isolation Kit (Qiagen). Isolated DNA was then amplified through PCR using Herculase II Fusion DNA Polymerase. DNA barcodes were then added to the amplified DNA using Nextera XT Index Kit (Illumina). DNA was read using a 500 cycle MiSeq Sequencing Kit.

LAT1 KO

2x10⁵ cas9 expressing LUAD cell lines were transfected with Dharmafect and LAT1 gRNA (CRISPR revolution). LAT1.1: UGUCUCCACAGUGGUGC; LAT1.2: CUUCACGCUGUAGCAGU. LAT1 knockdown was confirmed through western blot analysis.

Colony Assay Formation

1,000 cells were seeded in 6-well plate and incubated in either 50μM, 20μM, 2μM, or 0μM methionine for a total of 10 days. For our rescue experiment, after 7 days of incubating in 2μM methionine media, cells were returned to 20μM methionine for the remaining 3 days. Colonies were washed with 1x PBS and fixed with ice cold methanol before being stained with Coomassie blue. Colonies were manually counted, and intensity of stain was measured by ImageJ plugin, ColonyArea.

Wound Healing

1×10^6 cells were seeded onto 6-well plates and incubated in either 50 μ M, 20 μ M, 2 μ M, or 0 μ M methionine overnight. Wound was made by sterile pipette tip and wound was captured after 0-, 24-, and 48-hours. ImageJ was used to quantify the wound closure, and data were normalized to wound closure at 0-hours.

Cell motility

1×10^4 cells were seeded onto a 6-well plate and incubated in RPMI-1640 containing either 50 μ M methionine or 2 μ M methionine. Cells were then incubated for 48 hours, wherein images were taken every 10 minutes within the 48-hour time span using the Keyence live-cell imager. Cells were then tracked using the tracking software of Keyence Analyzer software to measure speed and distance.

In-vivo animal experiment

5×10^5 luciferase expressing H2009 cell lines were subcutaneously injected into the right flank of 8-week-old, male, NRG mice. When tumors first became palpable, mice were separated into two groups: one fed either a methionine high diet (0.86% methionine) or a methionine restricted diet (0.11% methionine) (Dyet). After 14 days, one cohort of 0.11% methionine mice were returned to 0.86% methionine. Tumor size was measured by both digital calipers and luminescence for a total of 28 days. Animals were euthanized and tumors were resected.

Immunoblotting

Tumor samples were prepared by crushing frozen tumor samples by mortar and pestle. A portion of pulverized tumor was then incubated in cell extraction buffer (CEB) containing protease and phosphatase inhibitors. 30 μ g of lysates were ran on a NuPAGE 4 to 12%

Bis-Tris PAGE gel and transferred to PVDF membrane. Membranes were blocked for 1 hour with 5% milk in TBS-T and probed with 1:750 dilution of mouse anti-LAT1 (Santa Cruz), 1:5000 rabbit anti-myc, 1:5000 rabbit anti-mTOR (Cell Signaling Technology), 1:5000 rabbit anti-p-mTOR (S2481) (Cell Signaling Technology), 1:5000 rabbit anti-p-mTOR (S2448) (Cell Signaling Technology), 1:5000 anti-AKT (Cell Signaling Technology), 1:5000 anti-p-AKT (Cell Signaling Technology), 1:5000 rabbit anti-Bax (Cell Signaling Technology), and 1:5000 rabbit anti-LC3B (Cell Signaling Technology) antibody overnight rocking at 4°C. Membranes were then washed and incubated with either HRP-conjugated anti-mouse or HRP-conjugated anti-rabbit (1:10000) secondary antibody for one hour. After final wash, ECL chemiluminescent reagent (Thermo Fisher) was used to detect protein levels.

Immunofluorescence

2×10^4 A549 cells were seeded into 4 chamber slides and incubated in RPMI containing either 50 μ M methionine or 2 μ M methionine for 3 days. Cells were fixed with 4% paraformaldehyde for 20 minutes, permeabilized using 0.1% Triton X-100 in 1x PBS for 30 minutes and blocked with 1% BSA in 1x PBS for 1 hour. We then stained our cells with anti-LAT1 mouse antibody with a 1:500 dilution and anti-LAMP1 rabbit antibody (Cell Signaling Technology) at a 1:500 dilution for 2 hours. Cells were washed with 1x PBS and incubated with either goat anti-rabbit Alexa Fluor 488 (Invitrogen) and donkey anti-mouse Alexa Fluor 568 (Invitrogen) secondary antibodies for 1 hour. Cells were washed with 1x PBS and incubated with 100ng/mL DAPI in 1x PBS for 3 minutes. Cells were then washed with 1x PBS, mounted using ClearMount mounting solution (Invitrogen), and images were taken on Nikon confocal microscope.

Macropinocytosis

1x10⁴ PC9 cells were seeded in 8-chamber slides and incubated in RPMI-1640 media with PBS (control), 100μM BCH, or 10mM BCH for 48 hours. Cells were then placed in serum-starved RPMI-1640 with respective treatment overnight. 50μM of 5- [N-ethyl-N-isopropyl] amiloride (EIPA) (Selleckchem) or DMSO was added 1 hour prior to returning cells to serum complete media and incubating with 1mg/mL of Dextran for 1 hour. Cells were washed with 1x PBS and 1mg/mL Concanavalin A for 1 hour and washed to remove unbound Concanavalin A. Cells were then fixed and permeabilized with 100% cold methanol and nucleus was stained using 100ng/mL DAPI in 1x PBS for 3 minutes. Slides were mounted using ClearMount mounting solution (Invitrogen), images were taken on Nikon confocal microscope using Z-stacking, and images were quantified using ImageJ.

Statistical analysis

All statistical analysis was performed using Graphpad Prism. Data are reported as average ±SEM, wherein p-values, statistical tests, and replicates are described in respective figures.

Results

Methionine restriction leads to decreased cellular proliferation

Previous work has shown that certain cancers, such as breast cancer, undergo tumor regression under methionine restrictions [92, 93]. Unfortunately, these studies failed to recapitulate a methionine restrictive environment, selecting for complete methionine starvation instead. Based on previous literature, we found the methionine concentration in human serum to range between 20 and 30 μ M [112]. With this in mind, we opted to investigate the changes brought on by excess methionine (50 μ M), serum-level methionine (20 μ M), methionine restriction (2 μ M) and complete methionine deprivation (0 μ M).

I performed an alamarBlue assay to investigate how different levels of methionine can impact the viability of lung adenocarcinoma (LUAD) across multiple days (Figure 6A-D). I compared the metabolic rate of resazurin, found in the alamarBlue, across the days with Day 0 and normalized my findings by LUAD incubated in 50 μ M methionine (Figure 6A-D). I found no change in cell viability of LUAD grown in 20 μ M vs 50 μ M methionine. However, after Day 2, multiple LUAD cell lines showed a dramatic decrease in 2 μ M and 0 μ M methionine compared to 50 μ M. I also investigated how the changes in methionine could affect non-malignant immortalized lung cells, HPL1D, and witnessed no significant changes in cell viability when comparing 20 μ M with 2 μ M methionine. This data recapitulates what others have found, wherein removing methionine from the media drastically decreases cancer cell viability, even if the presence of the immediate precursor of methionine (homocysteine), which was not seen in non-malignant fibroblasts [113]. One explanation to the decreasing resazurin

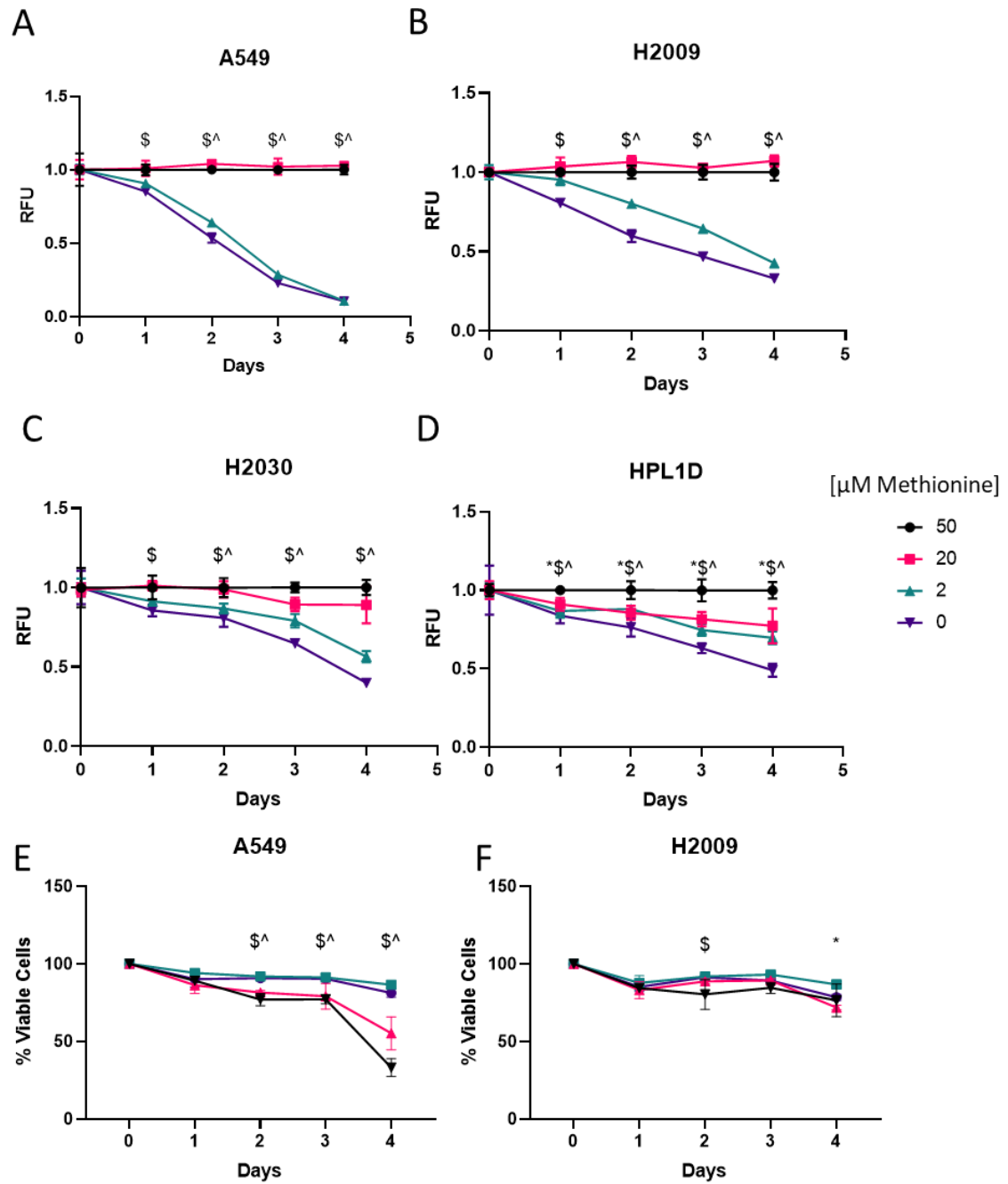


Figure 6. Methionine restriction decreases cellular proliferation without impacting viability.

A) Relative cell number of A549, B) H2009, and C) H2030 and D) non-malignant transformed epithelial lung cell (HPL1D) in decreasing concentrations of methionine in

RPMI-1640 media. E) Percentage of Annexin V negative/ PI negative of A549 and F) H2009 cells incubated in decreasing concentrations of methionine in RPMI-1640 media. Two-way ANOVA was used to compare each time-point with differences from relative cell number at 50 μ M methionine with Dunnet test. * p-value < 0.05 for 20 μ M vs 50 μ M, ^ p-value < 0.05 for 2 μ M vs 50 μ M, and \$ p-value < 0.05 for 0 μ M vs 50 μ M.

metabolism could be decreased cell number. To determine whether changes in methionine levels was inducing apoptosis in LUAD, I performed Annexin/PI staining. LUAD cells were placed in their respective media across 4 days with no media change and apoptosis was measured by flow cytometry daily (Figure 6E-F). Interestingly, my apoptotic results do not explain the drastic decrease of RFU witnessed in our alamarBlue study. For several LUAD cell lines, significant decrease of cell survival was not witnessed until after Day 3, and even then, did not match the same intensity as our alamarBlue study (Figure 6E-F).

Methionine restriction elicits a quiescent G2 phase cell cycle arrest.

With a decreasing amount of metabolized resazurin and no change in apoptosis, I next wanted to determine whether there were changes in proliferation due to cell-cycle arrest. I performed a clonogenic assay using 50, 20, 2, and 0 μ M methionine for 10 days (Figure 7A). I manually counted the colonies and found no significant difference between the different methionine concentrations (Figure 7B). Using ImageJ, I measured the average intensity of colony staining, a measure of proliferation; colonies containing more cells within them would stain darker than colonies with fewer cells. Interestingly, my data shows that there is a dramatic difference in staining in LUAD cells grown under 2 and 0 μ M methionine (Figure 7C). Together with my alamarBlue and annexin results, these data suggest that methionine restriction does not have an immediate impact on cellular survival, and instead lessens proliferation rate of LUAD cells.

We next sought to identify where in the cell-cycle we were witnessing a possible arrest. We incubated our LUAD cells in decreasing concentrations of methionine for 72-

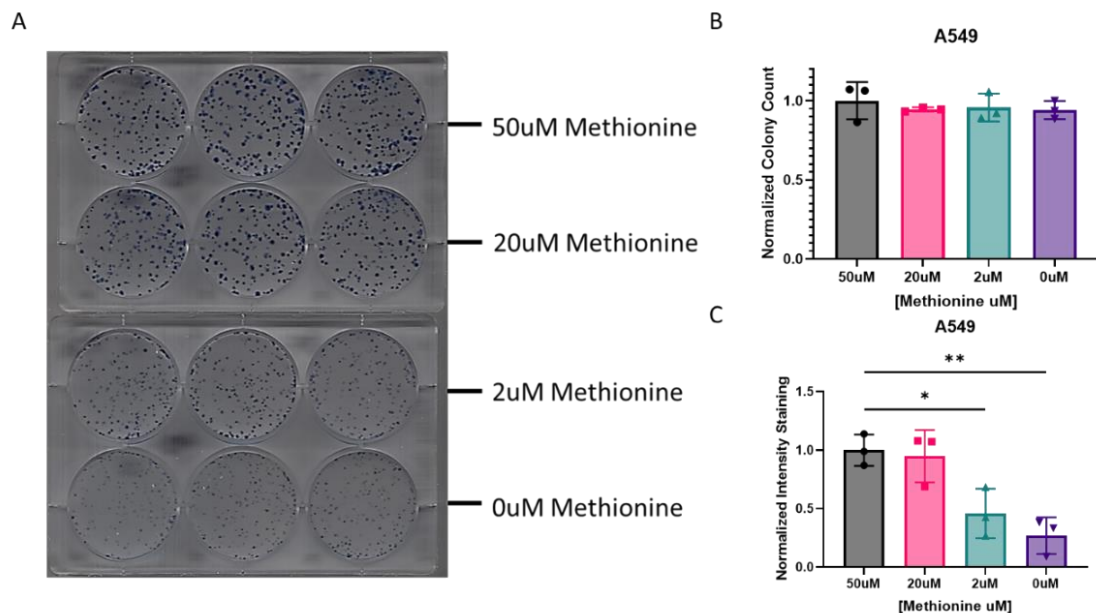


Figure 7. Methionine restriction decreases cellular proliferation.

A) Representative colony assay image of A549 cell lines seeded in RPMI-1640 containing either 50μM, 20μM, 2μM, or 0μM methionine after 10 days and stained with Coomassie stain. B) Normalized colony count of A549 colony assay. Data were gathered by manual counting and normalized to colony count of 50μM. One-way ANOVA was used to statistically analyze colony count and showed no significant differences C) Normalized Intensity staining of A549 colony assay. Data were gathered using ImageJ plugin ColonyArea and data collected was normalized to intensity of colonies in 50μM. Data of colony count and intensity was analyzed using one-way ANOVA with Dunnett test, * p-value < 0.032, ** p-value < 0.0021.

hours prior to performing a BrdU assay (Figure 8A). The data gathered from this experiment shows a decrease in S-phase and an increase in G1/G₀ and G2 phase for LUAD cells under methionine restriction (Figure 8B-C). A cell cycle arrest can mean either senescence or quiescence. Senescence is identified as a point in time when the cell has deteriorated to the point that it can no longer divide, mainly brought upon by age. Quiescence, on the other hand, is a reversible halt in the cell cycle, where cells will remain dormant until adequate conditions are met. To determine whether the cell cycle arrest observed under methionine restriction was indeed reversible, I performed a clonogenic assay experiment placing LUAD cells in either 20μM or 2μM methionine. After 7 days, one group originally placed in 2μM methionine was returned to 20μM methionine for the remaining 3 days (Figure 9A). What we witnessed was a drastic increase in proliferation, to a degree that the intensity of staining matched those that had never entered methionine restriction (Figure 9B-D). This data would suggest that cells enter a dormant state under methionine restriction, poised for proliferation and waiting for levels of methionine to return.

Altered motility observed under methionine restriction is due to proliferation.

Previous investigators have reported methionine restriction affects breast cancer motility and invasive potential. I performed a scratch wound assay to determine if LUAD cell lines would exhibit similar decreases in cell motility under methionine restriction. LUAD cell lines under either 2 or 0μM methionine showed a significant decrease in A549 cell line motility after 24- and 48-hours of methionine restriction, while H2009 cell line motility significantly decreased after 48-hours (Figure 10A-C).

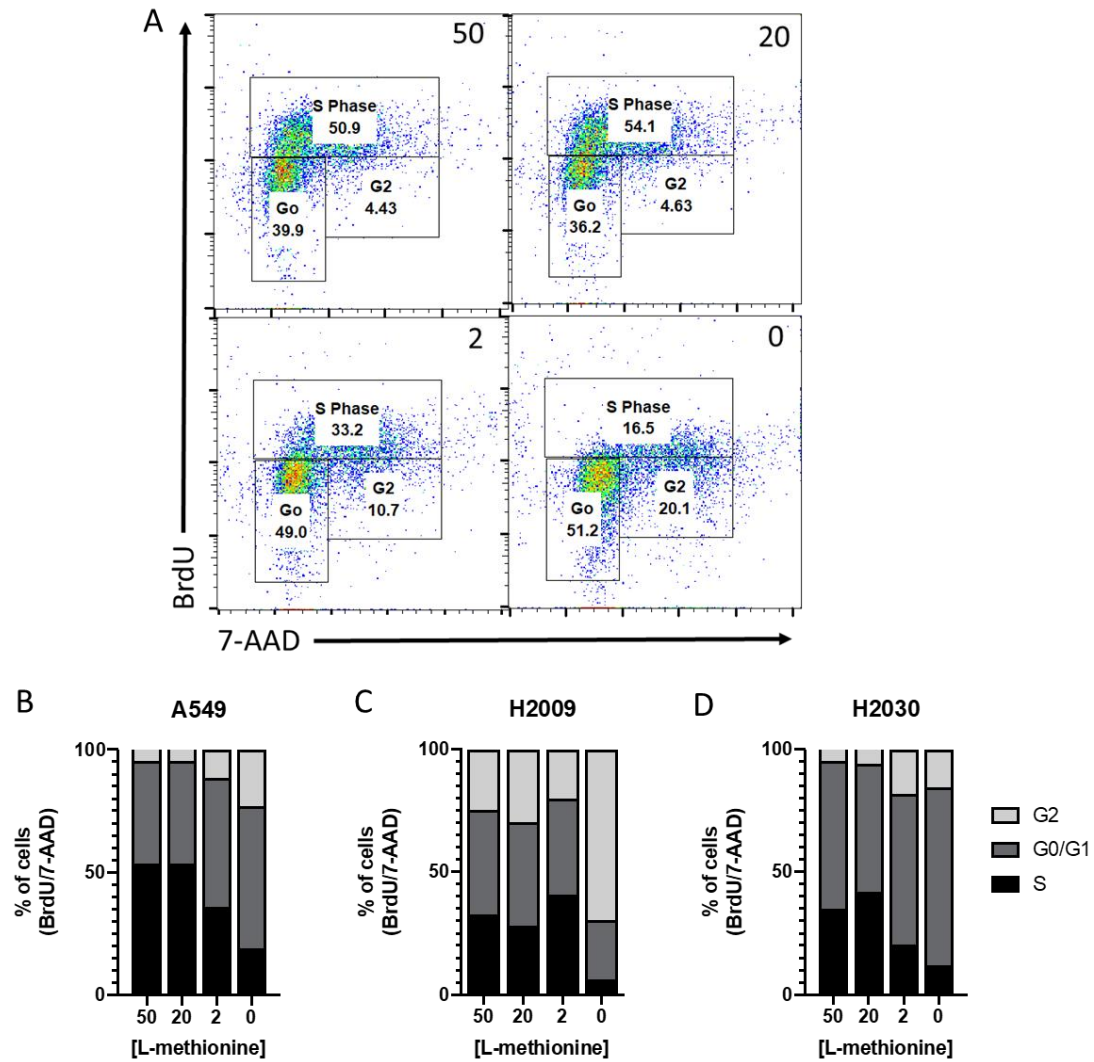


Figure 8. Methionine restriction elicits cell cycle arrest at G₀/G₁ and G₂ phase.

A) Representative of flow cytometry data on A549 using APC anti-BrdU antibody and 7-AAD. Cells were incubated in RPMI-1640 media containing either 50 μ M, 20 μ M, 2 μ M or 0 μ M methionine over 3 days. Cell lines were incubated with BrdU for 3 hours prior to fixing and staining. B) Data analysis of cell-cycle for A549, C) H2009, and D) H2030 cell lines.

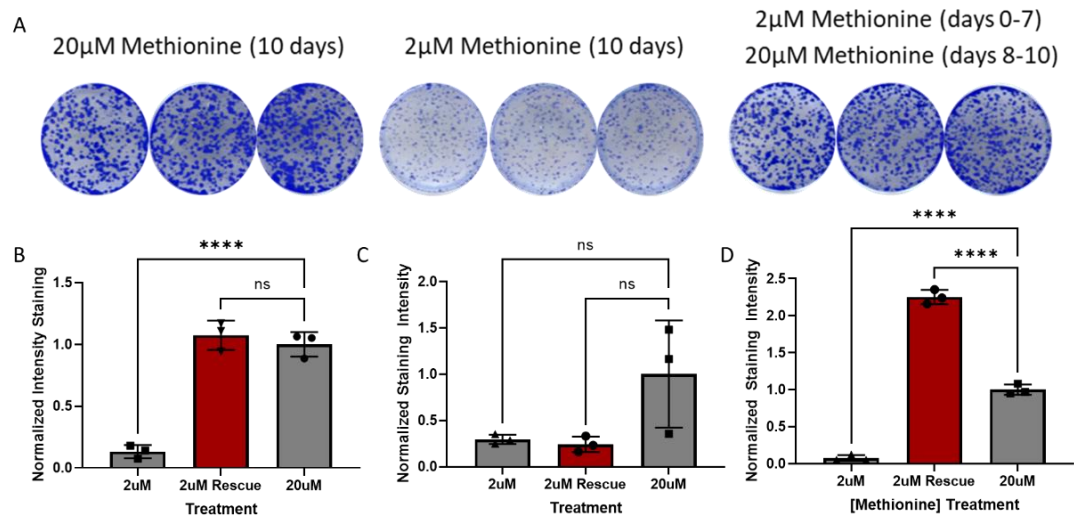


Figure 9. Slowed proliferation can be reversed following returning cells to high levels of methionine.

A) Representative images of colonies for A549 cells in respective media. Colonies were fixed with methanol, stained with Coomassie, and washed with PBS. B) A549 C) H2009 and D) H2030 colony staining intensity was measured using ColonyArea plugin of ImageJ. Red bar signifies cell lines placed in 2 μ M methionine for 7 days and returned to 20 μ M for the remaining 3 days. Data were analyzed using one-way ANOVA, comparing all samples with 20 μ M methionine, and using a Dunnet test ($n = 3$, **** p -value < 0.0001).

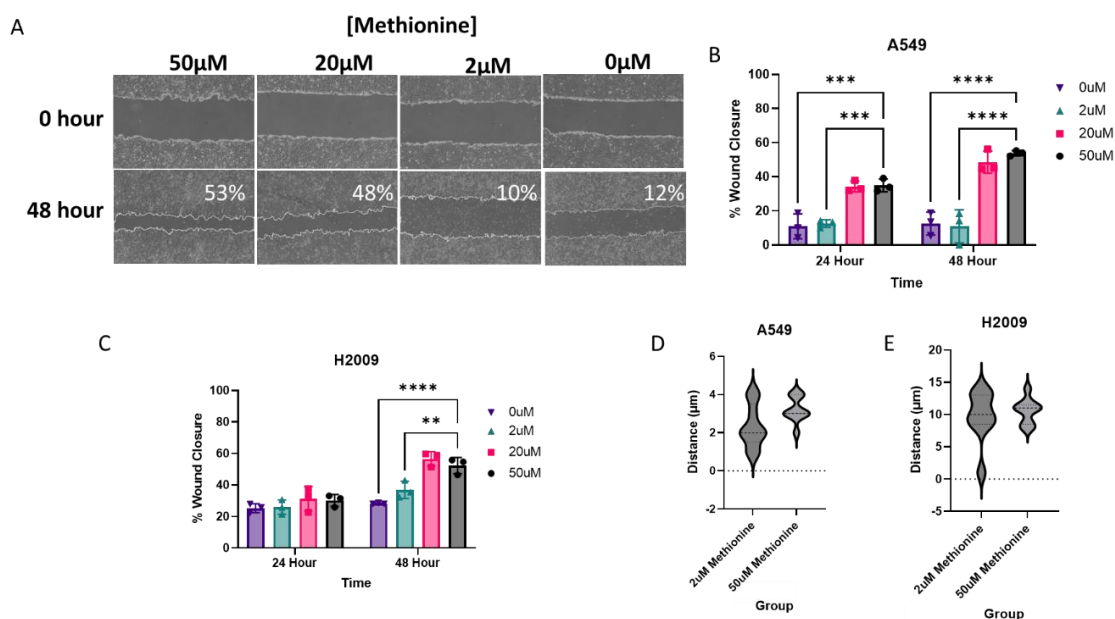


Figure 10. LUAD motility is not affected under methionine restriction.

A) Representative images of wound healing analysis. Average wound closer represented in text within 48-hour wound picture. B) Data analysis of wound healing in A549 and C) H2009 cell lines (n = 3). Data were normalized by wound area at 0 hour and analyzed using Two Way ANOVA with Dunnett test, comparing all data points with LUAD incubated in 50μM methionine. ** p-value < 0.0021, *** p-value < 0.0002, **** p-value < 0.0001. D) Cell motility assay using Keyence live-cell imager to measure distance traveled of individual A549 and E) H2009 cells (n = 9) in μm. Data were analyzed using student t-test.

As I saw changes in proliferation, I chose to verify that the wound closure was attributed to motility of LUAD cells. As such, I measured the distance traveled of LUAD cell lines in RPMI-1640 containing either 50 μ M or 2 μ M methionine using the Keyence BZX-800 live cell imager. To do this, I seeded LUAD cell lines such that I could differentiate single cells. LUAD cell lines were then incubated for 48 hours in our live cell imager, with images taken every 10 minutes. These images were then used to analyze the distance traveled by individual cells. My results show that there is no significant difference in total distance traveled over the course of 48 hours (Figure 10D-E). Taken together, my results suggest that methionine restriction does not impact motility of LUAD, but instead impacts proliferation.

Methionine restriction increases LAT1 expression and alters localization to lysosome.

To confirm our findings *in vivo*, we used immunocompromised NRGs mice and subcutaneously injected them with luciferase expressing H2009 cell lines (Figure 11A). These mice were then placed on either a methionine high diet (0.86% methionine) or a methionine low diet (0.11% methionine), with a separate methionine low cohort being returned to methionine high diet after 2-weeks. 2 weeks after changing the mouse diet from methionine high to methionine low resulted in a significant decrease in tumor progression for those mice in our methionine low group. (Figure 11B). Additionally, we witnessed a similar rescued phenotype in tumor progression for low methionine mice placed back into a high methionine diet as our in-vitro methionine restriction study.

Because the main transporter responsible for methionine uptake in cancer cells is LAT1, we investigated expression levels of LAT1 in tumors of mice under altered diet. We also investigated the expression levels of MYC, as MYC is a known enhancer of

LAT1 [40]. By western blot I saw LAT1 and MYC levels elevated in mice that had been, at one point, placed in 0.11% methionine diet (Figure 11C). However, densitometry analysis would show that the elevation for LAT1 observed in 0.11% methionine mice and elevation of MYC observed in methionine rescued mice were considered nonsignificant (Figure 11D-E). The significance observed by our densitometry is likely attributed to an outlier within the 0.86% methionine group. I also observed no significant changes in mTOR phosphorylation (Figure 11F-G) but did observe significantly elevated AKT phosphorylation in my 0.11% methionine mice and LC3b in both my methionine restricted mice and methionine rescued mice by densitometry (Figure 11H-I). It has previously been reported that, under stress, cancer cells activate AKT to modulate the microenvironment by enhancing vasculature [114]. As such, I believe the LUAD are upregulating LAT1 through MYC. Furthermore, the upregulation of AKT activation could be an attempt to increase vascularization to bring more nutrients to the tumor.

We went back to our *in-vitro* models to determine whether methionine restriction was also resulting in elevation of LAT1. We performed qPCR on our LUAD cell lines, using primers specific for LAT1, LAT2, LAT3, and LAT4. Interestingly, all LAT expression was observed to be elevated under methionine restriction (Figure 12A). We also investigated whether this increase in RNA expression was also observed in translated protein by western blot. We not only investigated LAT1 expression, but also probed for LC3b. Unfortunately, our LAT1 protein levels did not show any elevation in expression (Figure 12B-C); but like our *in-vivo* model, our cell lines were also showing a dramatic increase in MYC and LC3b under methionine restriction (Figure 12D-E).

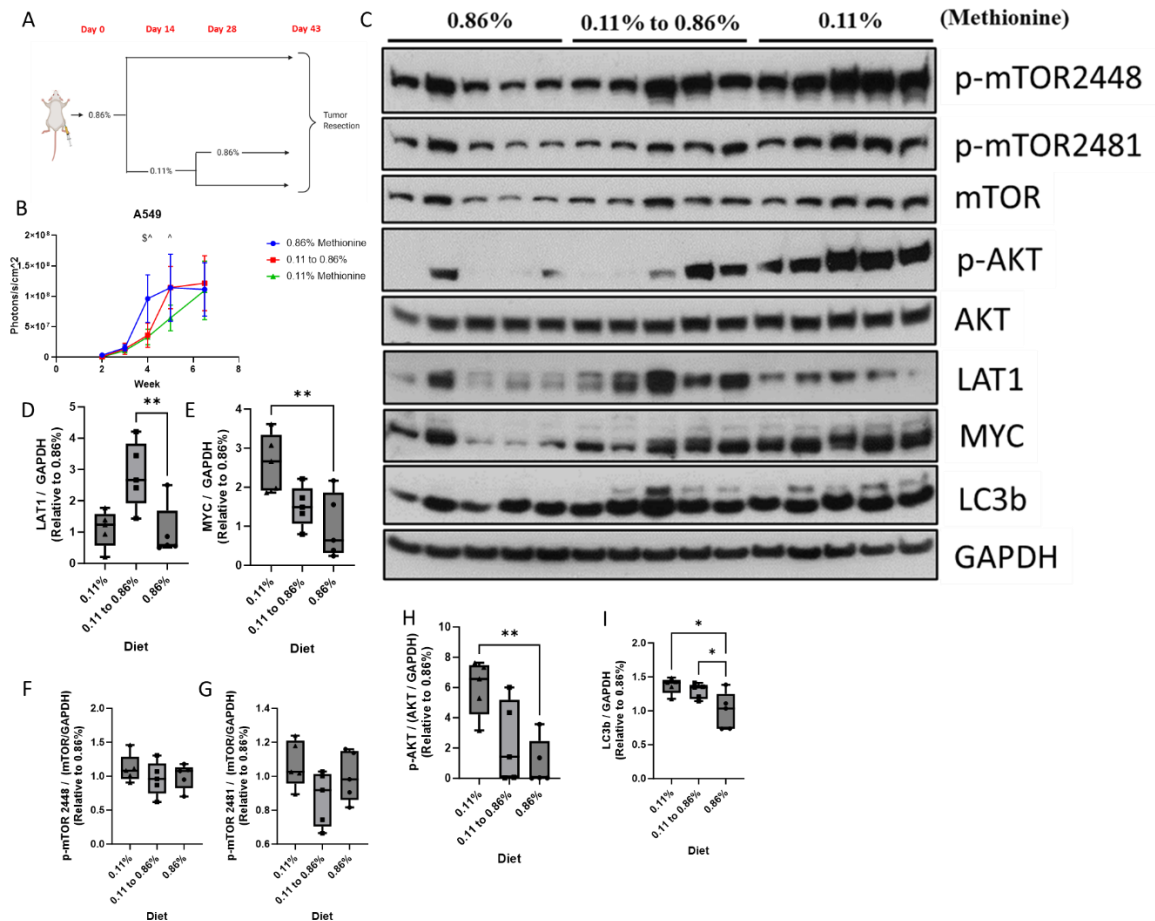


Figure 11. LUAD tumor growth is significantly decreased when animals are placed in low methionine diet.

A) Representation of study design. Luciferin expressing LUAD cell lines were subcutaneously injected in NRGS mice and placed in diet consisting of 0.86% methionine. After 14 days, mice were separated into our methionine high (0.86% methionine) and our methionine low (0.11% methionine) groups. After being in methionine low diet for 14 days, a third cohort was returned to our high methionine diet for the remainder of the study. B) Tumor growth measured weekly by AMI Imager. Data were analyzed using one-way ANOVA, comparing the photons/s/cm² of our experimental mice to our 0.86% methionine control mice. \$ denotes significant changes

between our 0.11 to 0.86% and our 0.86% animals, and ^ denotes significance between our 0.11% and our 0.86% animals (n = 5). C) Western blot analysis of tumors probing for LC3, myc, LAT1, AKT, phosphorylated AKT, mTOR, and phosphorylated mTOR (2481 and 2448). GAPDH was used as a loading control. D) Densitometry analysis of LAT1, E) MYC, F) phosphorylated mTOR at site 2448, G) phosphorylated mTOR at site 2481, H) phosphorylated AKT, and I) LC3b. LAT1, MYC, LC3b, total AKT, and total mTOR were normalized by GAPDH. Phosphorylated mTOR and AKT were normalized by normalized total mTOR and normalized total AKT, respectively. Data were analyzed using a one-way ANOVA with Tukey test, * p-value < 0.021 and ** p-value < 0.00332.

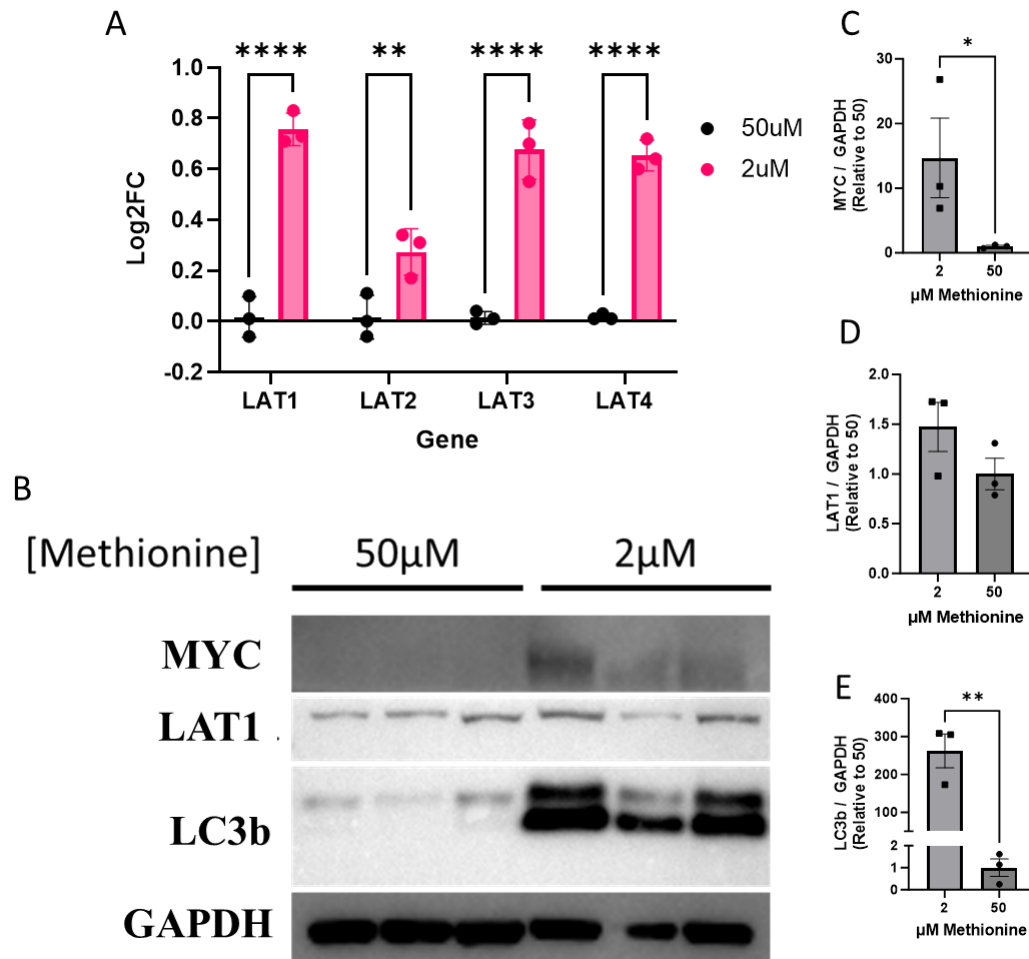


Figure 12. Methionine restriction leads to increased myc and LC3b in LUAD cell lines.

A) qPCR analysis of A549 investigating RNA expression of LAT1, 2, 3, and 4 comparing cell lines from A549 cell lines incubated in RPMI-1640 containing either 50μM or 2μM methionine (n=3) for 72 hours. Data were analyzed using two-way ANOVA with Sidak post-hoc test, ** p-value < 0.0021, **** p-value < 0.0001. B) Western blot of A549 cells grown in RPMI containing either 50μM or 2μM methionine for 72 hours and blotted for myc, LAT1, and LC3b. GAPDH was used as a loading control. C) Densitometry analysis of LAT1, D) MYC, and E) LC3b. LAT1, MYC, and

LC3b were normalized to GAPDH. Normalized densitometry data were analyzed using unpaired t-test, * p-value < 0.021 an ** p-value < 0.00332.

Amino acids are known to regulate mTOR phosphorylation, inhibiting mTOR activity under low nutrient levels [49, 53, 115]. It was surprising to witness increased mTOR phosphorylation under methionine restriction. LAT1 has been previously reported to localize to the membrane of the lysosome to facilitate the activation of mTOR [116, 117]. With this in mind, and with our results of LC3b, we hypothesized that the increase in mTOR activation in methionine restriction was accomplished by increasing autophagy in LUAD, shuttling the methionine from degraded proteins in the lysosome to the cytoplasm. We performed immunofluorescence on LUAD cell lines to determine whether methionine restriction was leading to LAT1 to relocate to the lysosome. We stained our LUAD cell lines with LAT1 and LAMP1, a marker for autophagy that is found on autophagic and endolysosomal organelles. Our results show LAT1 colocalizing with LAMP1, strengthening our hypothesis (Figure 13).

GeCKO screening identifies macropinocytosis as key pathway under methionine restriction.

My findings thus far would suggest that methionine restriction impacts the proliferation of LUAD without impacting survival. This is likely due to the increase in autophagy facilitating survival under methionine restriction. My next goal was to determine pathways that are critical for survival under methionine restriction. To do this, I performed a Genome-wide Crispr Knock-Out (GeCKO) screen (Figure 14A). As I have previously observed a dramatic decrease in cellular proliferation at 2 μ M methionine, I had first chosen to investigate the concentration of methionine that would elicit a 30% decrease in cellular proliferation. I used a range of methionine concentrations and recorded the normalized cell number to those grown in 50 μ M methionine.

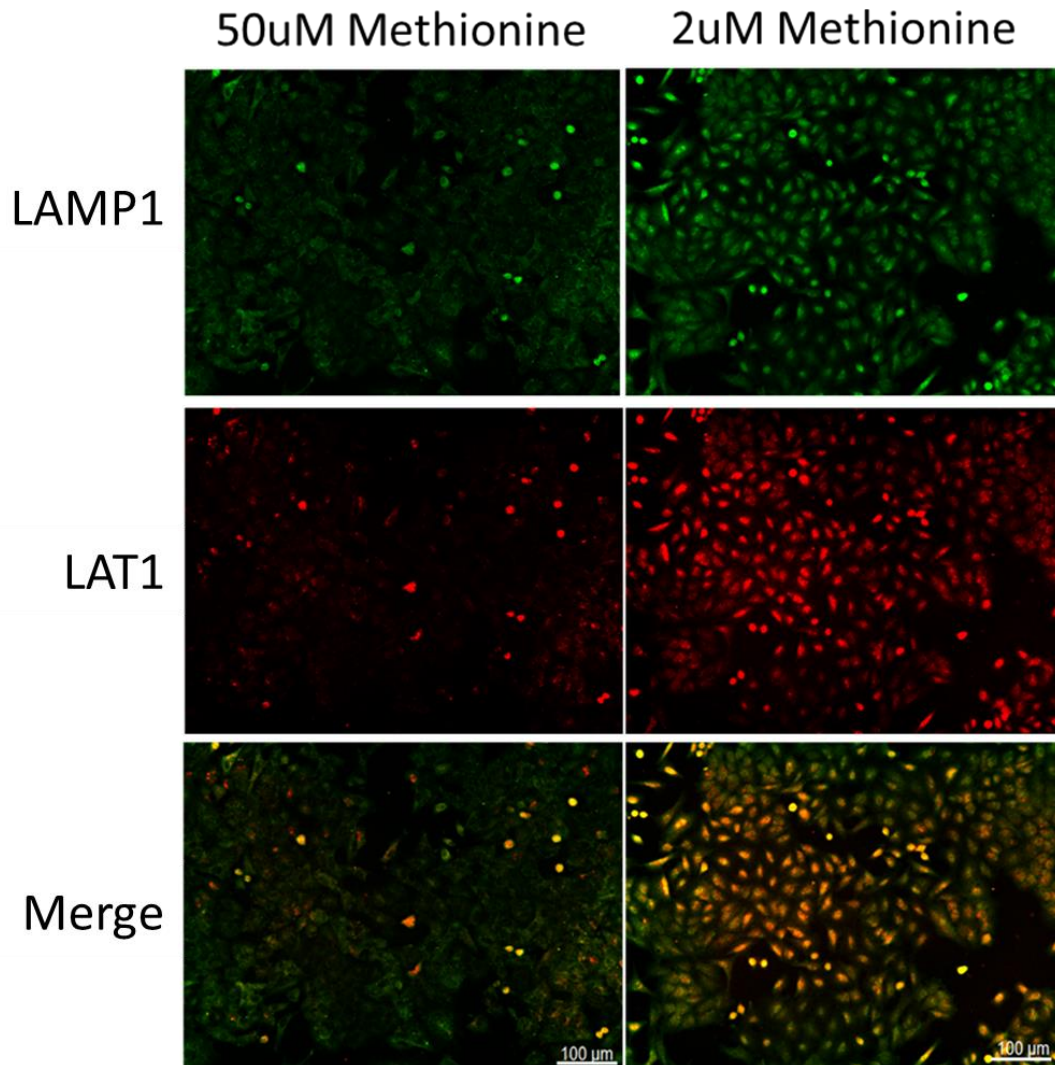


Figure 13. LAT1 localizes with LAMP1 under methionine restriction.

A549 were incubated in RPMI-1640 media containing either 50 μ M or 2 μ M methionine for 72 hours. Following fixing, cells were incubated with mouse anti-LAT1 (red) and rabbit anti-LAMP1 (green) antibody and stained with donkey anti-mouse and goat anti-rabbit secondary antibody. Images were captured on Nikon Confocal Microscope with 20x magnification.

From the range of concentrations chosen, 16 μ M methionine showed the desired decrease in cellular proliferation across multiple cell lines (Figure 14B). With this information, I incubated LUAD cell lines (A549 and H2009) and lung epithelial cell line, HPLD1, in 50 μ M methionine and 16 μ M methionine following CRISPR knockout. Our GeCKO screen identified in several genes that were shown to be synthetically lethal under methionine restriction, including SLC7A5 (LAT1) in LUAD but not in HPLD1. Interestingly, multiple genes associated with actin polymerization and endocytosis also showed synthetic lethality, specifically Cell Division Cycle 42 (CDC42), Syndecan 1 (SDC1), Early Endosome Antigen 1 (EEA1), Ras Homolog Family Member A (RhoA), Rho Associated Coiled-Coil Containing Protein Kinase 1 (ROCK1), Cytotoxic T-lymphocyte Associated Protein 4 (CTLA4), and Arrestin Domain-Containing Protein 4 (ARRD4), (Figure 14C).

These genes all share one endocytic pathway in common: macropinocytosis. Macropinocytosis is a non-selective form of endocytosis that cancer cells can utilize to take up cellular debris [118] and even amino acids [119]. With the knowledge that LUAD cell lines with macropinocytotic genes were not as fit to survive under lower methionine, I next asked if KO of LAT1 would result in upregulation of these genes. For this, I knocked out LAT1 using CRISPR and saw elevation of proteins associated with macropinocytosis, namely: Syndecan-1 (SDC1), ROCK1, and RhoA (Figure 15A). Unfortunately, we found that KO of LAT1 resulted in LUAD cell lines that were incapable of being reseeded. As such, I had opted to use a common LAT1 inhibitor, BCH. BCH is known to inhibit LAT1 at concentrations of \sim 100 μ M and all LATs at concentrations of 10mM. I investigated the effects of BCH treatment on LUAD

proliferation and saw BCH begins impacting relative LUAD cell numbers at 10mM (Figure 15B-C), and that BCH does not further decrease cell viability (Figure 15D-E). In order to investigate macropinocytosis in LUAD cell lines treated with BCH, I incubated LUAD cells with 70kDa Tetramethylrhodamine conjugated Dextran (Figure 16A). 70kDa Dextran was used to ensure uptake was because of macropinocytosis, as 70kDa is too large to be taken up by other means of endocytosis. To validate that uptake was indeed by macropinocytosis, I had also incubated cells with 50 μ M of 5-(N-ethyl-N-isopropylamyloride (EIPA), a macropinocytosis inhibitor [118]. Furthermore, Tetramethylrhodamine was used as our conjugated fluorophore as green fluorescence protein (GFP), the more common fluorophore, is pH sensitive [120]. Additionally, I used concanavalin-A (ConA), a lectin known to bind to glycoproteins such as those on the plasma membrane. Using ImageJ, I was able to isolate the internal structure of the cell from background using ConA. I then used ImageJ to measure particles remaining and normalized by DAPI count [121]. My results show that BCH administration, whether 100 μ M or 10mM, led to increased dextran uptake (Figure 16B). Additionally, EIPA treatment inhibited dextran uptake, further enforcing the idea that LAT1 inhibition leads to increased macropinocytosis.

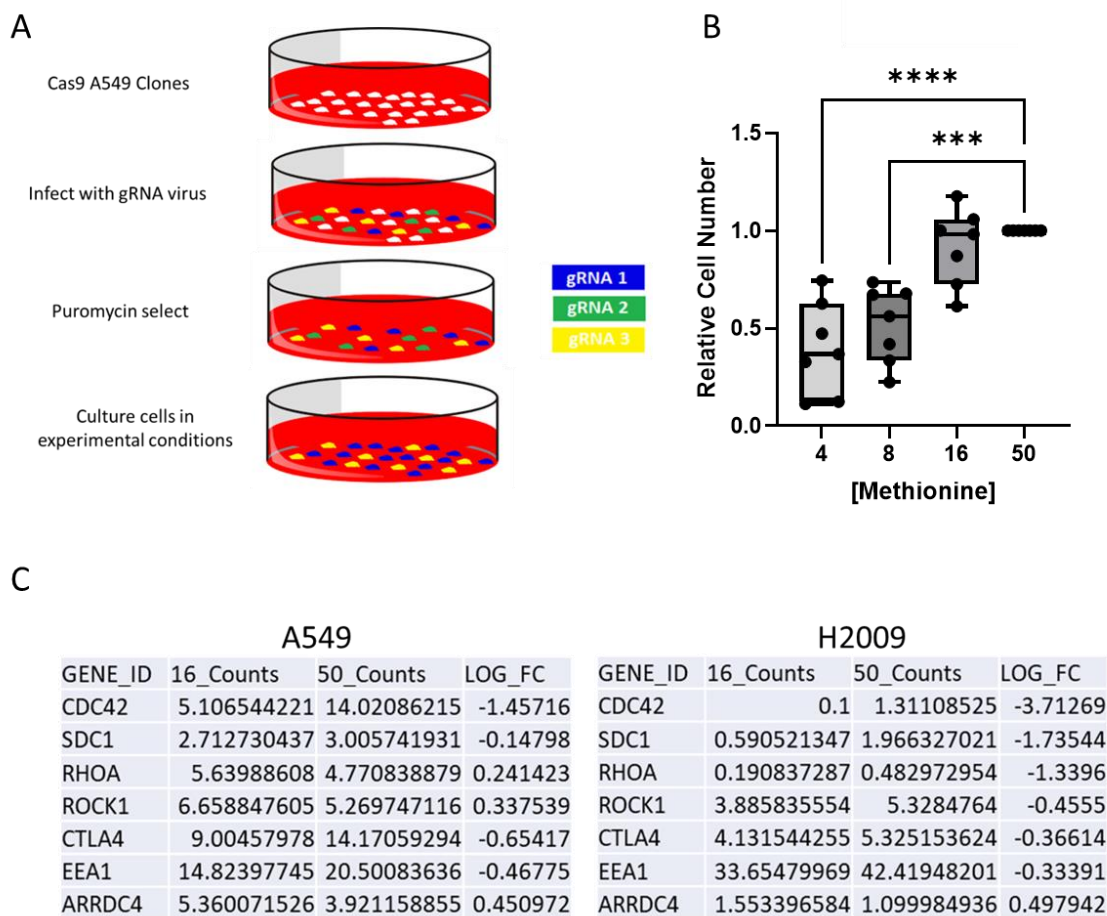


Figure 14. GeCKO screening results indicate macropinocytosis crucial for survival under methionine restriction.

A) Representative image illustrating the concept of GeCKO screening. After infection of gRNA, cells are placed in puromycin to select for cells that have successfully incorporated the virus. Cells were then transferred to either methionine high or methionine low media for 16 days. Samples were taken at the puromycin selection stage and after 16 days of treatment. B) Cell count measuring the impact of different methionine concentrations on cellular proliferation (n=6). Cells were seeded in respective media for 16 days, with cells reseeded every 4 days. Data were normalized to cell number at 50 μ M methionine and analyzed using one-way ANOVA with Dunnett

post-hoc test. **** p-value < 0.0001, *** p-value < 0.0002. C) GeCKO Screen results highlighting genes related to macropinocytosis.

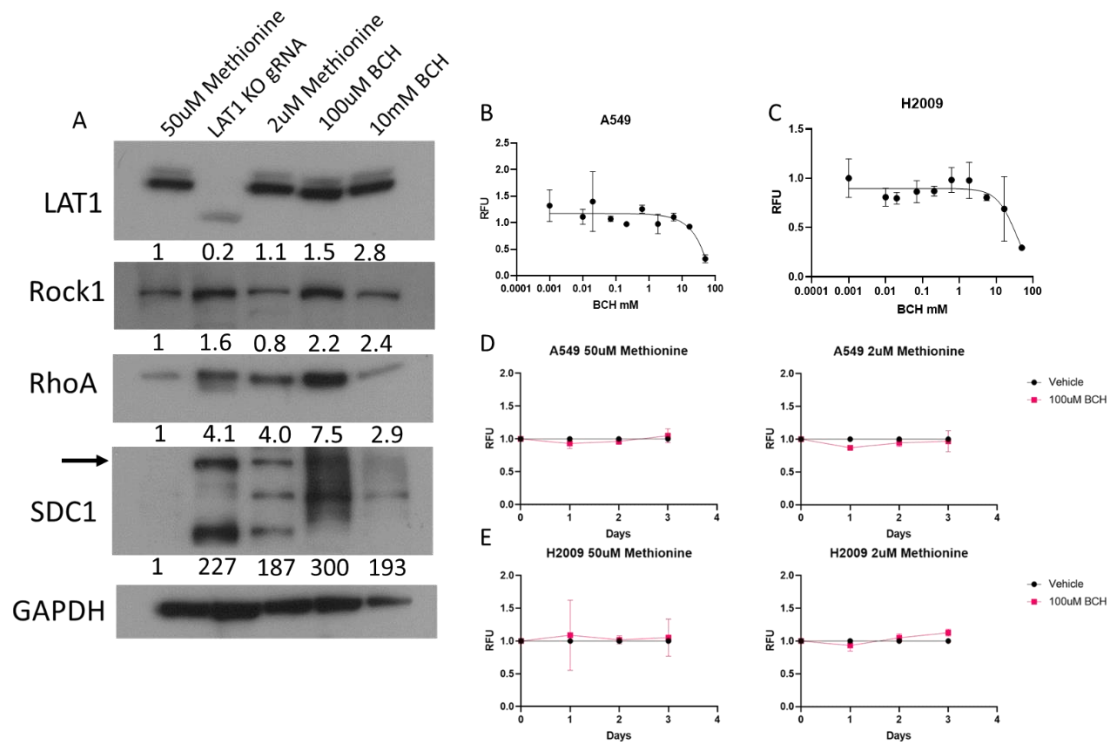


Figure 15. LAT1 KO and BCH administration impacts genes related to macropinocytosis.

A) Western blot analysis of A549 incubated in 50μM methionine media, 50μM methionine media with LAT1 KO by CRISPR, 2μM methionine media, 50μM methionine media with 100μM BCH, or 50μM methionine media with 10mM BCH for 72 hours. Membrane was probed for LAT1, to verify LAT1 KO, and macropinocytotic related genes: Rock1, RhoA, and SDC1. GAPDH was also probed as our protein loading control. Densitometry was measured using ImageJ, wherein GAPDH was used to normalize densitometry values. Normalized values were then compared against values of A549 incubated in 50μM Methionine. B) Cell viability of A549 and C) H2009 following increasing concentrations of BCH after 72 hours administration. Data were normalized

to RFU of cell lines incubated in 1 μ M BCH. D) Cell viability of A549 and E) H2009 following 100 μ M treatment of BCH in RPMI-1640 containing either 50 μ M or 2 μ M methionine over the course of 3 days. Data were normalized by RFU from cell lines in vehicle control at Day 0 for respective methionine concentrations.

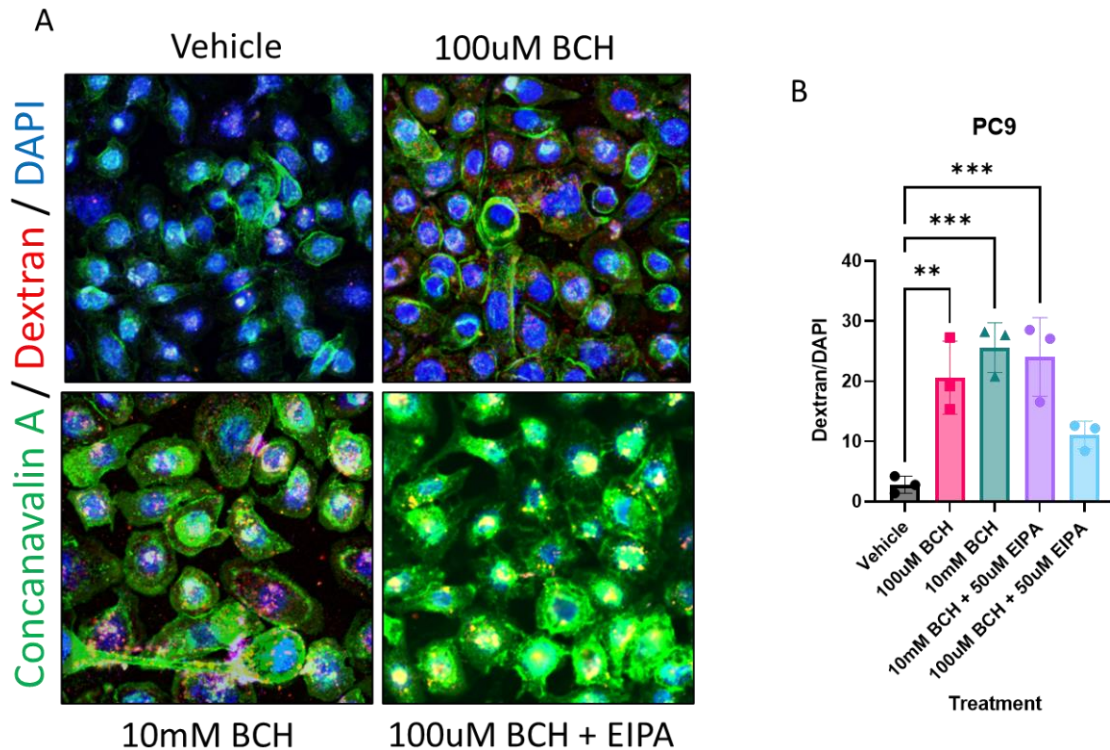


Figure 16. LAT1 inhibition leads to increased macropinocytosis.

A) PC9 cells were incubated with 100uM BCH or PBS as our vehicle control. Cells were incubated with Tetramethylrhodamine conjugated Dextran (Red), fixed with methanol, and cell wall was stained with Concanavalin A (green) and nucleus was stained with DAPI (blue). Images were captured using Nikon Confocal Microscope. B) Macropinocytosis data were measured by distinguishing intracellular regions using Concanavalin A in ImageJ. ImageJ was used to measure dextran content and normalized based on DAPI count. Data were analyzed using one-way ANOVA with Dunnett post hoc test. ** p-value < 0.0021, *** p-value < 0.0002.

Discussion

Methionine is an essential amino acid that is critical for cellular function. Cancer cells are highly dependent on methionine concentration, as others have shown removal of methionine and supplementation with its precursor, homocysteine, inhibits cellular proliferation on cancer cells but not non-malignant cells [122]. Studies investigating the role of methionine on breast cancer and prostate cancer have shown restricting methionine leads to anti-cancer activity, including decreasing cellular proliferation [93, 97, 113], decreasing metastasis [92, 123], and increasing cancer susceptibility to therapeutics [95, 124]. These findings have led to a new branch of potential therapeutics; focusing on nutritional modulation to treat cancer. This study focused on understanding the cellular effects of methionine restriction on LUAD.

In agreement with other studies investigating methionine restriction on breast and prostate cancer, we show that LUAD cell lines also exhibit a decrease in cellular proliferation following incubation with low levels of methionine. As proliferation is a consequence of cell cycle progression, we investigated at which stage LUAD cell lines were halted under methionine restriction and found cell lines to be arrested in the growth phase (G₂ and G₀). Interestingly, the slow growth that is observed in our methionine restrictive studies was rescued by returning cell lines to 20μM of methionine. Based on these results, we suggest that methionine restriction causes cells to enter a quiescent stage, wherein growth is paused, and cells are primed for proliferation when returned to a methionine-rich environment.

Previous studies have also suggested low methionine inhibits cancer cellular motility and invasive potential of breast and colorectal cancer [94, 123, 125, 126]. Our

wound healing assay did corroborate with these findings, showing methionine restriction decreased wound healing capabilities. However, because of the halt in proliferation that was observed, we chose to investigate cellular motility using live cell imaging and tracking software. Unlike our wound healing assay, our live cell imaging showed no significant difference in cellular motility in LUAD cell lines incubated in methionine restriction. We believe that the change in cellular motility observed in wound healing assays and invasive potential observed *in vivo* and invasion assays are a result of overall decreased cellular proliferation rather than a direct impact on cellular motility.

As cancers are highly dependent on nutrient availability for survival and progression, they upregulate transporter expression to satisfy their nutritional needs. Methionine is transported intracellularly through several SLC transporters, including LAT1, LAT2, LAT3, and LAT4. LAT1, specifically, has been observed to be upregulated in many different cancer types, which is believed to be through MYC transcriptional activation. LAT1 not only imports nutrients from the extracellular environment, but it has also been implicated in mTOR signaling on the lysosome [116, 117].

From our *in-vivo* models, we witnessed elevation of MYC, LAT1, AKT phosphorylation, and LC3b in tumors of mice that had previously been placed on a diet consisting of 0.11% methionine. In addition to LAT1 expression increasing in tumors of mice placed in low methionine diet, we also saw an elevation of LAT1,2,3, and 4 RNA expression of A549 cell lines placed in methionine restriction. Our immunofluorescence data also showed localization of LAT1 with LAMP1 under methionine restriction, providing further evidence that low methionine levels were leading to increased LAT1

localization to the lysosome. Interestingly, while we did not see significant LAT1 protein levels in our western blot, we saw a dramatic increase in signal by immunofluorescence. It's possible that more LAT1 may be found in the cellular debris of LUAD cell lines following CHAPS lysis buffer. Perhaps by using a harsher lysis buffer, such as RIPA, would result in a better comparison of LAT1 levels in 50 μ M methionine vs 2 μ M methionine.

We hypothesized that LUAD cell lines were upregulating autophagy as an attempt to survive low methionine environments. To determine what genes could be important in survival under methionine restriction, we performed a GeCKO screen to determine genes that were crucial for cell survival under methionine restriction. While we did see SLC7A5 and SLC1A5 to be synthetically lethal when knocked out in 16 μ M, as we expected it to be; we also witnessed knockdown of macropinocytosis associated genes CDC42, SDC1, RhoA, ROCK1, SLA4, and EEA1 caused synthetic lethality to LUAD cell lines under methionine restriction. Additionally, our screen showed knockout of ARRDC4, a gene which regulates and inhibits macropinocytosis, did not result in lethality for LUAD cell lines under methionine restriction by our GeCKO screen. Macropinocytosis is a process that allows cells to non-specifically engulf molecules in the surrounding environment. In addition to seeing these changes in methionine restriction, we also saw elevated expression of Rock1, RhoA, and SDC1 in A549 cells that had LAT1 knocked out by CRISPR. While A549 cell lines expanded following LAT1 KO, trypsinizing our cells and subculturing them led to no cell adherence. Due to the issue of reseeding the LAT1 knocked out A549 cell lines, we focused our attention on studying macropinocytosis using the LAT1 inhibitor, BCH.

Using a concentration of BCH to either inhibit LAT1 or all LATs showed similar results of increased macropinocytotic protein expression were detected. Interestingly, we saw that administration of BCH did not impact cell viability, which we speculated was because of enhanced macropinocytosis sustaining cellular methionine concentrations. Our dextran studies further supported this idea, showing that BCH increased uptake of 70kDa dextran while EIPA, a known macropinocytosis inhibitor, reduced dextran uptake to basal levels. Overall, my data suggest that methionine restriction leads to decreased cellular activity due to a halt in the cell cycle at G_2 and G_0 , while LAT1 inhibition leads to cells utilizing macropinocytosis to transport extracellular nutrients intracellularly (Figure 17).

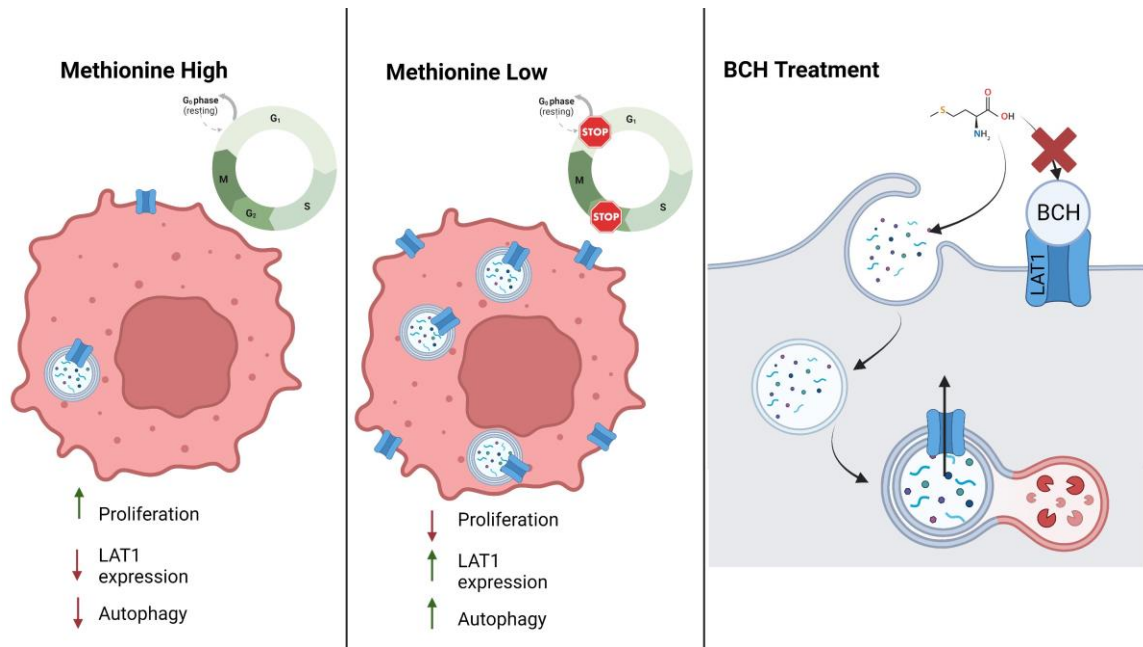


Figure 17. Graphical representation of methionine restriction and BCH treatment effects

Methionine restriction leads to an arrest at the G₂ phase of the cell cycle, resulting in a decrease in proliferation. Additionally, LAT1 expression and autophagy are greatly upregulated under methionine restriction. This is also observed when treating our LUAD with LAT1 inhibitor, BCH, where we also observe an increase in macropinocytosis.

CHAPTER 3: DECRYPTING THE CROSSTALK BETWEEN LUNG ADENOCARCINOMA AND *ESCHERICA COLI*

Introduction

Solid tumors, such as lung cancer, can be seen as separate organs consisting of heterogeneous cell types that make up the tumor microenvironment (TME) [55-59, 61, 65-67]. While previously believed to consist of mammalian cells that were reprogrammed by the tumor, it has come to light that other organisms also influence the TME, namely fungi and bacteria [78, 83, 89, 127, 128].

Our understanding of bacterial: tumoral relationship has led to the appreciation of certain bacterial species acting as oncomicrobes [80]. *Helicobacter pylori*, for instance, has been implicated in the development of colorectal cancer through inducing DNA damage including mutations and double-stranded breaks [81, 84]. Others have also reported the loss of microbiome, specifically tumor microbiome, through combination of antibiotics led to a decrease in overall tumor progression and metastasis [78, 129]. Furthermore, the microbiome has also been shown to act as nutritional reservoirs for tumors, wherein bacteria were taking up the nitrogenous waste product of tumors, in the form of ammonia, and converting it to L-arginine [130].

Bacteria are single celled organisms that can be separated into two categories: gram-positive and gram-negative. Gram-positive cells have a thick peptidoglycan cell wall that test positive during a gram stain, while gram negative cells have a thinner

peptidoglycan cell wall. Many gram-negative cells, such as *Escherichia coli*, have lipopolysaccharides (LPS), a bacterial toxin made of lipids and polysaccharides, on the outer cell wall [131]. Our immune cells can regulate gram-negative cells by targeting LPS using Toll-like Receptors (TLR), with TLR4 being the most recognized to interact with LPS [132]. Stimulation of TLR4 with LPS results in activation of the innate immune system to produce inflammatory signals through NF- κ B and cJUN activation [133-135]. However, TLR4 is not exclusively expressed on immune cells as previous studies have reported expression of TLR4 observed on multiple cancer types including lung cancer [136]. Stimulation of TLR4 has been shown to upregulate proteins related to lung cancer progression such as VEGF, TGF- β , and IL-8. It is evident that the bacteria play a role in cancer development and progression, and that biomolecules such as LPS found on most gram-negative bacteria may influence signaling pathways of lung cancer. However, the extent by which bacteria may influence lung adenocarcinoma (LUAD) remains poorly understood.

In this study, we investigate the effects of *E. coli* on LUAD phenotype. Our earlier study investigated the impact of methionine restriction on LUAD. While methionine is considered essential in mammalian cells, bacterial cells have dedicated pathways for the synthesis of methionine *de novo*. We investigated whether the supplementation of *E. coli* grown RPMI-1640 media can rescue the phenotype of LUAD in methionine restriction. Additionally, we performed radiolabeling studies to delineate the LUAD: *E. coli* interaction, as well as to determine the relevance of methionine to this interaction. We also performed RNA-seq to identify transcriptomic changes in LUAD brought on by the presence of *E. coli* biomolecules. We hypothesized that the phenotypic

changes observed in LUAD when incubated with *E. coli* biomolecules was largely due to stimulation of TLR4 through LPS binding. We found that the presence of *E. coli* biomolecules induced increased transcription of glycolytic enzymes as well as proteins that promote epithelial-to-mesenchymal transition (EMT). While we did observe an increase in glycolysis and invasive potential, our data suggests that *E. coli* induces this phenotype in a TLR4-independent manner. However, from treating our *E. coli* supplemented with RNase, charcoal, and dialysis, we witnessed changes in HKII, cJUN, and claudin expression in LUAD cell lines.

Methods and Materials

Cell Culture

Human LUAD cell lines (A549, H2009, and PC9) were obtained from American Type Culture Collection (ATCC, Manassas, VA, USA). Cells were maintained in RPMI-1640 (Gibco-ThermoFisher, Waltham, MA, USA), supplemented with 10% FBS, and grown at 37 degrees in a humidified 5% CO₂ incubator. For our bacterially supplemented media, *E. coli* were grown in 2mL lysogeny broth (LB) media for 24 hours on a shaker at 37°C. Afterwards, *E. coli* were added to RPMI-1640 supplemented with 10% FBS and 1% L-glutamine at a final OD of 0.1 and allowed to grow overnight. Following incubation, *E. coli* cells were removed from the media by centrifugation (12,000 x g for 10 minutes) and filter sterilization (0.2μ). For inhibition of TLR4, cells were incubated in C34 (MedChemExpress, NJ, USA) at a final concentration of 5μM for 2 days.

Bacterially supplemented media was treated in 4 separate manners: filtered dialysis, charcoal stripping, RNase supplementation, and heat-shock. 14mL of bacterially supplemented media was filter dialyzed using Ultracel®-3K (Amicon, Burlington, MA, USA) at a centrifugal force of 4000 x g for 1 hour. Charcoal stripping was performed by 0.28g of Dextran Coated Charcoal (Sigma Aldrich, Burlington, MA, USA) into 14mL of bacterially supplemented media and incubated rocking overnight at 4°C. Media was then centrifuged at 2000 x g for 15 minutes to remove charcoal. Bacterially supplemented media was also treated with RNaseA at a final concentration of 100μg/mL prior to administration to LUAD cells.

Radiolabeling of cell lines

For determining whether a crosstalk exists between bacteria and cancer cells, we utilized ^{14}C uniformly labeled glucose. Cells, either bacterial or LUAD, were grown in RPMI media supplemented with $0.1\mu\text{Ci/mL}$ glucose for 24 hours for bacteria and 72 hours for LUAD. Cells were collected and washed with PBS before being placed in unlabeled RPMI for an additional 24 hours. The new labeled RPMI was centrifuged, followed by filter sterilization before being used. Cell lines were grown in newly labeled RPMI media before being collected, washed, and lysed with RPMI containing 0.1% SDS.

RNA Sequencing

Human LUAD cell lines, A549 and H2009, were incubated in bacterially supplemented RPMI-1640 media for 48 hours. Following incubation, RNA was isolated from LUAD cells using EZNA Total RNA Kit (Omega, Norcross, GA, USA). RNA sample integrity and concentration were determined by Agilent 2100 Bioanalyzer (Agilent Technologies, Santa Clara, CA). Libraries were prepared from $1\mu\text{g}$ RNA using the Universal Plus mRNA-Seq with NuQuant® (Tecan, Switzerland), and Universal Plus UDI S02622 were used to barcode the libraries. Size, purity, and quantitation of libraries was performed using the Agilent Bioanalyzer (Agilent Technologies, Santa Clara, CA). Libraries were quantified by Qubit dsDNA HS kit (ThermoFisher, Q33231) and size analysis done with the HS NGS Fragment Kit (Agilent, DNF-474-0500) on the Agilent Fragment Analyzer. Libraries were diluted to 2nM with Illumina Resuspension Buffer (RSB), equivolume pooled, then further diluted to 750pM with Resuspension buffer with Tween. PhiX positive control was spiked in to a final of 2%. Denaturation and final dilution was done onboard instrument and libraries sequenced on a P2 100 cycle kit (Illumina, 20046811)

with 101 sequencing cycles and 2 index reads of 8bp each on the NextSeq 2000 instrument. FASTQ generation was performed with BaseSpace DRAGEN analysis version 1.2.1. Raw sequencing files were downloaded from Illumina's BaseSpace onto the KBRIN server for analysis. Sequences were directly aligned to the *Mus musculus* reference genomes assembly (mm39.fa) using STAR (version 2.6) [137] to generate alignment files in bam format. Differential expression analysis was performed using two tools, Cuffdiff2 [138] and DESeq2 [139]. For the Cuffdiff2 analysis, Cuffnorm was used to produce FPKM (Fragments Per Kilobase Million) normalized counts. The counts were then filtered to include only genes with minimum expression of one FPKM in three or more samples and an average expression of at least one FPKM. For the DESeq2 analysis, raw read counts were obtained from the STAR aligned bam format files using HTSeq version 0.10.0 [140]. The raw counts were normalized using the Relative Log Expression (RLE) method and then filtered to exclude genes with fewer than 10 counts across the samples.

Lactate Levels

For LUAD cell lines, cells were incubated in RPMI-1640 media, bacterially supplemented media, or bacterially supplemented media with C34 inhibitor for 48 hours. 100µL of media was collected from LUAD plates and diluted 1:1000 with 1x PBS. Lactate measurement in diluted media was analyzed using Lactate Glo Assay (Promega, Madison, WI, USA) and luminescence was measured using SpectraMax iD3 (Molecular Devices, San Jose, CA, USA). Luminescence recorded was then normalized by cell count. For measuring lactate levels following bacterial addition, LUAD cell lines were

incubated in RPMI-1640 without addition of penicillin/streptomycin for 48 hours. The resulting media was collected, and bacteria was added to an OD of 0.1. Bacteria were incubated on a rocker for 24 hours at 36°C. Media was then collected, centrifuged at 12,000 x g for 10 minutes, and filter sterilized with 0.2 µ filter. Resulting media was diluted 1:1000 with 1x PBS and measured using the Lactate Glo Assay.

Deoxyglucose measurement

LUAD cells were incubated in 6-well dish with RPMI-1640 or bacterially supplemented media. 2 µCi/ml of ¹⁴C-2-deoxyglucose (PerkinElmer, Waltham, MA, US) was added to LUAD cell lines and incubated for 1 hour. LUAD cells were harvested, washed with 1x PBS, and lysed with 1% SDS in RPMI-1640. Radioactivity of the cell lysate was measured by scintillation counter, with counts per minute being normalized based on BCA protein concentration.

Wound Healing Assay

LUAD cell lines were incubated in 6-well dish at a confluency of 2x10⁶ overnight. Wound was created using a pipette tip and layered with 200µL Matrigel (Corning, Glendale, AZ, USA) at a final concentration of 8mg/mL infused either with RPMI-1640 or bacterially supplemented media. LUAD cells were then incubated in RPMI-1640 media for 72 hours and cellular motility was captured every 24-hours. Wound closure was determined by ImageJ, normalizing percentage wound closure by wound area at 0-hours.

Migration and Invasion Assay

8µm pore size transwell inserts (Corning, Glendale, AZ, USA) were for measuring LUAD invasive potential. Inserts were hydrolyzed with ice cold 1x PBS, 200µL of Matrigel at a final concentration of 8mg/mL was layered atop the membrane and incubated at 37°C incubator for 1 hour. LUAD cells were then seeded in the top chamber at a density of 5×10^4 in either serum-starved RPMI-1640 media, serum-starved bacterially supplemented media, or serum-starved bacterially supplemented media with C34 inhibitor. The bottom chamber contained RPMI-1640 supplemented with 10% FBS. Cells were incubated for 48 hours and then fixed with ice cold 100% methanol, followed by the removal of non-invasive cells. Cells were then stained using Hema 3 (Fisher Scientific, Hampton, NH, USA), captured using BZX-800 Keyence microscope (Keyence, Osaka, Japan), and analyzed using BZX-800 analyzer.

Immunoblotting

Whole cell lysate was performed using 1x CHAPS buffer containing protease and phosphatase inhibitors. 30µg of lysates were ran on a NuPAGE 4 to 12% Bis-Tris PAGE gel and transferred to PVDF membrane. Membranes were blocked overnight with 5% milk in TBS-T and probed with anti- ZO1 (1:5000), E-cadherin (1:5000), Claudin-1 (1:5000), SNAI1 (1:5000), cJUN (1:5000), Hexokinase I (1:5000), Hexokinase II (1:5000), Lactate Dehydrogenase A (1:5000), and Pyruvate Kinase M2 isoform (1:5000) antibody overnight at 4°C. All antibodies were procured from Cell Signaling Technology at Danvers, MA, USA. Membranes were then washed and incubated with HRP-conjugated anti-rabbit (1:10000) secondary antibody for one hour. ECL

chemiluminescent reagent (Thermo Fisher) was used to detect protein levels. Membranes were also probed with anti-GAPDH (Cell Signaling Technology, Danvers, MA, USA) as a loading control.

Real Time PCR

Total RNA was isolated from cell pellets using E.Z.N.A Total RNA Kit I (OMEGA) according to the manufacture's protocol. 1µg isolated RNA was converted to cDNA using High-Capacity RNA-to-cDNA kit (Applied Biosystems). Gene expression was determined by qPCR using SYBR green and the following primers: IL1β Forward: GGCATCCAGCTACGAATCTC, IL1β Reverse: TCGTTATCCCATGTGTCGAA, cJUN Forward: AACGACCTTCTATGACGATGCCCTC, cJUN Reverse: GCGAACCCCTCCTGCTCATCTCTC, GAPDH Forward: GTCTCCTCTGACTTCAACAGCG, and GAPDH Reverse: ACCACCCTGTTGCTGTAGCCAA was used as our housekeeping genes. Fold change was normalized to our 50µM methionine control and transformed to log base 2 to delineate statistical significance.

Statistical analysis

All statistical analysis was performed using GraphPad Prism. Data are reported as average ±SEM, wherein p-values, statistical tests, and replicates are described in respective figures.

Results

E. coli supplementation can rescue LUAD proliferation under methionine restriction.

As mentioned previously, bacteria have a dedicated pathway that is responsible for the *de novo* synthesis of methionine. Prior work from the lab had shown that the methionine synthesis pathway was upregulated and methionine metabolism was downregulated in bacteria isolated from tumors in human patients [90], I sought to investigate the potential of bacteria acting as a methionine reservoir for LUAD. To that end, I performed a clonogenic assay. Briefly, LUAD cell lines were incubated in 2 μ M methionine for 7 days. Following this 7-day incubation, one group (Bacteria) was placed in media containing 1:1 of 2 μ M methionine media and 2 μ M methionine media that was previously used to grow *E. coli*. To account for the possibility that the nutrients in the *E. coli* grown media was completely replenished, my control (Vehicle) was placed in media containing 1:1 of 2 μ M methionine media and 1x PBS. Cells were incubated for the remaining 3 days and stained with Coomassie (Figure 18A). My results show an increase in colony staining for LUAD cells grown with bacteria (Figure 18B). This data would suggest that the *E. coli* are able to rescue LUAD proliferation following 2 μ M methionine incubation. As I observed bacteria could rescue the proliferation of our LUAD cells under methionine restriction, I next sought to investigate signaling pathways that could be affected by the administration of bacterial biomolecules. ERK activation is associated with higher proliferation and the pathway leading to ERK's hyperactivation is implicated with more aggressive LUAD phenotypes [141]. Activation of tyrosine kinase receptors, such as Epidermal Growth Factor Receptor (EGFR), leads to a cascade of signaling that leads to the phosphorylation of ERK1/2, which facilitates in cellular proliferation and

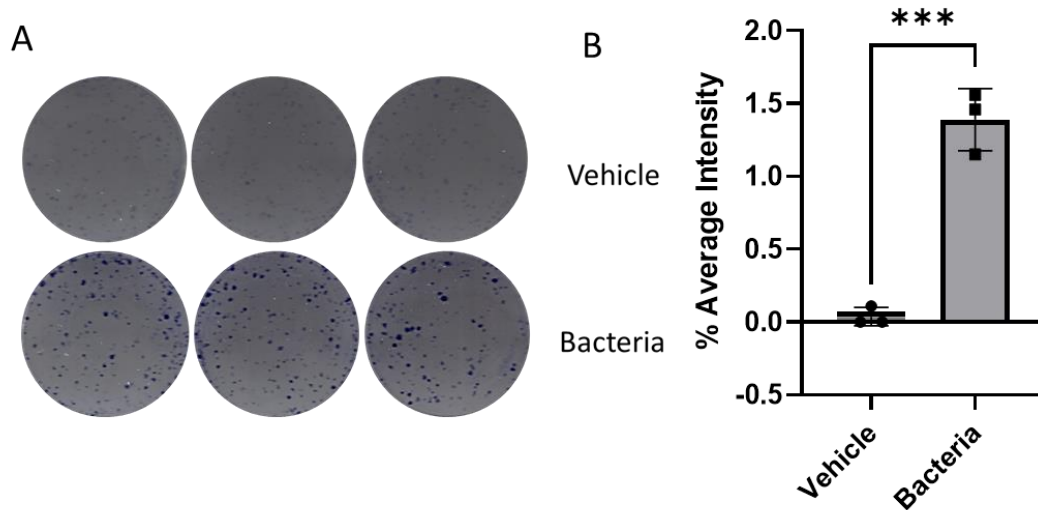


Figure 18. *E. coli* synthesized methionine can rescue cancer phenotypes.

A) Clonogenic assay of cells in 2 μ M methionine media in the presence or absence of bacteria. B) Average intensity of colony staining gathered from ImageJ plugin, ColonyArea, and normalized to vehicle control. Data were analyzed using a student's t-test, *** p-value < 0.0002.

survival. Additionally, the receptor can also lead to activation of AKT that activates mTOR, which is also responsible for cellular survival. Interestingly, previous research has shown the ERK1/2 pathway and the AKT pathway can cross-inhibit one another [142].

I chose to investigate the effects of *E. coli* biomolecule supplementation under methionine restriction on mTOR, ERK1/2, and AKT activation. For this, I incubated our LUAD cells in either RPMI-1640 media containing 50 μ M methionine with PBS supplementation, 2 μ M methionine with PBS supplementation, and 2 μ M methionine with *E. coli* biomolecule supplementation. Interestingly, my data showed LUAD cell lines grown in methionine restriction had elevated levels of phosphorylated AKT (Figure 19A-B). Not only did *E. coli* biomolecule supplemented media diminish the activation of AKT, but we see a dramatic increase in ERK1/2 activation (p-p44/42) (Figure 19C). By densitometry, I saw no significant difference in the downstream mediator mTOR phosphorylation (Figure 19 D-E). However, I did see a dramatic decrease in cleaved caspase 3 in *E. coli* biomolecule supplemented media (Figure 19F). My data suggest that *E. coli* biomolecules are leading to the activation of ERK1/2 signaling, which may be protecting cancers from stress that would lead to apoptosis.

Crosstalk between LUAD and E. coli

With the impact of *E. coli* biomolecule supplementation on LUAD signaling and proliferation, I next asked if LUAD cell lines were taking up the biomolecules. I decided to use C¹⁴-glucose to radiolabel my *E. coli* cells. In this manner, I can confidently determine whether LUAD take up *E. coli* biomolecules, as they should be the only source of radiolabeling.

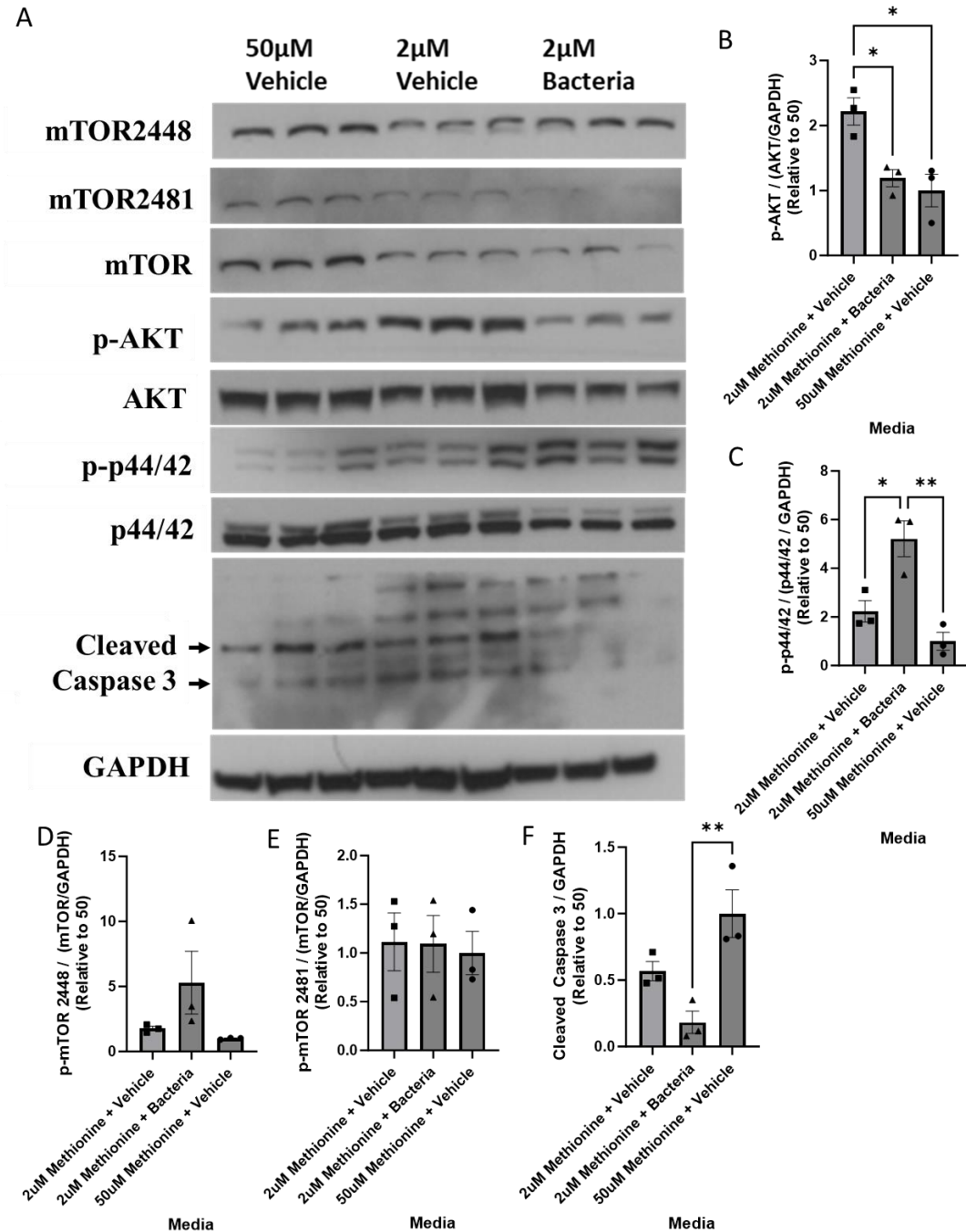


Figure 19. Altered signaling in LUAD in the presence of bacteria.

A) Western blot analysis of A549 in 50μM methionine, 2μM methionine, or 2μM methionine with bacterially supplementation. B) Densitometry analysis of p-mTOR 2448, C) p-mTOR 2481, D) p-AKT, E) p-p44/42 and F) cleaved caspase 3. Total mTOR, AKT,

and p44/42 were normalized to GAPDH. Normalized total proteins were then used to normalize their phosphorylated versions. Data were analyzed using one-way ANOVA with Tukey test, * p-value < 0.0332, ** p-value < 0.0021.

In this study, I inoculated *E. coli* with RPMI-1640 containing 0.1 μ Ci/mL of uniformly labeled ^{14}C -glucose for 24 hours. I then isolated the media excreted from the labeled bacteria and incubated our LUAD cells in the newly acquired *E. coli* supplemented media for either 1, 6, or 24 hours. The LUAD cell lines were then washed and measured by scintillation counter (Figure 20A). My findings showed a time-dependent increase in labeling for A549 (Figure 20B) and H2009 (Figure 20C), suggesting that the *E. coli* biomolecules were being taken up by LUAD cell lines. Because my earlier studies showed the importance of methionine, I next investigated how disruption of the methionine synthesis pathway in *E. coli* would impact the labeling of LUAD cells. For this, I used our WT and metA mutant *E. coli* taken from the Keio collections and incubated them in RPMI-1640 containing 2 μ M methionine. The media was then filter sterilized and administered to LUAD cell lines for 24 hours. These results show less labeling in the LUAD cell lines given biomolecules from metA mutant *E. coli* than LUAD cell lines given biomolecules from WT *E. coli* (Figure 20D-E).

As I saw *E. coli* were able to label LUAD cell lines, I next investigated whether LUAD cell lines could also label *E. coli*. To do this, I performed a similar study by radiolabeling LUAD cell lines with ^{14}C -glucose for 72 hours to allow for complete incorporation of labeled carbon. LUAD cell lines were then placed in unlabeled RPMI-1640 for 24 hours, after which the media was taken, and filter sterilized. The resulting filter sterilized LUAD was then used to grow *E. coli* for 24 hours before reading ionization events on the scintillation counter (Figure 21A). From our scintillation count, we see a significant increase in *E. coli* radiolabeling using media from both LUAD cell lines (Figure 21B), suggesting a crosstalk between the *E. coli* and LUAD.

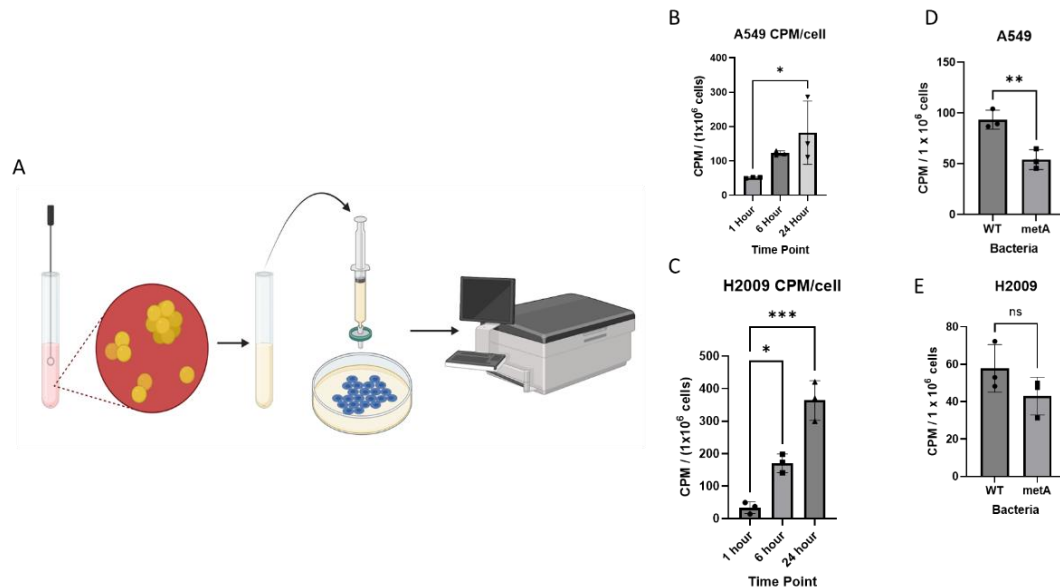


Figure 20. LUAD can take up *E. coli* biomolecules.

A) Schematic for radiolabeling LUAD cell lines with bacterial metabolites. Uniformly labeled ^{14}C -Glucose was used to label bacterial cells. B) Scintillation counter CPM for A549 cells incubated in either no bacterially labeled supplemented media (Cold) or bacterially labeled supplemented media after 1, 6, and 24 hours. Data were normalized based on cell count. C) Scintillation counter CPM for H2009 cells incubated with bacterially labeled supplemented media for 1, 6, and 24 hours. Data were normalized based on cell count. Data were analyzed using one-way ANOVA with Dunnet test, * p-value < 0.0332, *** p-value < 0.0002 D) Scintillation counter CPM for A549 cells and E) H2009 cells incubated with filter sterilized medium from *E. coli* WT vs metA mutant. Data were analyzed using unpaired t-test, ** p-value < 0.0021.

E. coli biomolecules elicit a number of transcriptomic changes in LUAD cell lines

I have previously shown that multiple LUAD cell lines and *E. coli* cells can label one another through secreted biomolecules. I have also shown the proliferation of LUAD cell lines under low nutritional environment conditions is rescued upon administering bacterially supplemented media (Figure 9A-D). To gain a better understanding of the impact of *E. coli* biomolecules, I performed RNA sequencing on A549 and H2009 cell lines (Figure 22A). To identify Differentially Expressed Genes (DEG), gene expression in LUAD cell lines in RPMI-1640 media vs *E. coli* supplemented media were compared using DESeq2 [139]. Interestingly, analyzing the RNA-seq data using a KEGG pathway uncovered both glycolysis/gluconeogenesis and the Hippo pathway as upregulated in both cell lines following treatment with *E. coli* biomolecule supplementation (Figure 22B-C).

I focused my attention on genes expressed similarly in both cell lines, of which over 900 genes were recorded, and concentrated on those regarding the pathways mentioned above (Figure 23A). Regarding glycolysis/gluconeogenesis, addition of *E. coli* biomolecules led to increases in Hexokinase I (HKI), Hexokinase II (HKII), Lactate Dehydrogenase (LDHA), Pyruvate Kinase M isoform (PKM), 6-phosphofructo-2-kinase/fructose-2,6-biphosphatase 3 and 4 (PFKFB3/4), Aldolase (ALDOA and ALDOC), Phosphoglycerate kinase 1 (PGK1), Phosphoglycerate mutase 1 (PGAM1), and Enolase 2 (ENO2). Furthermore, PFKFB3/4 was observed to be within the top 10 upregulated DEGs in A549 cells and within the top 20 upregulated DEGs in H2009 cells (Table 2-3). Both HKII and PKM are irreversible steps that are only found in glycolysis and not in gluconeogenesis. Meanwhile, I was unable to identify enzymes that were

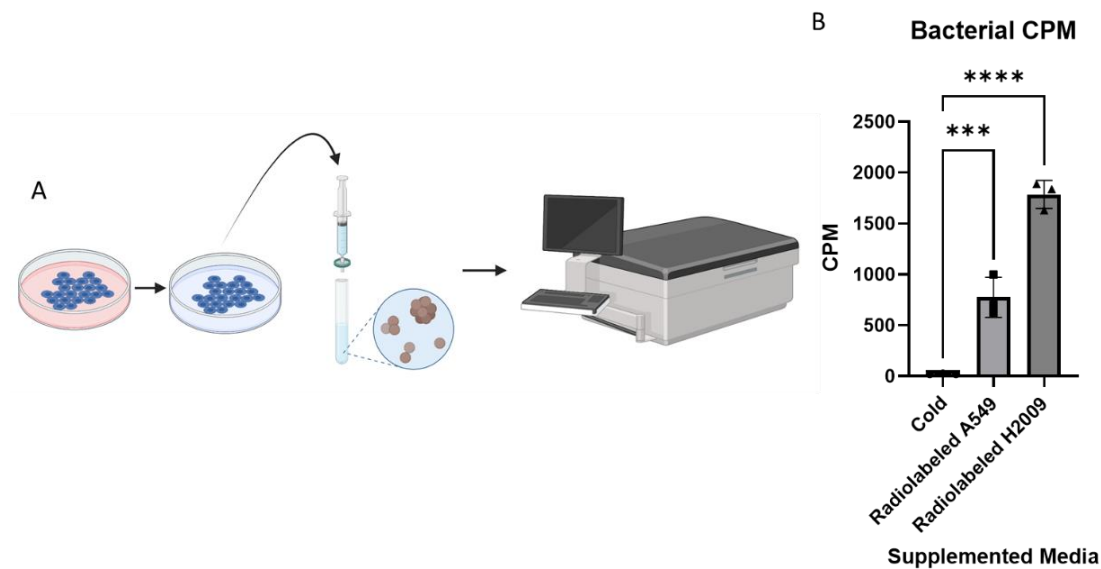


Figure 21. *E. coli* can take up LUAD biomolecules.

A) Schematic for radiolabeling bacteria with LUAD metabolites. Uniformly labeled ^{14}C -glucose was used to label LUAD cell lines. B) Scintillation counter CPM for bacteria following 24 hours of incubation in LUAD supplemented media, with cold being LUAD unlabeled supplemented media. Data were analyzed using a one-way ANOVA with Dunnet test, *** p-value < 0.0002, **** p-value < 0.0001.

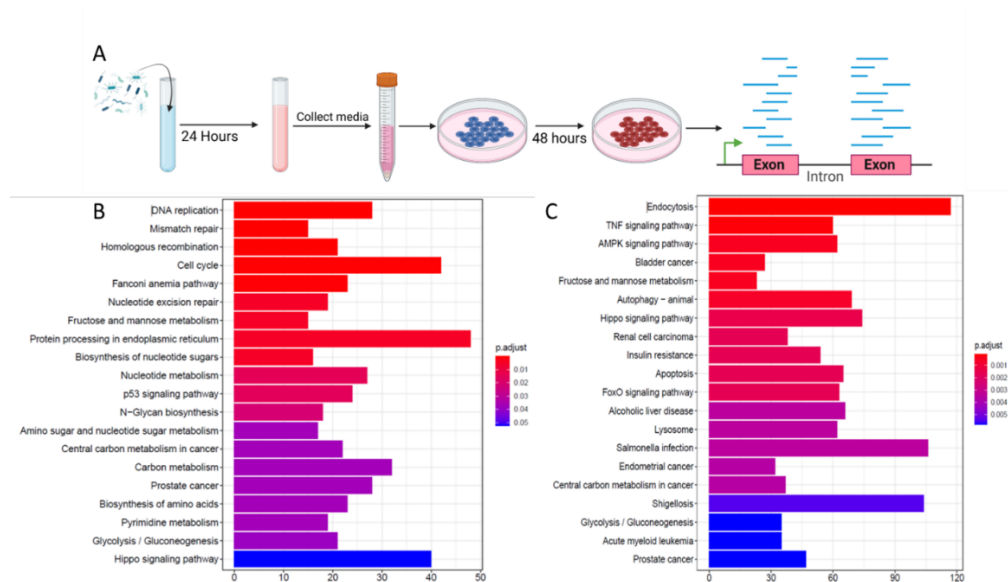


Figure 22. KEGG analysis reveals multiple pathways impacted by *E. coli* biomolecules in LUAD.

A) Pipeline for analysis of RNA-seq taken from lung adenocarcinoma cell lines after *E. coli* biomolecule treatment. B) Top 20 KEGG pathways enriched under the presence of *E. coli* supplementation for A549 and C) H2009 cells. Adjusted p-values for each comparison included in the figure key.

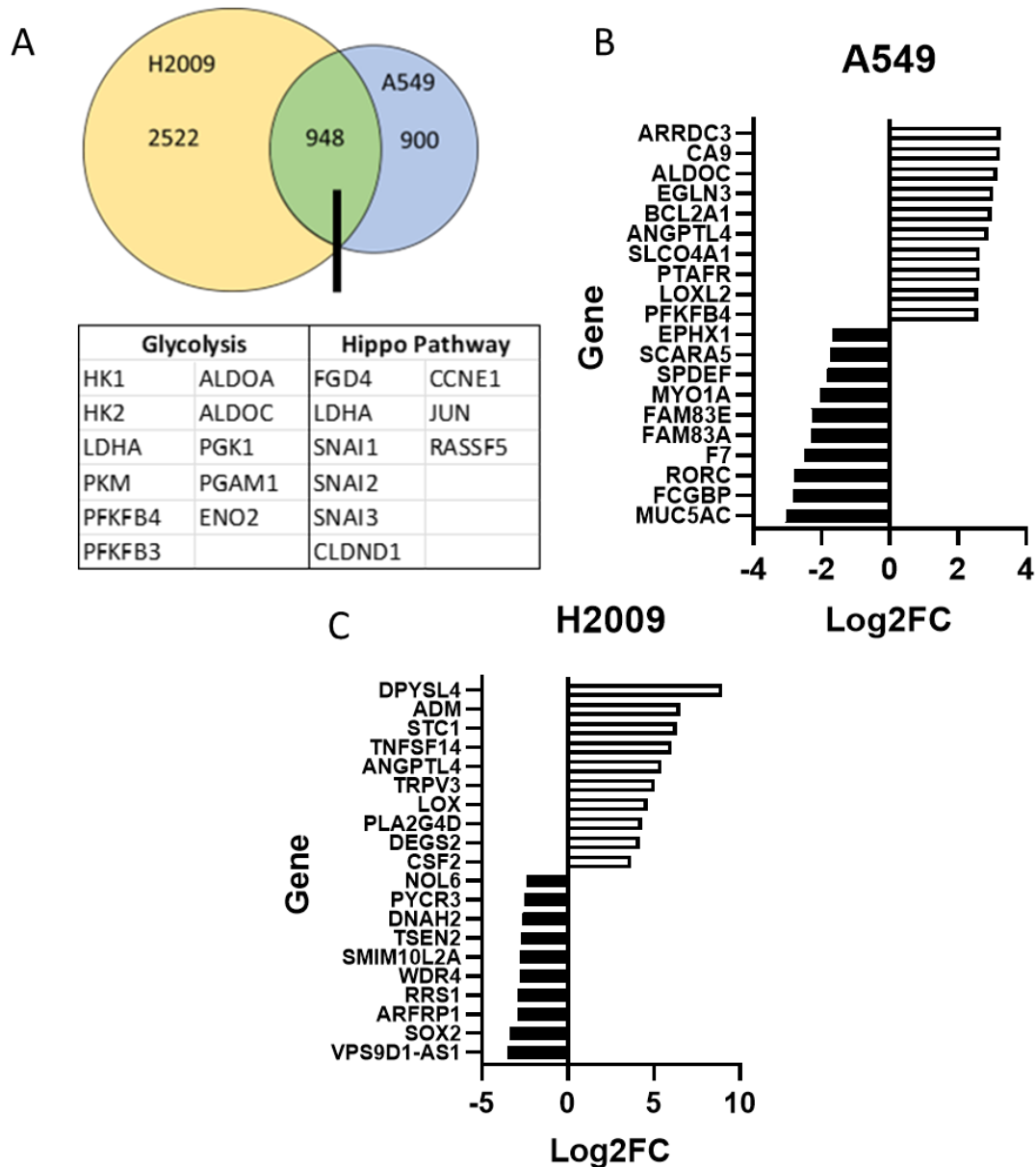


Figure 23. Differentially expressed genes of LUAD incubated in *E. coli* biomolecules.

A) Venn diagram representing the unique and shared LUAD genes upregulated under *E. coli* supplementation. Genes related to Glycolysis and the Hippo pathway have been placed in a table below the venn diagram. B) Top 10 upregulated and downregulated LUAD genes in A549 and C) H2009 cells under *E. coli* supplementation. Transcriptomic data from RNA-seq analysis was filtered by $p\text{-value} < 0.05$ and sorted by $\log_2\text{FC}$.

considered irreversible in gluconeogenesis. As such, I believe that the effects of *E. coli* on LUAD have a direct relationship with glycolysis.

The Hippo Pathway is a conserved signaling pathway that is involved in several cellular processes such as proliferation, metabolism, and cancer development [143]. Previous studies have also linked the Hippo Pathway with EMT in cancer [144]. The shared genes between cell lines involving the Hippo Pathway include FYVE, RhoGEF and PH Domain Containing 4 (FGD4), LDHA, Snail Family Transcriptional Repressor 1, 2, and 3 (SNAIL1/2/3), Claudin Domain Containing 1 (CLDN1), Cyclin E1 (CCNE1), Jun Proto-Oncogene, AP1 Transcription Factor Subunit (JUN), and Ras Association Domain Family Member 5 (RASSF5). Additionally, investigating A549 and H2009 cells independently showed several adhesion associated genes to be downregulated in the presence of *E. coli* biomolecules (Table 4-5). I chose to investigate the effects of these bacterial biomolecules on EMT.

Bacterial biomolecules increase glycolysis in LUAD cell lines.

It is common knowledge that cancer cells upregulate glycolysis and shuttle pyruvate into lactate, even in environments with sufficient oxygen. This phenomenon is termed the Warburg Effect. The reason behind this shift to a less energy efficient metabolic process remains a topic of debate. I performed gene set enrichment analysis (GSEA) on the RNA-seq data and observed similar results indicating that LUAD cell lines incubated in bacterially supplemented media had enriched genes associated with glycolysis (Figure 24A). Furthermore, I investigated the protein levels of several enzymes associated with glycolysis: HK1, HK2, PKM2, and LDHA. In this study, I had chosen to incorporate a group that was treated with 0.5µg/mL of LPS. LPS is a

Ensembl ID	Gene Symbol Description	Log ₂ FC	P-value	Q-value
ENSG00000101187	SLCO4A1 solute carrier organic anion transporter family member 4A1 [Source:HGNC Symbol;Acc:HGNC:10953]	2.651	4.998e-82	9.042e-78
ENSG00000059804	SLC2A3 solute carrier family 2 member 3 [Source:HGNC Symbol;Acc:HGNC:11007]	2.474	1.104e-78	9.986e-75
ENSG00000170525	PFKFB3 6-phosphofructo-2-kinase/fructose-2,6-biphosphatase 3 [Source:HGNC Symbol;Acc:HGNC:8874]	2.390	8.299e-77	5.004e-73
ENSG00000134013	LOXL2 lysyl oxidase like 2 [Source:HGNC Symbol;Acc:HGNC:6666]	2.609	6.027e-74	2.726e-70
ENSG00000109107	ALDOC aldolase, fructose-bisphosphate C [Source:HGNC Symbol;Acc:HGNC:418]	3.166	1.369e-71	4.954e-68
ENSG00000167772	ANGPTL4 angiopoietin like 4 [Source:HGNC Symbol;Acc:HGNC:16039]	2.902	1.107e-67	3.338e-64
ENSG00000171314	PGAM1 phosphoglycerate mutase 1 [Source:HGNC Symbol;Acc:HGNC:8888]	1.793	1.554e-62	4.016e-59
ENSG00000114268	PFKFB4 6-phosphofructo-2-kinase/fructose-2,6-biphosphatase 4 [Source:HGNC Symbol;Acc:HGNC:8875]	2.590	8.299e-51	1.601e-47
ENSG00000169403	PTAFR platelet activating factor receptor [Source:HGNC Symbol;Acc:HGNC:9582]	2.643	8.853e-51	1.601e-47
ENSG00000131668	BARX1 BARX homeobox 1 [Source:HGNC Symbol;Acc:HGNC:955]	2.419	3.631e-50	5.972e-47
ENSG00000107159	CA9 carbonic anhydrase 9 [Source:HGNC Symbol;Acc:HGNC:1383]	3.240	5.656e-50	8.526e-47
ENSG00000079308	TNS1 tensin 1 [Source:HGNC Symbol;Acc:HGNC:11973]	2.343	1.771e-41	2.465e-38
ENSG00000134333	LDHA lactate dehydrogenase A [Source:HGNC Symbol;Acc:HGNC:6535]	1.465	4.782e-41	6.179e-38
ENSG00000117525	F3 coagulation factor III, tissue factor [Source:HGNC Symbol;Acc:HGNC:3541]	2.191	1.575e-39	1.781e-36
ENSG00000113369	ARRDC3 arrestin domain containing 3 [Source:HGNC Symbol;Acc:HGNC:29263]	3.264	9.760e-39	9.808e-36
ENSG00000129521	EGLN3 egl-9 family hypoxia inducible factor 3 [Source:HGNC Symbol;Acc:HGNC:14661]	3.044	1.837e-38	1.749e-35
ENSG00000140379	BCL2A1 BCL2 related protein A1 [Source:HGNC Symbol;Acc:HGNC:991]	2.992	2.499e-38	2.261e-35
ENSG00000118503	TNFAIP3 TNF alpha induced protein 3 [Source:HGNC Symbol;Acc:HGNC:11896]	2.140	8.015e-38	6.904e-35
ENSG00000185033	SEMA4B semaphorin 4B [Source:HGNC Symbol;Acc:HGNC:10730]	1.301	6.359e-36	5.229e-33
ENSG00000188042	ARL4C ADP ribosylation factor like GTPase 4C [Source:HGNC Symbol;Acc:HGNC:698]	1.612	2.253e-32	1.772e-29

Table 2. Top 20 upregulated genes in A549 incubated in *E. coli* biomolecules

$p \leq 0.05$; $q \leq 0.05$; $|\log_2FC| \geq 0$; counts ≥ 10 across samples).

Ensembl ID	Gene Symbol Description	Log ₂ FC	P-value	Q-value
ENSG00000167772	ANGPTL4 angiopoietin like 4 [Source:HGNC Symbol;Acc:HGNC:16039]	5.437	6.415e-223	1.300e-218
ENSG00000112033	PPARD peroxisome proliferator activated receptor delta [Source:HGNC Symbol;Acc:HGNC:9235]	2.539	9.653e-167	9.782e-163
ENSG00000159167	STC1 stanniocalcin 1 [Source:HGNC Symbol;Acc:HGNC:11373]	6.322	1.172e-117	7.917e-114
ENSG00000125735	TNFSF14 TNF superfamily member 14 [Source:HGNC Symbol;Acc:HGNC:11930]	6.061	4.290e-107	1.739e-103
ENSG00000197461	PDGFA platelet derived growth factor subunit A [Source:HGNC Symbol;Acc:HGNC:8799]	3.312	7.178e-101	2.424e-97
ENSG00000079385	CEACAM1 carcinoembryonic antigen related cell adhesion molecule 1 [Source:HGNC Symbol;Acc:HGNC:1814]	2.317	5.279e-96	1.528e-92
ENSG00000114268	PFKFB4 6-phosphofructo-2-kinase/fructose-2,6-biphosphatase 4 [Source:HGNC Symbol;Acc:HGNC:8875]	3.233	2.269e-90	5.748e-87
ENSG00000168350	DEGS2 delta 4-desaturase, sphingolipid 2 [Source:HGNC Symbol;Acc:HGNC:20113]	4.161	8.615e-88	1.939e-84
ENSG00000153531	ADPRHL1 ADP-ribosylhydrolase like 1 [Source:HGNC Symbol;Acc:HGNC:21303]	2.525	2.336e-86	4.735e-83
ENSG00000143369	ECM1 extracellular matrix protein 1 [Source:HGNC Symbol;Acc:HGNC:3153]	3.501	1.732e-81	3.191e-78
ENSG00000159337	PLA2G4D phospholipase A2 group IVD [Source:HGNC Symbol;Acc:HGNC:30038]	4.290	2.622e-81	4.428e-78
ENSG00000113083	LOX lysyl oxidase [Source:HGNC Symbol;Acc:HGNC:6664]	4.624	2.987e-81	4.657e-78
ENSG00000151640	DPYSL4 dihydropyrimidinase like 4 [Source:HGNC Symbol;Acc:HGNC:3016]	8.973	3.258e-81	4.716e-78
ENSG00000072682	P4HA2 prolyl 4-hydroxylase subunit alpha 2 [Source:HGNC Symbol;Acc:HGNC:8547]	2.886	2.053e-80	2.774e-77
ENSG00000187193	MT1X metallothionein 1X [Source:HGNC Symbol;Acc:HGNC:7405]	3.003	2.223e-76	2.650e-73
ENSG00000148926	ADM adrenomedullin [Source:HGNC Symbol;Acc:HGNC:259]	6.527	9.578e-76	1.078e-72
ENSG00000143816	WNT9A Wnt family member 9A [Source:HGNC Symbol;Acc:HGNC:12778]	2.616	1.804e-74	1.924e-71
ENSG00000167971	CASKIN1 CASK interacting protein 1 [Source:HGNC Symbol;Acc:HGNC:20879]	3.258	1.066e-73	1.080e-70
ENSG00000164400	CSF2 colony stimulating factor 2 [Source:HGNC Symbol;Acc:HGNC:2434]	3.689	1.380e-73	1.332e-70
ENSG00000167723	TRPV3 transient receptor potential cation channel subfamily V member 3 [Source:HGNC Symbol;Acc:HGNC:18084]	5.034	8.156e-73	7.513e-70

Table 3. Top 20 genes upregulated in H2009 incubated in *E. coli* biomolecules

p≤0.05; q≤0.05; |log₂FC|≥0; counts ≥ 10 across samples).

Ensembl ID	Gene Symbol Description	Log ₂ FC	P-value	Q-value
ENSG00000022567	SLC45A4 solute carrier family 45 member 4 [Source:HGNC Symbol;Acc:HGNC:29196]	-1.448	1.473e-58	3.332e-55
ENSG000000215182	MUC5AC mucin 5AC, oligomeric mucus/gel-forming [Source:HGNC Symbol;Acc:HGNC:7515]	-3.047	3.830e-40	4.619e-37
ENSG000000147689	FAM83A family with sequence similarity 83 member A [Source:HGNC Symbol;Acc:HGNC:28210]	-2.291	1.857e-39	1.976e-36
ENSG00000054277	OPN3 opsin 3 [Source:HGNC Symbol;Acc:HGNC:14007]	-1.219	6.130e-32	4.620e-29
ENSG00000057593	F7 coagulation factor VII [Source:HGNC Symbol;Acc:HGNC:3544]	-2.502	2.094e-31	1.515e-28
ENSG000000143819	EPHX1 epoxide hydrolase 1 [Source:HGNC Symbol;Acc:HGNC:3401]	-1.689	4.660e-31	3.242e-28
ENSG000000168079	SCARA5 scavenger receptor class A member 5 [Source:HGNC Symbol;Acc:HGNC:28701]	-1.745	1.052e-27	5.949e-25
ENSG000000105523	FAM83E family with sequence similarity 83 member E [Source:HGNC Symbol;Acc:HGNC:25972]	-2.281	4.108e-26	1.955e-23
ENSG000000109501	WFS1 wolframin ER transmembrane glycoprotein [Source:HGNC Symbol;Acc:HGNC:12762]	-0.915	7.746e-26	3.503e-23
ENSG000000166866	MYO1A myosin IA [Source:HGNC Symbol;Acc:HGNC:7595]	-2.047	9.487e-26	4.086e-23
ENSG000000182704	TSKU tsukushi, small leucine rich proteoglycan [Source:HGNC Symbol;Acc:HGNC:28850]	-0.986	7.968e-25	3.133e-22
ENSG000000198074	AKR1B10 aldo-keto reductase family 1 member B10 [Source:HGNC Symbol;Acc:HGNC:382]	-1.547	7.234e-24	2.617e-21
ENSG000000275395	FCGBP Fc fragment of IgG binding protein [Source:HGNC Symbol;Acc:HGNC:13572]	-2.842	6.958e-23	2.331e-20
ENSG000000116761	CTH cystathionine gamma-lyase [Source:HGNC Symbol;Acc:HGNC:2501]	-1.345	8.669e-23	2.851e-20
ENSG000000275993	SIK1B salt inducible kinase 1B (putative) [Source:HGNC Symbol;Acc:HGNC:52389]	-0.948	1.617e-21	4.433e-19
ENSG000000143365	RORC RAR related orphan receptor C [Source:HGNC Symbol;Acc:HGNC:10260]	-2.800	7.501e-21	1.995e-18
ENSG000000227471	AKR1B15 aldo-keto reductase family 1 member B15 [Source:HGNC Symbol;Acc:HGNC:37281]	-1.610	9.318e-21	2.443e-18
ENSG000000171903	CYP4F11 cytochrome P450 family 4 subfamily F member 11 [Source:HGNC Symbol;Acc:HGNC:13265]	-1.137	1.619e-20	4.012e-18
ENSG000000141376	BCAS3 BCAS3, microtubule associated cell migration factor [Source:HGNC Symbol;Acc:HGNC:14347]	-1.113	2.586e-20	6.238e-18
ENSG000000124664	SPDEF SAM pointed domain containing ETS transcription factor [Source:HGNC Symbol;Acc:HGNC:17257]	-1.822	4.417e-19	9.989e-17

Table 4. Top 20 downregulated genes in A549 incubated in *E. coli* biomolecules
p≤0.05; q≤0.05; |log₂FC|≥0; counts ≥ 10 across samples).

Ensembl ID	Gene Symbol Description	Log ₂ FC	P-value	Q-value
ENSG00000165271	NOL6 nucleolar protein 6 [Source:HGNC Symbol;Acc:HGNC:19910]	-2.405	1.035e-112	5.244e-109
ENSG00000132382	MYBBP1A MYB binding protein 1a [Source:HGNC Symbol;Acc:HGNC:7546]	-1.985	3.115e-77	3.946e-74
ENSG00000261373	VPS9D1-AS1 VPS9D1 antisense RNA 1 [Source:HGNC Symbol;Acc:HGNC:48915]	-3.506	1.127e-71	9.519e-69
ENSG00000160193	WDR4 WDR4 WD repeat domain 4 [Source:HGNC Symbol;Acc:HGNC:12756]	-2.784	2.115e-70	1.588e-67
ENSG00000179051	RCC2 regulator of chromosome condensation 2 [Source:HGNC Symbol;Acc:HGNC:30297]	-1.216	2.201e-64	1.274e-61
ENSG00000184678	HIST2H2BE histone cluster 2 H2B family member e [Source:HGNC Symbol;Acc:HGNC:4760]	-2.167	4.194e-60	2.023e-57
ENSG00000179041	RRS1 ribosome biogenesis regulator homolog [Source:HGNC Symbol;Acc:HGNC:17083]	-2.903	5.385e-58	2.372e-55
ENSG00000183914	DNAH2 dynein axonemal heavy chain 2 [Source:HGNC Symbol;Acc:HGNC:2948]	-2.626	7.063e-58	2.982e-55
ENSG00000108963	DPH1 diphthamide biosynthesis 1 [Source:HGNC Symbol;Acc:HGNC:3003]	-2.171	3.985e-57	1.615e-54
ENSG00000181449	SOX2 SRY-box 2 [Source:HGNC Symbol;Acc:HGNC:11195]	-3.375	1.343e-55	5.236e-53
ENSG00000162836	ACP6 acid phosphatase 6, lysophosphatidic [Source:HGNC Symbol;Acc:HGNC:29609]	-2.223	1.573e-55	6.017e-53
ENSG00000185215	TNFAIP2 TNF alpha induced protein 2 [Source:HGNC Symbol;Acc:HGNC:11895]	-2.296	4.328e-55	1.624e-52
ENSG00000104524	PYCR3 pyrroline-5-carboxylate reductase 3 [Source:HGNC Symbol;Acc:HGNC:25846]	-2.562	8.199e-54	2.724e-51
ENSG00000178947	SMIM10L2A small integral membrane protein 10 like 2A [Source:HGNC Symbol;Acc:HGNC:34499]	-2.772	1.778e-52	5.721e-50
ENSG00000154743	TSEN2 tRNA splicing endonuclease subunit 2 [Source:HGNC Symbol;Acc:HGNC:28422]	-2.760	3.157e-51	9.410e-49
ENSG00000105289	TJP3 tight junction protein 3 [Source:HGNC Symbol;Acc:HGNC:11829]	-1.289	2.103e-50	5.919e-48
ENSG00000101246	ARFRP1 ADP ribosylation factor related protein 1 [Source:HGNC Symbol;Acc:HGNC:662]	-2.906	4.004e-50	1.082e-47
ENSG00000156521	TYSND1 trypsin domain containing 1 [Source:HGNC Symbol;Acc:HGNC:28531]	-2.077	7.108e-49	1.800e-46
ENSG00000213965	NUDT19 nudix hydrolase 19 [Source:HGNC Symbol;Acc:HGNC:32036]	-1.695	3.188e-48	7.880e-46
ENSG00000103351	CLUAP1 clusterin associated protein 1 [Source:HGNC Symbol;Acc:HGNC:19009]	-2.322	3.659e-48	8.935e-46

Table 5. Top 20 downregulated genes in H2009 incubated in *E. coli* biomolecules ($p \leq 0.05$; $q \leq 0.05$; $|\log_2FC| \geq 0$; counts ≥ 10 across samples).

major constituent of the bacterial cell wall of gram-negative bacteria, such as *E. coli*. Interestingly, my western blot data showed a dramatic increase in HKII expression and not of HK1, PKM2, or LDHA (Figure 24B-F) in *E. coli* supplemented media and not vehicle or LPS administration. It has been shown that incubation with LPS is known to induce cytokines such as interleukin 1 β (IL1 β) [145, 146] and enhanced glycolysis [147]. To test whether the results from my LPS data were due to nonfunctional LPS, I performed qPCR and saw that there was indeed an increase in IL1 β and cJUN mRNA expression in LUAD cell lines incubated with 0.5 μ g/mL LPS (Figure 25A-B).

As the RNA-seq data revealed elevated RNA expression of glycolytic enzymes and my western blot data showed elevation of HKII protein, I next investigated whether bacterial supplementation was enhancing glucose uptake. For this, I incubated LUAD cell lines in either our vehicle control, bacterially supplemented media, or 0.5 μ g/mL of LPS for 16 hours followed by incubating with labeled 2-deoxyglucose for 1 hour and measuring radioactivity by scintillation count. The counts per minute (CPM) were then normalized to protein concentration gathered by BCA. My results show that supplementation of *E. coli* biomolecules, but not LPS, significantly increased glucose uptake in A549 and PC9 (Figure 26A-B). However, due to issues acquiring CPM above background for H2009 and H2030, I was only able to compare vehicle with bacteria. While my H2009 cells showed a similar significance in glucose uptake, H2030s showed no significant change (Figure 26C-D).

As mentioned earlier, cancer cells favor lactate production over shuttling pyruvate into the citric acid cycle. To this end, we investigated whether bacterially secreted biomolecules enhanced lactate production of glycolysis. We chose to investigate lactate

production using a luciferin coupled assay and examined the effects of vehicle, bacterially supplemented media, and the addition of 0.5µg/mL lipopolysaccharides (LPS) on lactate production. Interestingly, we witnessed a dramatic increase in all three of our LUAD cell lines incubated with bacterially supplemented media but no significant increase in LPS administration compared to vehicle (Figure 27A-C). I further investigated the lactate in the *E. coli* supplemented media to determine how much the *E. coli* was contributing to the lactate levels observed. From this data, I validated LUAD as the main source of lactate observed (Figure 27D)

Previous reports have suggested bacteria capable of utilizing the nitrogenous waste byproduct of cancer cells [130]. Additionally, others have shown a direct link between cancer and the bacteria, wherein the azurin synthesized by *P. aeruginosa* was upregulating Aldolase A in breast cancer, which in turn facilitated adherence of *P. aeruginosa* onto breast cancer [127]. I investigated whether lactate produced by LUAD cell lines is also taken up by *E. coli*. Lactate levels found in media previously used to grow LUAD cell lines before and after 24-hour incubation with bacteria were measured using the luciferin coupled lactate assay and witnessed a dramatic decrease in lactate levels (Figure 28). Taken together, these findings would suggest that the bacteria are increase glycolysis in LUAD, resulting in increased production of lactate that is then released into the extracellular matrix, which can then be taken up by the microbiome.

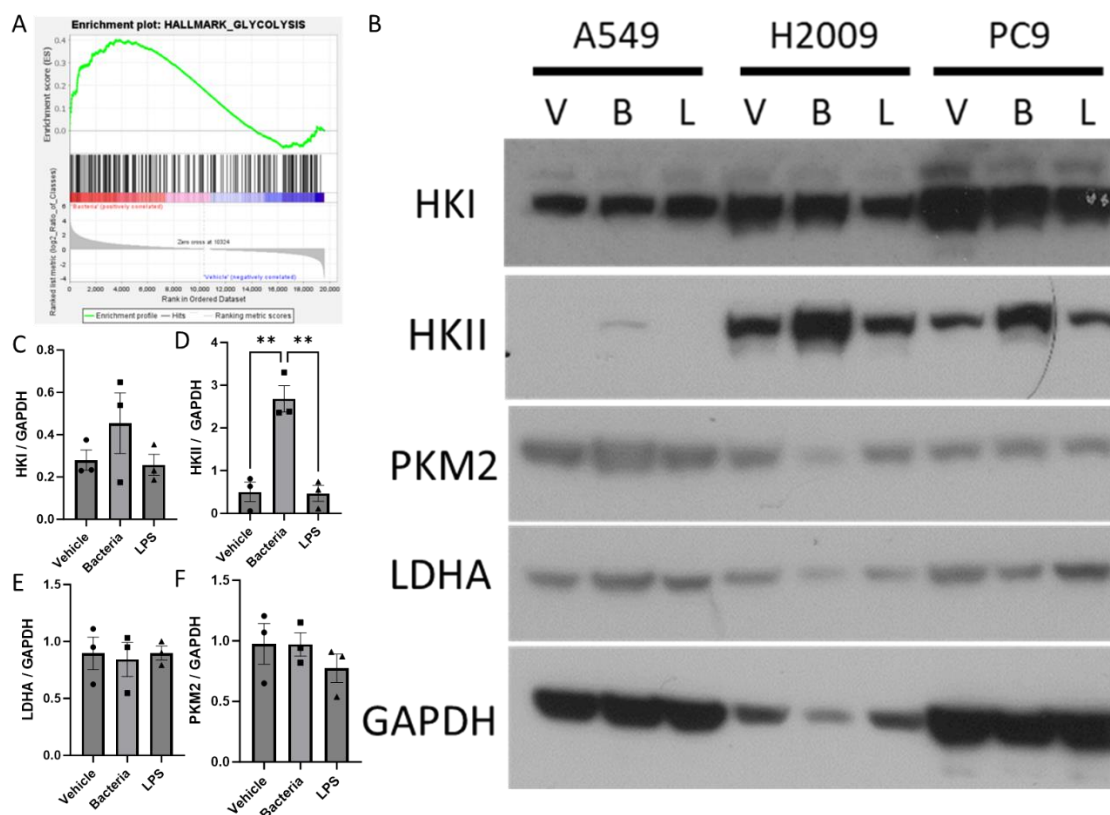


Figure 24. *E. coli* supplemented media enhances enzymes related to glycolysis in LUAD.

A) Gene set enrichment analysis (GSEA)-enrichment plot of representative gene sets in A549 incubated with *E. coli* supplemented media for genes involved in glycolysis. B) Western blot representing multiple glycolytic enzymes. V = Vehicle (1:1, RPMI: PBS), B = Bacteria (1:1, RPMI: Bacterially infused media), and L = LPS (1:1, PRMI: PBS + 0.5µg/mL LPS).

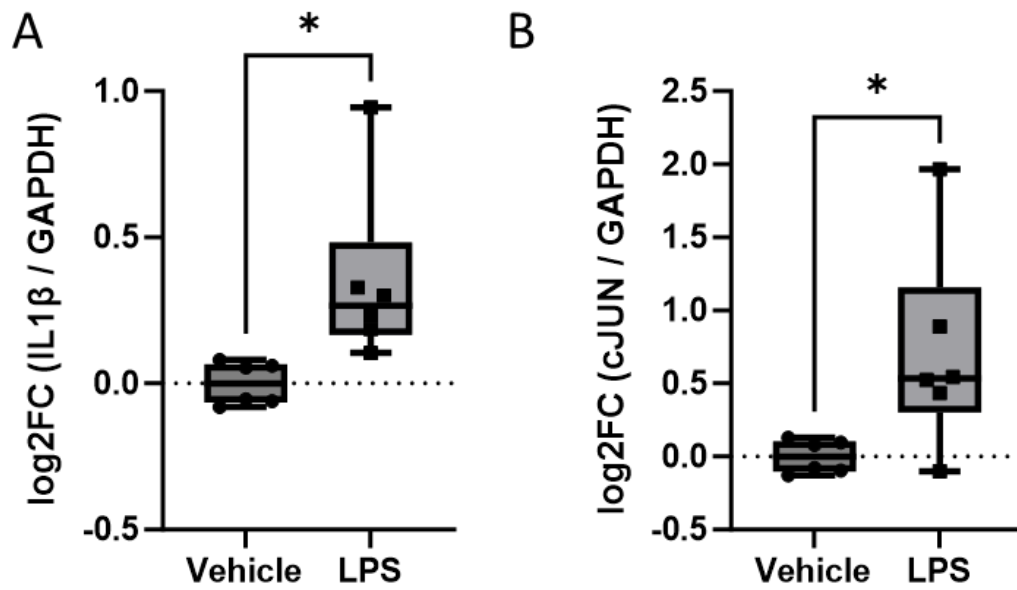


Figure 25. LPS increases IL1 β and cJUN mRNA transcription in LUAD cell lines.

A) qPCR analysis of IL1 β and B) cJUN mRNA expression in LUAD cell lines incubated in Vehicle (1x PBS) or LPS (0.5 μ g/mL LPS) for 16 hours. Data were normalized to GAPDH levels and statistically analyzed using unpaired t-test, * p-value < 0.0332.

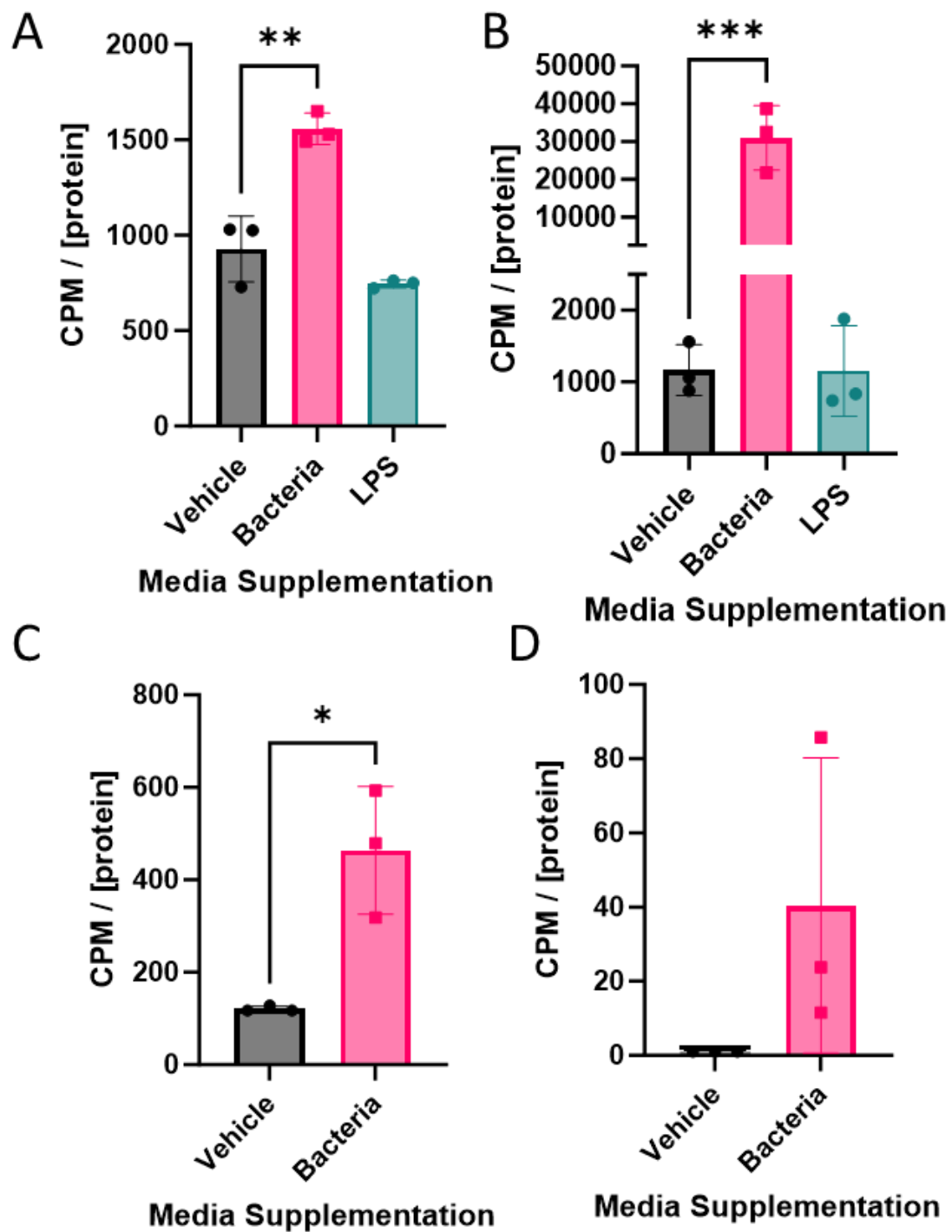
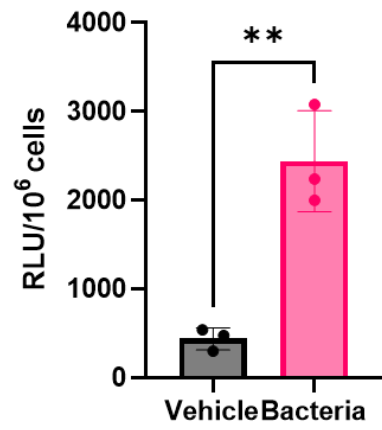


Figure 26. *E. coli* supplementation increases glucose uptake in LUAD cell lines.

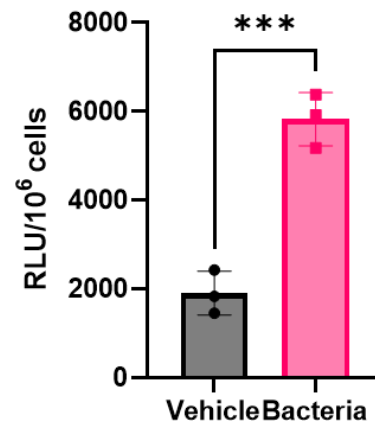
A) A549 and B) PC9 cells were incubated in either Vehicle (1:1 RPMI: PBS), Bacteria (1:1 RPMI-1640: Bacteria Supplemented media), or LPS (1:1 RPMI: PBS + 0.5 μ g/mL

for 16 hours followed by 2 hours of incubation with radiolabeled deoxyglucose. Counts per minute were normalized to protein concentrations and data were analyzed using one-way ANOVA with Tukey test; ** p-value < 0.00332, *** p-value < 0.0002. C) H2009 and D) H2030 cells were incubated in either Vehicle (1:1 RPMI: PBS) or Bacteria (1:1 RPMI-1640: Bacteria Supplemented media) for 16 hours followed by 2 hours of incubation with radiolabeled deoxyglucose. Counts per minute were normalized to protein concentrations and data were analyzed using unpaired t-test, * p-value < 0.021.

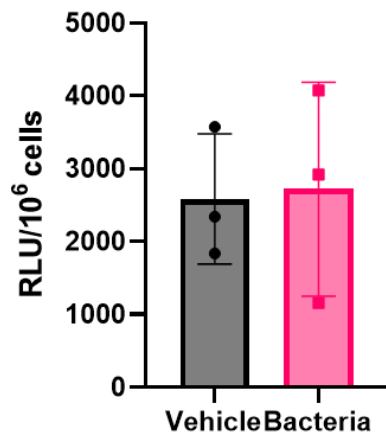
A



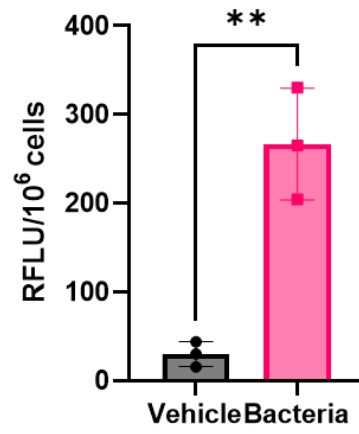
B



C



D



E

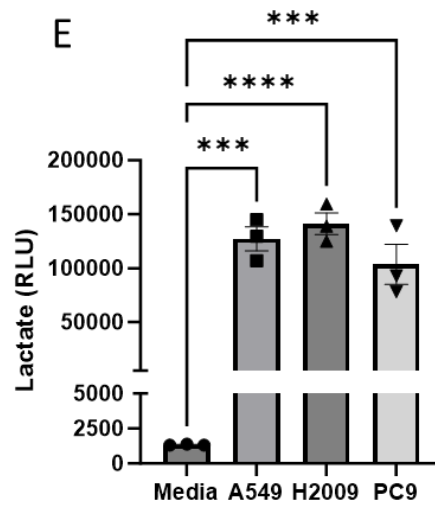


Figure 27. *E. coli* supplementation increases lactate production.

A) Lactate production of LUAD cell lines A549, B) H2009, C) H2030, and D) PC9, under Vehicle (1:1, RPMI: PBS) and Bacteria (1:1, RPMI: Bacterially infused media).

Lactate production was measured using lactate-glo and luminescence was normalized based on cell count. Data were analyzed using a student t-test; ** p-value < 0.0021 and

*** p-value < 0.0002. D) Lactate measured in *E. coli* supplemented media before

(Media) and after 16-hour incubation with LUAD cell lines (A549, H2009, and PC9).

Lactate was measured using lactate-glo and data were analyzed using one-way ANOVA,

*** p-value < 0.0002, ***** p-value < 0.0001.

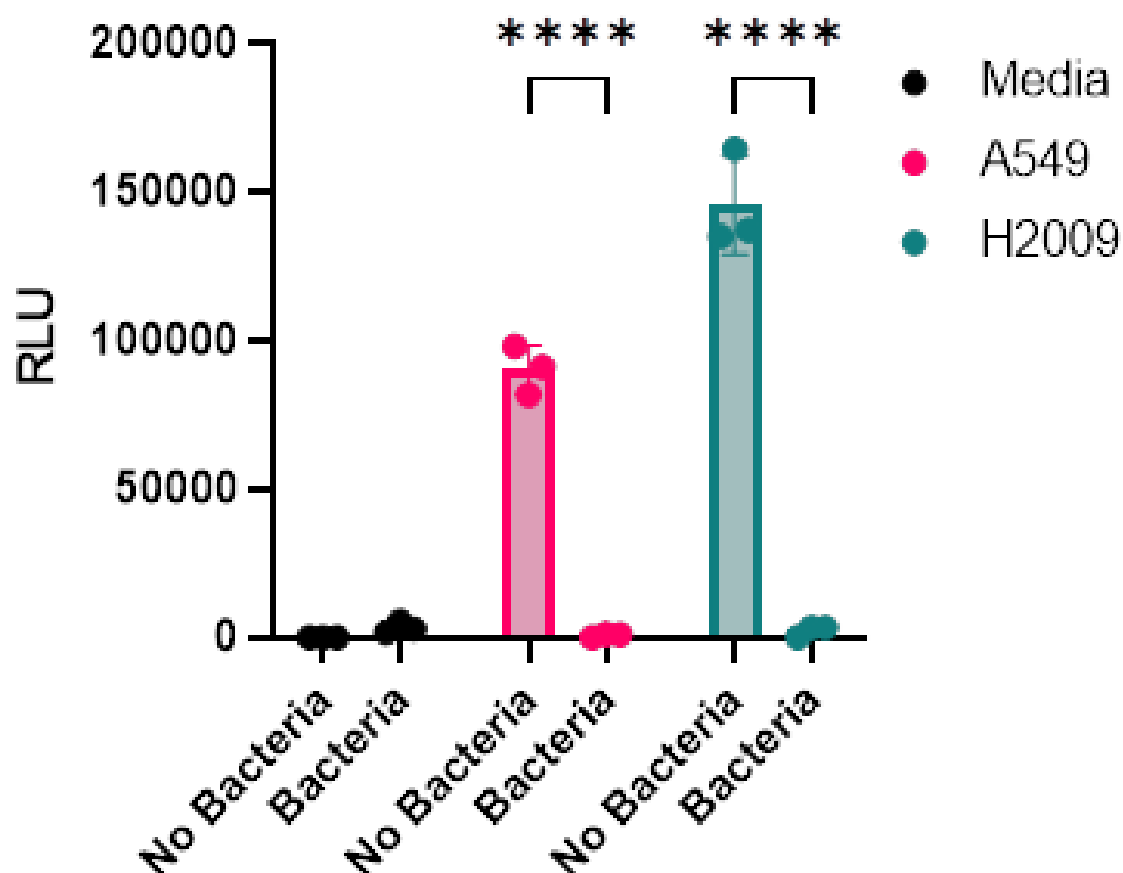


Figure 28. *E. coli* can take up lactate released by LUAD cell lines.

Lactate levels, in counts per second, in LUAD media before (0 Hour) and after (24 Hour) being incubated with *E. coli*. Lactate was measured using lactate-glo assay and relative luminescent units were compared using Two-way ANOVA with Dunnett post-hoc test.

**** p-value < 0.0001.

E. coli biomolecules enhance invasive potential of LUAD cell lines.

Previous literature has shown that bacteria play a role in cancer metastasis, where antibiotic treatment diminishes lung cancer metastasis while inoculating germ free mice with bacteria increased lung cancer metastasis [78]. As the RNA-seq KEGG data showed the Hippo pathway was shown to be within the top 20 upregulated pathways in LUAD cell lines incubated in *E. coli* supplemented media by KEGG analysis, and the Hippo pathway is related to EMT signaling, I chose to investigate the impact of *E. coli* biomolecules on LUAD invasive and motility potential. GSEA further confirmed upregulation of EMT profile in LUAD cell lines incubated in *E. coli* biomolecules compared to those incubated in RPMI-1640 alone (Figure 29A). Performing western blot and probing for EMT specific markers revealed SNAIL, a known inducer of EMT, was dramatically increased following the addition of bacterial biomolecules in A549 and PC9 (Figure 29B).

Metastasis requires the cell to intravasate into the vasculature as well as extravasate to the desired organ. To identify whether the bacterial biomolecules were acting as chemoattractants and promote metastasis, I performed a wound healing assay, where the wound was coated with either RPMI infused matrigel (Vehicle) or *E. coli* supplemented infused matrigel (Bacteria) (Figure 30A). If the *E. coli* biomolecules were acting as chemoattractants, then LUAD cell lines incubated with bacterially infused Matrigel would lead to increased wound closure. This was not the case, as I saw no significant difference in wound closure between RPMI infused vs *E. coli* infused Matrigel (Figure 30B-C).

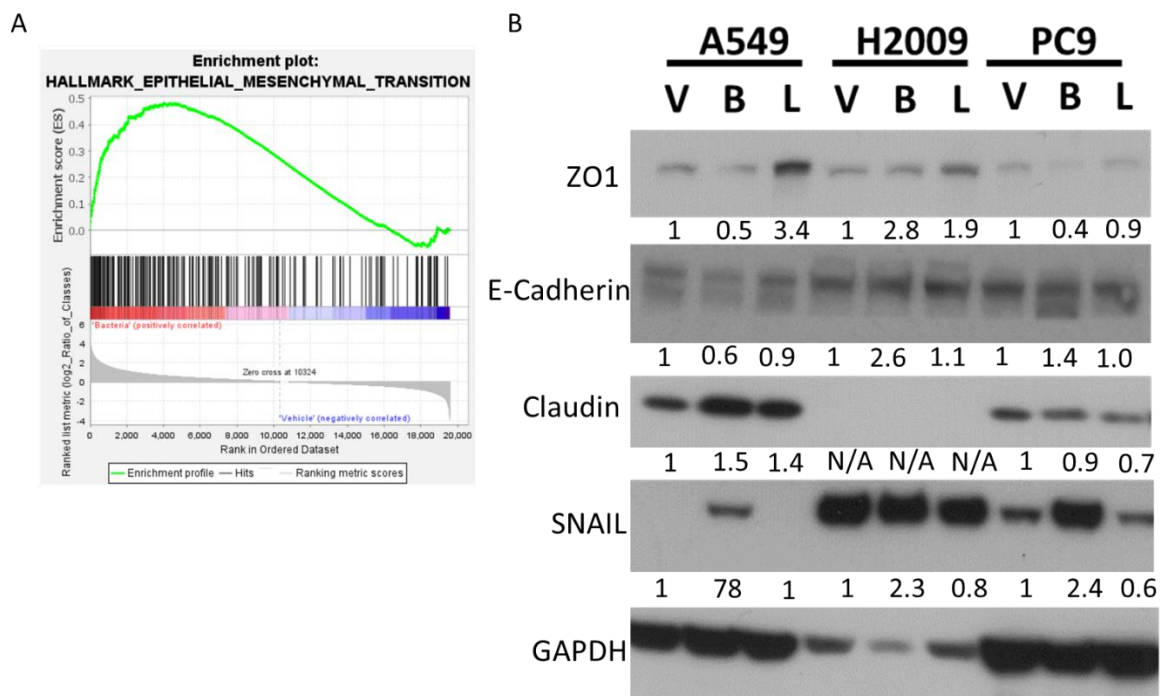


Figure 29. *E. coli* supplementation shows elevated EMT markers.

A) Gene set enrichment analysis (GSEA)-enrichment plot of representative gene sets in A549 incubated with *E. coli* supplemented media for genes involved in EMT progression.

B) Western blot depicting the expression levels of key EMT markers. V = Vehicle (1:1, RPMI: PBS), B = Bacteria (1:1, RPMI: Bacterially infused media), and L = LPS (1:1, RPMI: PBS + 5 μ M LPS). Densitometry was measured using ImageJ. Values were normalized against GAPDH values. Normalized densitometry values were then compared against each respective LUAD cell line's (A549, H2009, and PC9) V value.

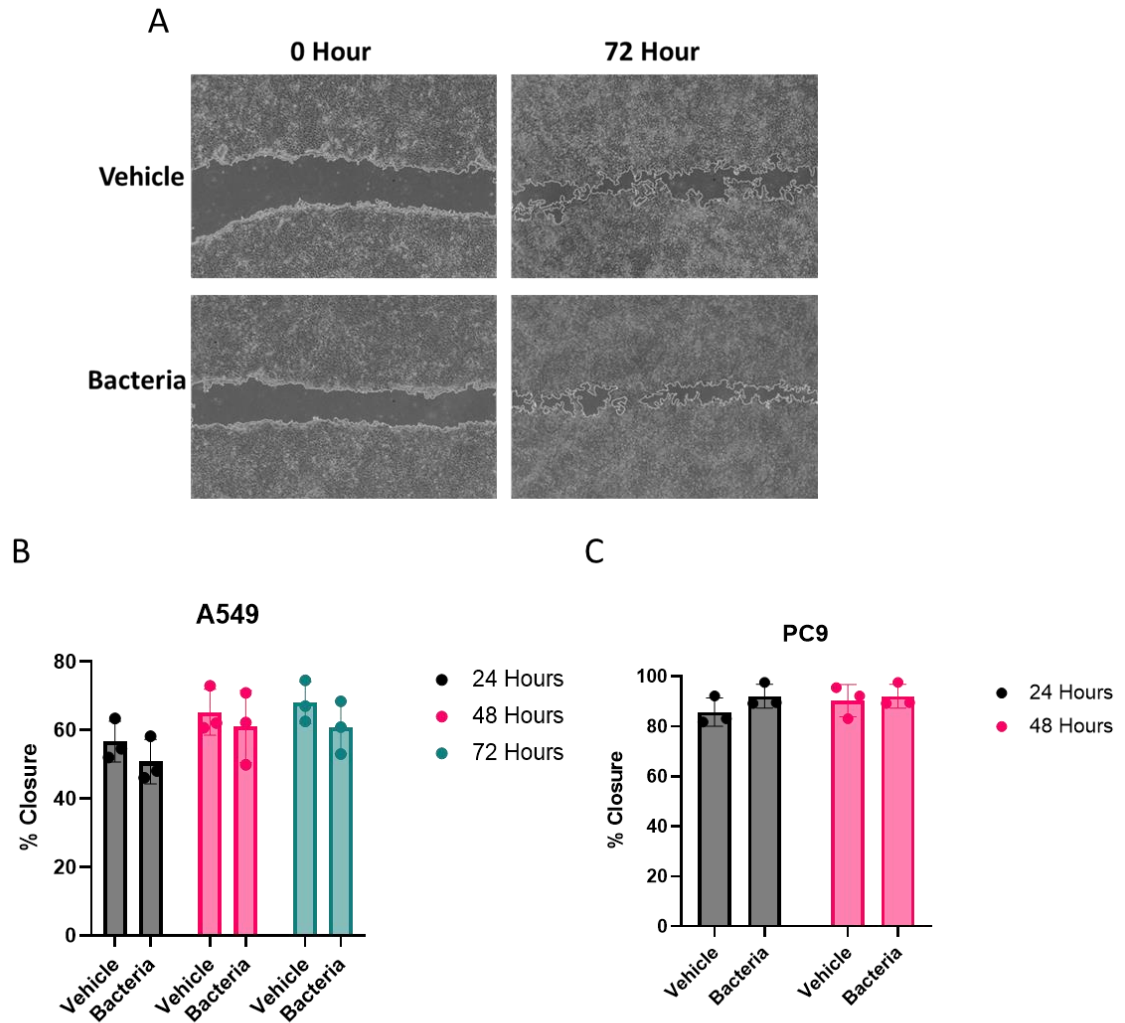


Figure 30. LUAD cell lines do not use *E. coli* biomolecules as chemoattractant.

A) Representative images of wound healing assay following bacterial treatment on LUAD cell lines. Following wound formation, wound was filled with Matrigel infused with either RPMI media or bacterially supplemented media. B) A549 and C) PC9 wound closure data analysis (n = 3). Data were analyzed using two-way ANOVA with Tukey post-hoc test.

As my results suggest the *E. coli* biomolecules were not acting as chemoattractants, I next investigated the impact of bacterial biomolecules on motility invasive potential. For motility, LUAD cell lines were incubated with either RPMI-1640 media with PBS (Vehicle) or *E. coli* biomolecule (Bacteria) supplementation. Individual cell motility was captured and analyzed using BZX-800 and showed no significant change in motility (Figure 31A). I next performed an invasion assay using transwell chambers wherein the bottom chamber contained serum complete RPMI-media and the top chambers contained either serum starved RPMI-media or serum starved *E. coli* supplemented media. After 48-hours, I stained invaded cells and observed a significant increase in normalized invasive potential in LUAD cell lines incubated in bacterially supplemented media (Figure 31B-C). Taken together, my data would suggest that *E. coli* biomolecules do not act as a chemoattractant for LUAD cell lines, but instead facilitates the LUAD invasion.

Phenotypic changes observe in bacterial biomolecules presence is TLR4 independent.

My data shows clear evidence that *E. coli* biomolecules can impact the phenotype of LUAD cell lines directly. However, the mechanism by which *E. coli* were increasing glycolysis or inducing EMT remained unclear. Previous literature has linked LPS induction of TLR4 with increased proliferation and metastasis in cancers [148-152]. Activation of TLR4 is known to lead to increased activation of the MAPK pathway, which is known to result in upregulation of HIF1 alpha expression and activity and results in increased expression of HKII [153-156]. My earlier western blot data had shown increased ERK phosphorylation, an enzyme found in the MAPK pathway, and

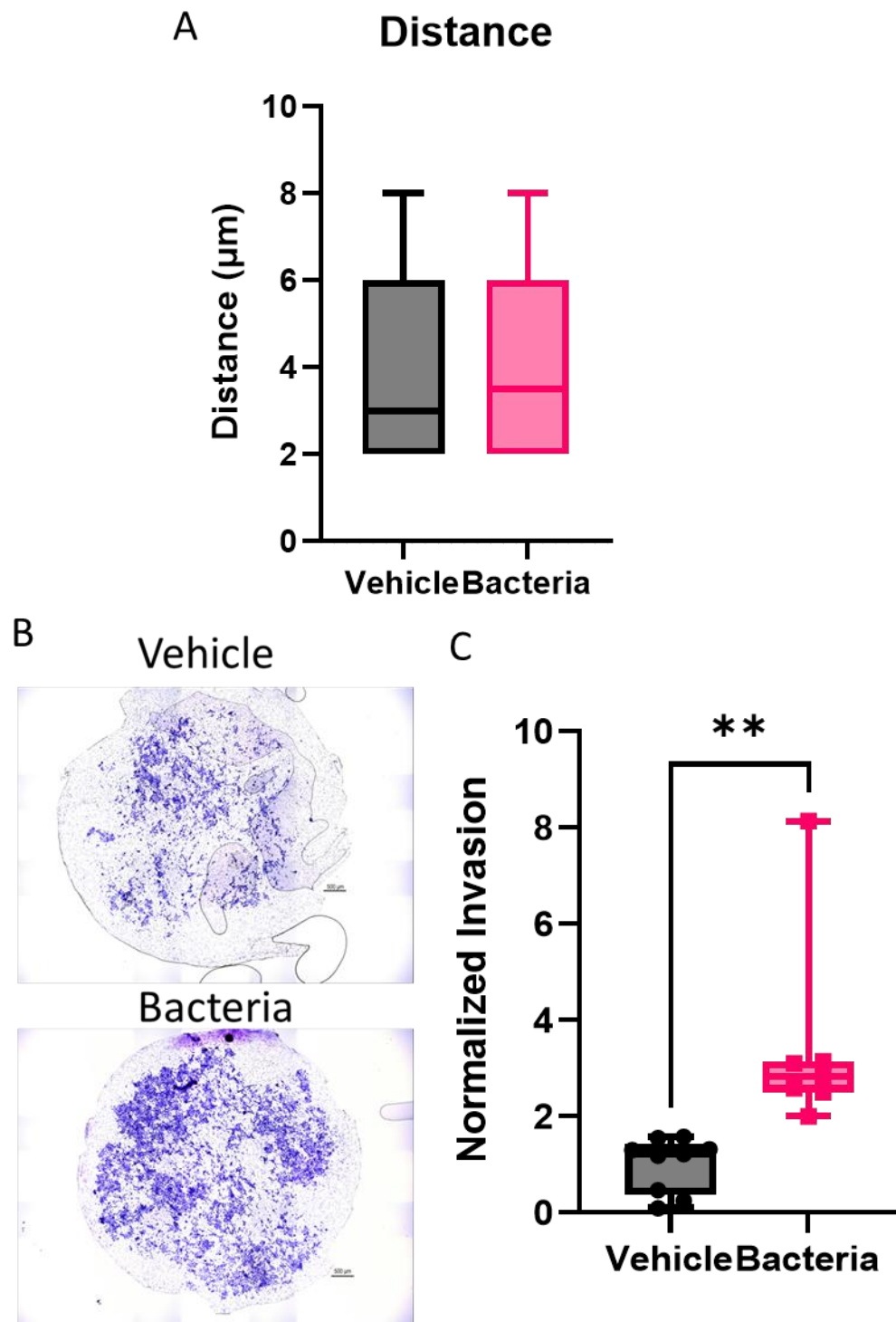


Figure 31. LUAD invasion, but not motility, increases with *E. coli* biomolecules.

A) Single cell motility data captured on BZX-800 Live Cell Imager after 48 hours. Distance traveled, in μm , was measured using BZX-800 Analyzer and data points (n = 20) were analyzed using unpaired t-test. B) Visual representation of invasion assay of A549 treated with serum-starved RPMI-1640 media supplemented with either PBS (Vehicle) or *E. coli* biomolecules (Bacteria). Note: Trans well membrane shown for Bacteria does not represent outlier. C) Normalized invasive potential of Vehicle vs Bacteria. Data were acquired using BZX-800 Analyzer Hybrid Cell Count software and normalized to average invasive count of Vehicle. Normalized data were analyzed using unpaired t-test, ** p-value < 0.0021.

decreased phosphorylation of AKT in LUAD cell lines incubated with *E. coli* (Figure 19). ERK is known to crosstalk with AKT, acting as an inhibitor against AKT phosphorylation [142, 157]. In addition to the association of MPAK with HKII, activation of the MAPK pathway has been previously shown to increase expression of the protooncogene cJUN [158]. Interestingly, the RNA-seq data revealed cJUN was also significantly upregulated in both cell lines when treated with *E. coli* biomolecules and was further confirmed in our western blot analysis (Figure 32A-B).

To determine the importance of the TLR4 receptor activation on the EMT and glycolysis, I used a potent TLR4 inhibitor, C34 [159, 160]. Previous investigators have reported a decrease in tumor progression with C34 treatment, showing the increased proliferation of colorectal cancer by palmitic acid being lessened by treating cells with 5 μ M of C34 [161]. I performed alamarBlue assay on several cell lines and ensured that C34 was not toxic to our cell lines at 5 μ M (Figure 33). Additionally, C34 was shown to decrease p38 phosphorylation in a dose dependent manner (Figure 34A-B).

With the knowledge that C34 was non-toxic to our cells at 5 μ M and was sufficient to decrease p38 phosphorylation, I continued to investigate the effects of TLR4 inhibition on glycolysis. LUAD cells were treated with 5 μ M C34 or equal volume of DMSO in media with and without *E. coli* biomolecules. Western blot data showed a modest decrease HKII expression following treatment of C34 with or without bacterial exposure by densitometry (Figure 35A). Investigating the lactate production of LUAD cell lines showed no significant difference when LUAD cells incubated in *E. coli* biomolecules were treated with Vehicle or C34 (Figure 35B-D). In addition to

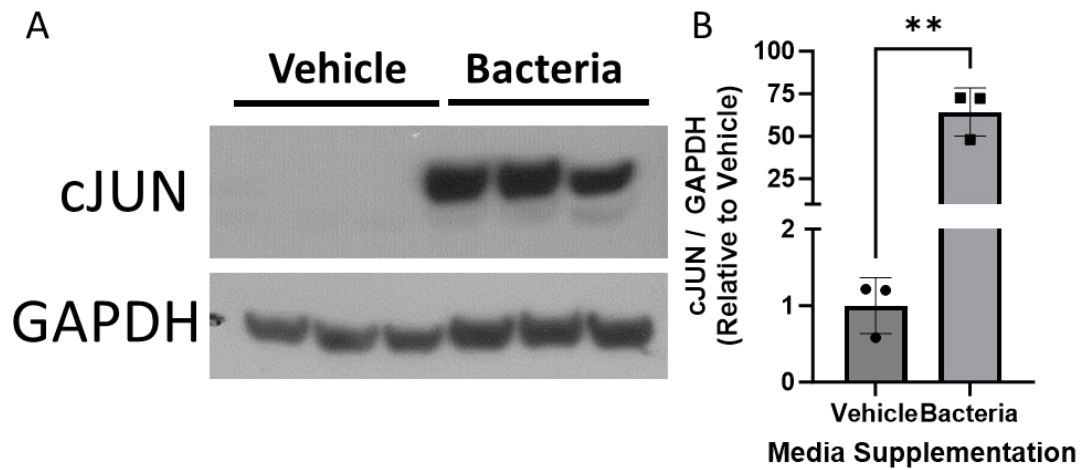


Figure 32. Increased cJUN expression in LUAD cells incubated with *E. coli* biomolecules.

A) Western blot of LUAD cells incubated in either Vehicle (1:1, RPMI-1640: PBS) or Bacteria (1:1, RPMI-1640: *E. coli* supplemented media) probed for anti-cJUN and anti-GAPDH antibody. B) Densitometry analysis of western blot. Values were normalized by GAPDH and further normalized to average expression found in Vehicle. Data were analyzed using unpaired t-test, ** p-value < 0.0021.

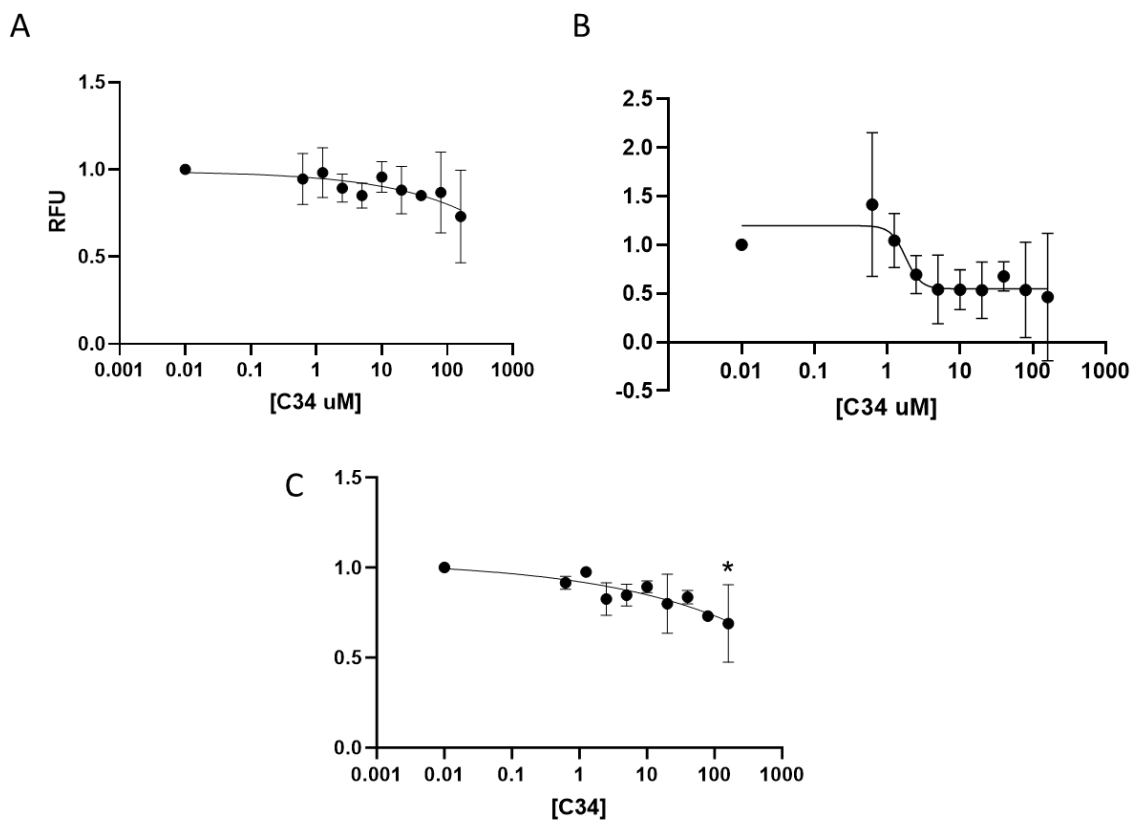


Figure 33. Effects of C34 inhibition on cell viability.

A) AlamarBlue data of A) A549, B) H2009, and C) PC9 measuring cell viability following increasing concentrations of C34 after 24 hours. Data were normalized by relative fluorescent units (RFU) of $0.01\mu\text{M}$ C34 and analyzed using one-way ANOVA comparing RFUs to $0.01\mu\text{M}$ C34 RFU; * p-value < 0.0332.

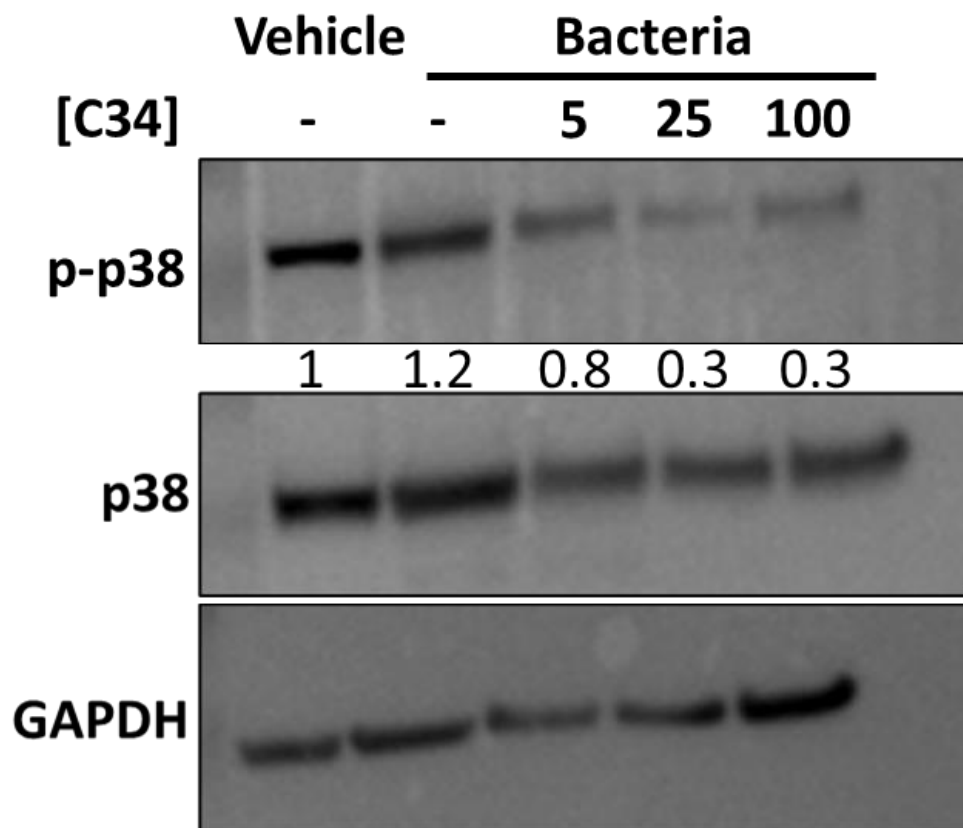


Figure 34. MAPK phosphorylation decreases on C34 administration.

Western blot analysis of A549 incubated in increasing concentrations of C34 for 24 hours. Membrane was probed for anti-phosphorylation MAPK (p-p38), anti-MAPK (p38), and GAPDH. Densitometry was measured using ImageJ where values were normalized to GAPDH. Phosphorylated p38 was normalized to p38, and LUAD incubated in *E. coli* biomolecules were normalized to vehicle control.

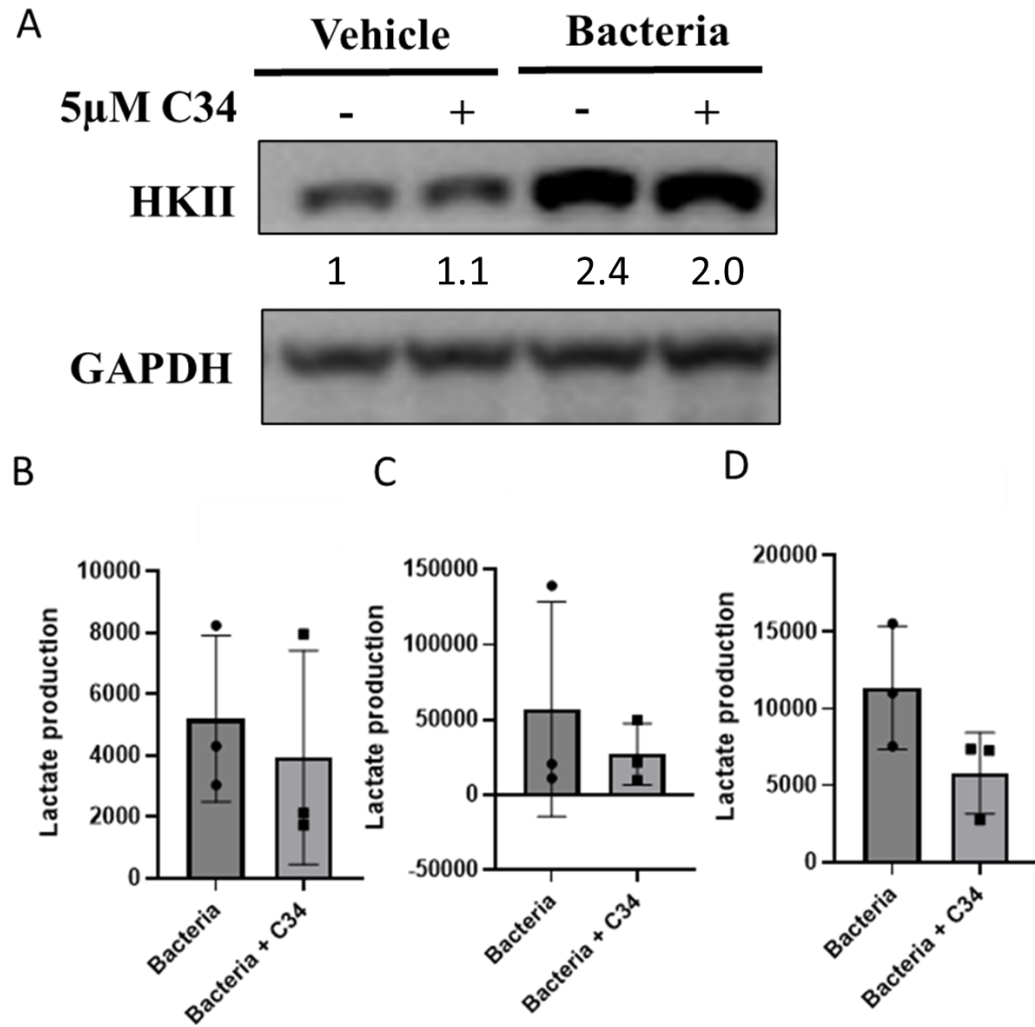


Figure 35. TLR4 inhibition does not lead to decreased glycolysis in LUAD cells treated with *E. coli* supplemented media.

A) Western blot analysis of A549 incubated in vehicle (1:1, RPMI-1640: PBS) or Bacteria (1:1, RPMI-1640: *E. coli* supplemented media) and either DMSO (-) or 5 μ M TLR4 inhibitor, C34 (+) for 24 hours. The membrane was blotted with anti-hexokinase II (HKII) and anti-GAPDH. Densitometry was measured using ImageJ where values were normalized to GAPDH and compared against Vehicle without C34 treatment. B) Lactate-glo assay measuring lactate production in

luminescence in A549, B) H2009, and C) PC9 cells incubated with *E. coli* supplemented media and treated with either DMSO or C34. Data were analyzed using a student t-test and showed no significance.

investigating the effects of C34 on LUAD incubated with *E. coli* biomolecules, I also investigated the effects of C34 on invasion. My results indicate that C34 does not inhibit invasive potential of LUAD incubated with bacteria (Figure 35).

In addition to investigating TLR4, I also explored the *E. coli* biomolecules to identify the type of biomolecule eliciting the phenotypic changes. For this, I treated the *E. coli* supplemented media by removing possible bacterial RNA with RNase, removal of lipid-based biomolecules using dextran-coated charcoal, and removal of molecules larger than 3kDa using spin columns. A549 cells were then incubated with the treated media for 48 hours and whole cell lysate was analyzed by western blot. My data shows treating the *E. coli* supplemented media with RNase led to decreasing levels of HKII but increasing levels of Claudin and cJUN when compared to LUAD cell lines incubated with untreated media (Figure 36). It has previously been shown that some bacteria, such as *Staphylococcus aureus*, can secrete immunomodulatory RNA into the extracellular matrix which acts as a ligand against specific TLRs [162, 163] . In addition to RNA impacting the cell phenotype, I also show that both removal of lipids and molecules over 3kDa in size resulted in increased levels of Claudin but decreasing levels of cJUN and HKII relative to A549 incubated with untreated media (Figure 36). Interestingly, RNase treatment behaved opposite to charcoal and dialysis in respects to cJUN expression. I believe that bacterial RNA plays an inhibitory role against cJUN. These results show that different bacterially derived molecules may have differing impacts on LUAD phenotype.

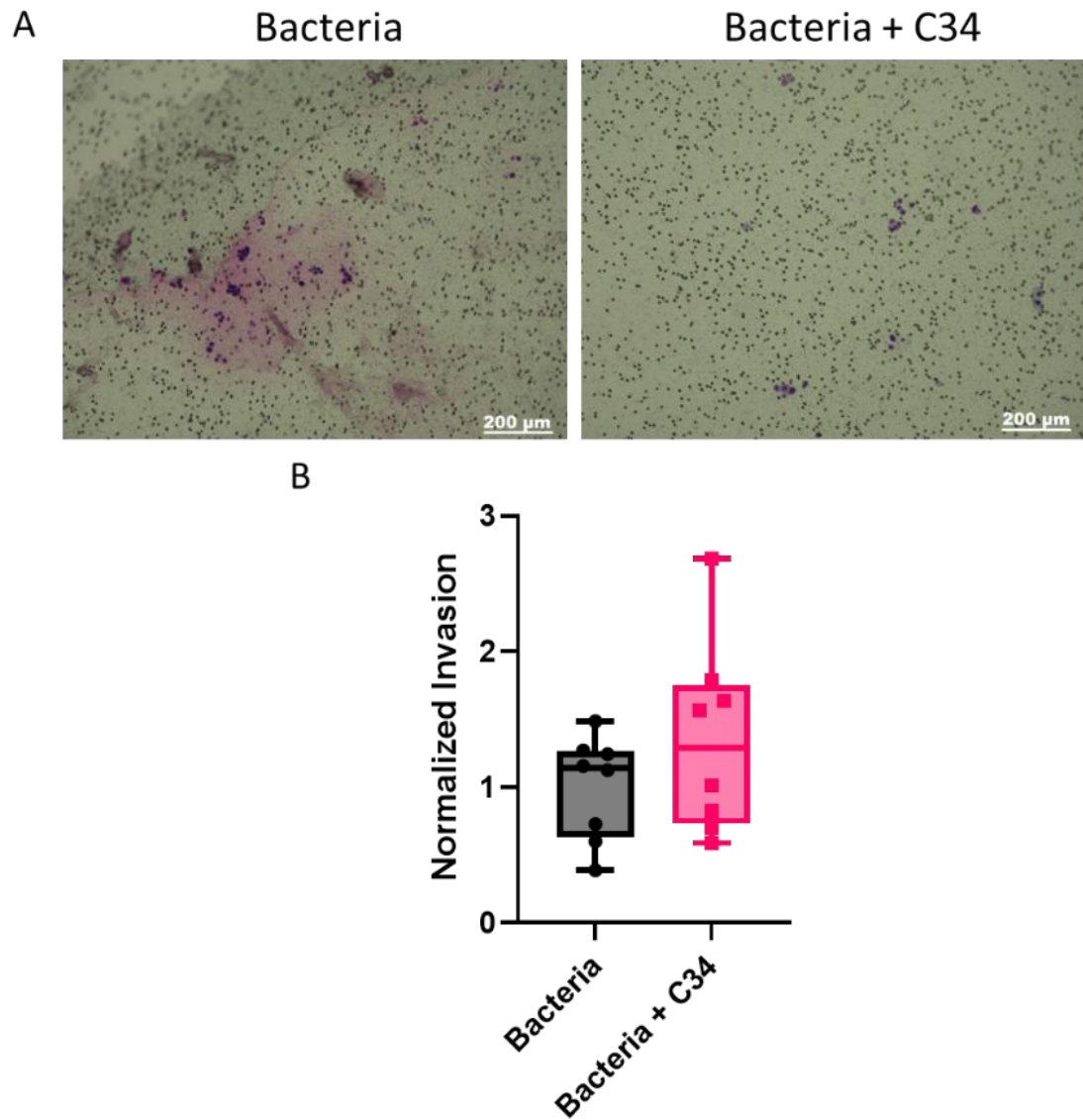


Figure 36. TLR4 inhibition does not lower invasive potential of LUAD incubated in *E. coli* supplemented media.

A) Representative image of invasion assay taken at 10x magnification. B) Data analysis of invasion transwell taken from Keyence Live Cell Imager and analyzed using Keyence Analyzer. Data were normalized by average normalized invasion in LUAD cells in *E.*

coli supplemented media with DMSO control. Normalized data were analyzed using student t-test and showed no significance.

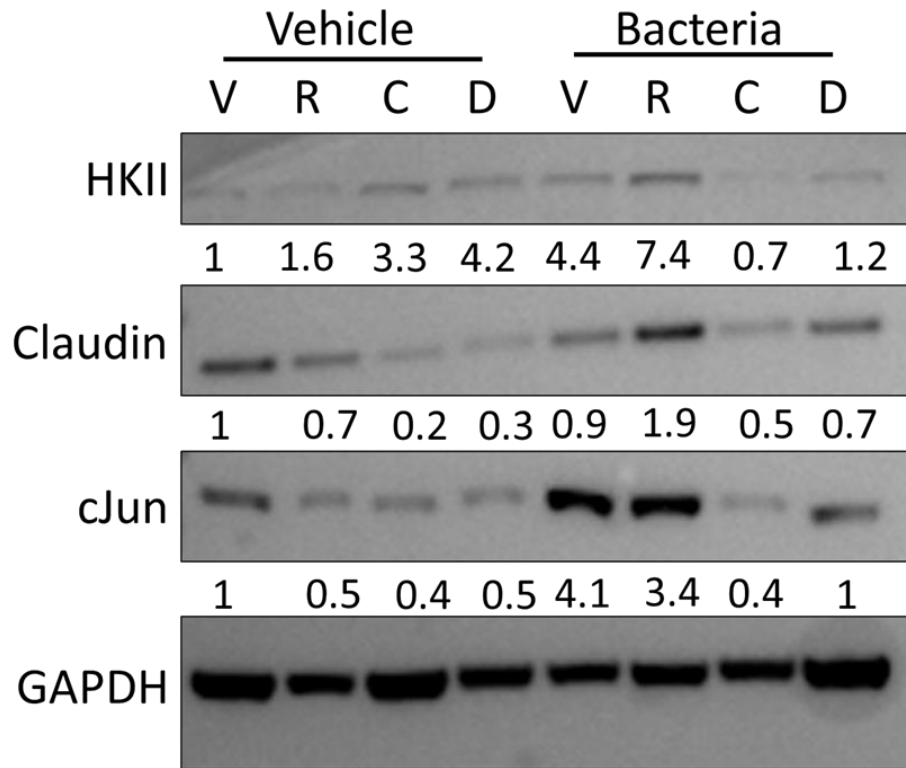


Figure 37. *E. coli* RNA, lipids, and biomolecules > 3kDa impacts LUAD phenotype.

Western blot analysis of A549 treated with either Vehicle (1:1, RPMI-1640: *E. coli* supplemented media) or Bacteria (1:1, RPMI-1640: *E. coli* supplemented media) untreated (V), treated with 100ng/mL RNase (R), charcoal stripped (C), or removal of molecules > 3kDa (D). Membrane was blotted with anti-HKII, -Claudin, -cJUN, and -GAPDH. Densitometry was measured by ImageJ, using respective GAPDH to normalize values, and compared against Vehicle V.

Discussion

Recent studies have linked the tumor microbiome with cancer progression and metastasis [78, 81, 89, 127, 130, 164]. These studies have not only highlighted the importance of the tumor microbiome on cancer but have also suggested the possibility of a direct crosstalk between the tumor cells and the microbiome [90, 127]. In this study, I further evaluated the impact on the microbiome directly onto the LUAD by using RNA-seq to identify transcriptomic changes that may highlight pathways that are tied with bacteria. Of the differentially genes expressed in LUAD cell lines exposed to *E. coli* biomolecules, several of these genes were related to glycolysis and the Hippo pathway.

It is well known that cancer cells are highly addicted to glucose and convert pyruvate into lactate even in aerobic environments, a phenomenon known as the Warburg Effect [165]. The RNA-seq data gathered in this thesis shows the presence of *E. coli* biomolecules further enhances the Warburg Effect observed in my LUAD cell lines. In addition to observing increase glucose uptake in the presence of *E. coli* biomolecules, I also show that lactate production is also increased. Previously, it was believed that lactate was another waste product of cancer cells, but lactate has also been shown to play a role in signaling, metastasis, and even a fuel source for cancer cells [166]. In addition to lactate, others have investigated the role of nitrogenous waste produced by tumors; showing *E. coli* cells can utilize the nitrogenous waste to generate arginine for immune cells [167]. I asked if the lactate produced by cancer cells could also be taken up by *E. coli*. My results show that the lactate produced by LUAD cells can be taken up by *E. coli*. It should be noted that the LUAD media used for this experiment was not further

supplemented with additional glucose. The lack of glucose supplementation could be what is driving *E. coli* to take up lactate.

In addition to an elevation of glycolysis, the RNA-seq data also hinted at bacterial biomolecules having an impact on the Hippo pathway. The Hippo pathway is related to several cellular phenotypes including survival and motility [144]. To narrow my studies to a specific phenotype, I investigated the top 20 downregulated and upregulated DEGs. Not only did I observe several genes associated with adherence downregulated, but I also report multiple genes within the SNAIL family (SNAI1, SNAI2, and SNAI3) upregulated. As such, I focused on the role of *E. coli* biomolecules on LUAD motility and invasion. Investigating the protein expression of multiple EMT markers showed a significant elevation of SNAIL. I next investigated whether the biomolecules released from *E. coli* could be a chemoattractant for the LUAD cell lines. My results showed no increase in invasion in our modified wound-healing assay, which incorporated the use of Matrigel infused with either media or *E. coli* supplemented media, suggesting that the bacterial biomolecules were not acting as chemoattractants, such as chemokines. Additionally, I also show that incubating LUAD cell lines with *E. coli* biomolecules did not influence inherent LUAD motility. However, my invasion assay showed a significant increase in invasive potential towards a known chemoattractant, serum, when LUAD cell lines were serum starved and *E. coli* biomolecules were supplemented.

As my study explores the direct relationship between LUAD and bacteria, I next wanted to determine the mechanism by which *E. coli* were eliciting the phenotypic changes in LUAD cell lines. As *E. coli* are gram negative bacterial cells, their cell walls has a large abundance of LPS. LPS is known to impact immune cells by activating

TLRs, namely TLR4, on the surface of immune cells and leading to phenotypic changes such as increased in glycolysis [153]. Cancer cells are also known to have TLR4 receptors where activation has been shown to increase survival, proliferation, and even metastasis [147, 148, 151, 152, 168]. To determine whether the effects we were observing were related to stimulation of the TLR4 receptor, we used a potent TLR4 inhibitor known as C34. I performed alamarBlue to determine the effects of C34 on LUAD cell viability and saw a significant decrease in viability at 5 μ M with H2009, but not A549 or PC9. By western blot I show a decrease in MAPK phosphorylation, a pathway known to be downstream of TLR4 [169-171], with C34 incubation in a dose-dependent manner. Due to the decrease in cell viability in H2009 following C34 incubation, I performed my experiments using 5 μ M C34. I observed no change in expression levels of HKII on treating cells with C34, and no change in lactate production. To this end, I concluded that the increase in glycolysis observed in the presence of *E. coli* supplementation was not mediated by TLR4 activation. Additionally, I saw no significant change in invasive potential for LUAD cells treated with C34, suggesting the change in invasive potential is also not mediated by TLR4 activation.

A previous study has shown a crosstalk between *Pseudomonas aeruginosa* and multiple cancers including prostate, ovarian, and breast [127]. My *in-vitro* data shows that there exists a direct crosstalk between LUAD and *E. coli*. I investigated how *E. coli* synthesized RNA, lipids, and biomolecules > 3kDa impact LUAD phenotype by treating *E. coli* supplemented media with RNase, charcoal, and dialysis spin column, respectively. My results show RNA remove increased cJUN expression while removal of lipids or biomolecules > 3kDa decreased cJUN levels, suggesting bacterial RNA inhibits

cJUN expression. While our knowledge of the relationship between LUAD and the microbiome remains in its infancy, understanding the LUAD: microbiome interaction could prove beneficial in targeting specific phenotypes such as metastasis. Adding to this idea of tumor: microbiome interaction, previous investigators have also established methods into developing and studying a synthetic microbiome [172]. Future studies will benefit in using a synthetic microbiome to study the impact of specific microbial families on LUAD progression, *in-vivo*. These future studies will not only broaden our understanding of the microbiome shift on LUAD progression, but also has the potential to grant us new therapeutic avenues to target and treat LUAD.

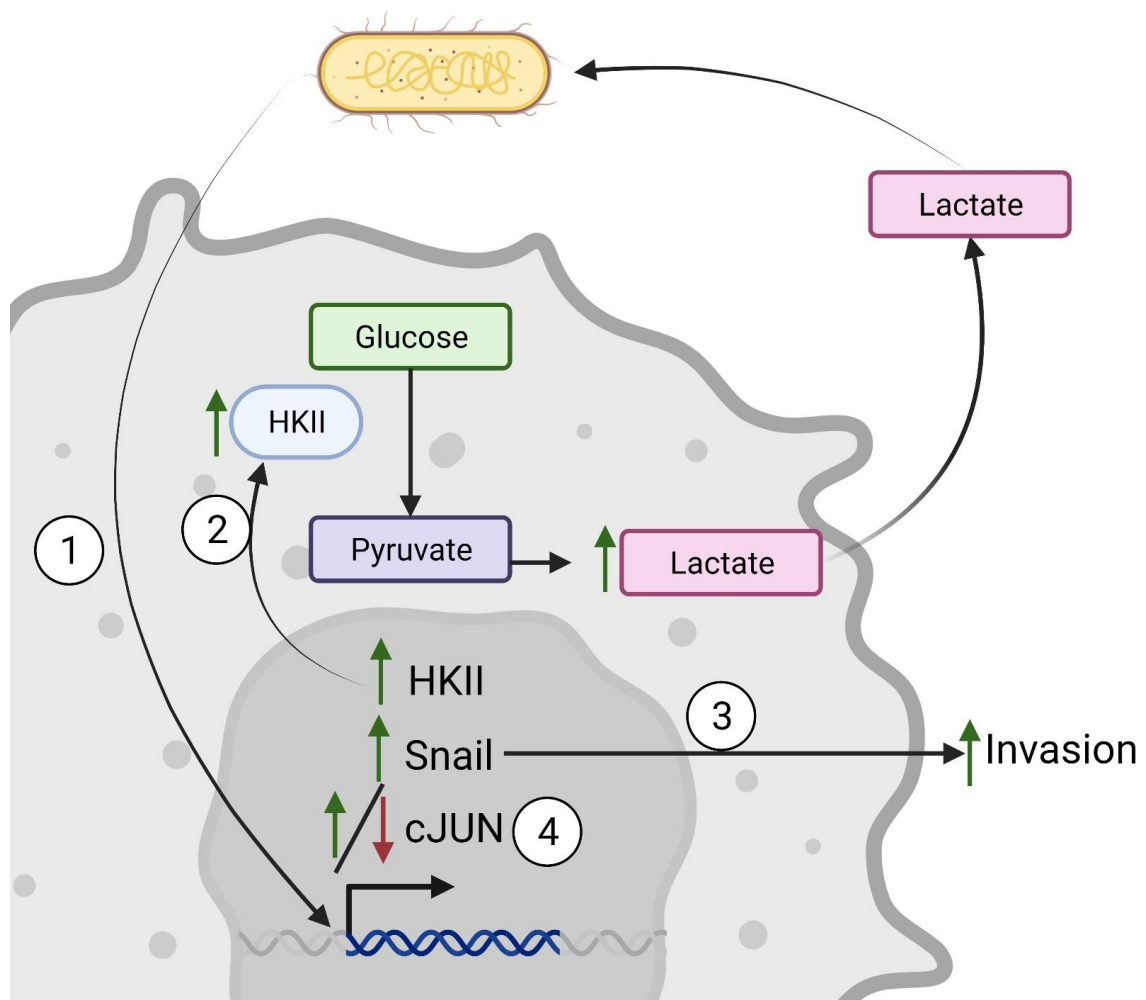


Figure 38. Graphical summary of relationship between *E. coli* and LUAD.

1: *E. coli* can interact with LUAD through biomolecules including RNA, lipids, and biomolecules > 3kDa. 2: *E. coli* secreted biomolecules lead to upregulation of HKII and enhances glycolysis, leading to increased lactate levels which bacteria can take up. 3: *E. coli* increases expression of SNAIL and increasing invasive potential of LUAD. 4: *E. coli* secreted lipid and biomolecules > 3kDa increase cJUN protein levels, while RNA decreases cJUN protein levels.

CHAPTER 4: OVERALL CONCLUSIONS AND FUTURE DIRECTIONS

This thesis was started from a simple question of how methionine restriction would impact LUAD. These early studies opened the doors to collaborating with individuals in the British Columbia Cancer Center that were investigating the microbiome in patients diagnosed with LUAD. This led to an exciting, albeit more complex, project that required me to move past focusing on LUAD and towards broadening my scope to encompass microbiology.

In Chapter 2, I focus on investigated the role of methionine restriction on LUAD. As others have seen methionine restriction led to decreased proliferation, survival, and motility in breast, colorectal, and prostate cancer [92, 94, 95, 97, 124, 173], I chose to investigate whether that was also true in LUAD. One of the limitations from previous studies was the complete removal of methionine rather than restricting the concentration of methionine within the media. As such, I incorporated a range of methionine concentrations. I had found that at 2 μ M methionine, LUAD cells exhibited a similar decrease in proliferation, but no change in survival and no dramatic change in cellular motility. This 2 μ M methionine concentration is a better at representing methionine restriction based on previous literature of methionine concentration in the plasma [112]. Overall, I believe that methionine restriction shifts LUAD from a highly proliferative state to a low proliferative state, relying on macropinocytosis to scavenge for sources of methionine.

While Chapter 2 focused on the effects of methionine restriction on LUAD, Chapter 3 shifted the focus into *E. coli* and LUAD. The radiolabeling studies I had performed shows a crosstalk between LUAD and *E. coli*. This finding ultimately led to me performing RNA-seq on two LUAD cell lines, A549 and H2009, wherein over 900 genes were recorded being differentially expressed in the presence of *E. coli* biomolecules. Of these over 900 genes, 11 were well known glycolytic genes and 9 were associated with the Hippo Pathway. Notably, 4 of the 9 genes found in the Hippo Pathway were directly tied to EMT. With this knowledge, I was able to show that there is an increase in glycolysis and EMT for LUAD cells incubated with *E. coli* biomolecules. Of the enzymes related to glycolysis and EMT, it was HKII that exhibited a dramatic increase in expression when LUAD were exposed to *E. coli* biomolecules.

While it is commonly known to be the first committed step in glycolysis, recent findings have discovered a novel moonlighting function that facilitates EMT [174]. It has been suggested that HKII acts as a scaffolding protein, binding to the cyclic-AMP-dependent protein kinase A regulatory subunit 1a (PRKAR1a) and Glycogen synthase kinase 3 (GSK3), ultimately facilitating phosphorylation of GSK3 by PRKAR1a [174]. GSK3 has been previously shown to inhibit EMT [175], and phosphorylation has been shown to inhibit GSK3 [176]. Furthermore, HKII has also been suggested to facilitate glycosylation of SNAIL through O-GlcNAcylation [174]. Glycosylation of SNAIL prevents phosphorylation by GSK, which would lead to degradation, thus stabilizing SNAIL [177]. With my data showing *E. coli* biomolecules also increasing SNAIL expression, it would be interesting to see if the EMT observed is facilitated by HKII.

I continued by investigating TLR4, a receptor most known to be influenced by bacteria that has implications in both glycolysis and EMT. I used a potent TLR4 inhibitor, C34, to investigate if inhibition of TLR4 would lead to decreased glycolysis or EMT in LUAD incubated with *E. coli* biomolecules. Unfortunately, I saw no significant change in glycolysis or EMT. I believe the increase in glycolysis and EMT observed when incubating LUAD with *E. coli* biomolecules is not attributed to activation of TLR4.

This thesis contains several strengths that expand our knowledge of LUAD, methionine availability, and the relationship between LUAD and *E. coli*. Previous work investigating methionine availability *in-vitro* in cancer cells have used a system that is completely devoid of methionine [93, 96, 123, 178]. My work focused on using a methionine concentration that would better reflect restriction, rather than deprivation. Secondly, my data is the first to use GeCKO screening to identify genes that could be considered synthetically lethal when combined with methionine restriction. Future studies can use the information gathered from my GeCKO screen to find novel targets against LUAD when treated with a methionine inhibitor, such as BCH. Thirdly, my data is the first to culture LUAD with *E. coli* biomolecules and identify DEGs directly influenced by *E. coli*. While this thesis focused on *E. coli* biomolecules influencing glycolysis and EMT/invasive potential in LUAD *in-vitro*, several other pathways remain to be investigated. My earlier work investigating the effects of LUAD Lastly, I have also investigated treating the *E. coli* supplemented media with RNase, Charcoal, and dialysis to characterize the biomolecules secreted by *E. coli*.

This work is not without its pitfalls or limitations. For starters, my work revolved around three LUAD cell lines; A549, H2009, and PC9. Two of these cell lines, A549 and

H2009, are KRAS-mutant LUAD while PC9 are EGFR mutants. While KRAS and EGFR constitute the most known mutations in LUAD [8, 173, 179], others still exist that may result in different observable results. Furthermore, it would strengthen my findings if I were to have included more cell lines with KRAS, such as H2122 or H2030, or EGFR mutations, such as HCC2279 or HCC827.

One major criticism between *in-vitro* and *in-vivo* studies is the results from *in-vitro* do not always recapitulate *in-vivo*. Others are attempting to bridge the gap between *in-vitro* vs. *in-vivo* by moving from 2D cell culture work to 3D [180-182]. The *in-vitro* work performed in these experiments were all performed in 2D culture, and it would be interested to see if I see similar results if I were to move to a 3D culture. A 3D culture would involve growing my LUAD cells in a non-adherent 96-well dish to form organoids. These organoids would then be planted onto a culture dish and placed in either high methionine or methionine restriction. Unlike the 2D culture where the methionine is dispersed evenly across the lawn of LUAD cells, in a 3D tumor organoid the methionine would need to penetrate through the outer wall of LUAD cells to be taken up by the LUAD cells found in the core. In this scenario, I believe I would see an increase in cell death, as those LUAD cells within the core of the organoid would be starved of methionine.

It should also be noted that my findings investigated only one bacterial species, *E. coli*, of the large mass found within the microbiome. The microbiome is a complex amalgamation of organisms that are known for nitrogen fixation and providing nutrients. As such, I can investigate how different microbes can impact LUAD development. However, one major limitation of these kinds of studies is that there is no accurate way to

regulate the growth of bacteria in culture. The microbiome in our body is tightly regulated, where our immune cells and other cells in the microbiome keep individual species from overgrowing. This is not the case for our bacterial culture where the *E. coli* are able to continue growing until they reach a growth plateau. It is possible the LUAD phenotype observed in Chapter 3 is due to the large amount of *E. coli* producing these biomolecules. While in our body, they may be supplying such biomolecules, the impact of *E. coli* may be dramatically lessened due to their population size compared to other cells in the microbiome. Thus, future studies would benefit from *in-vivo* models to understand the influence of the microbiome on tumor progression.

The use of a synthetic oligo mouse microbiome (OMM) would be key in combating these limitations[172, 183, 184]. Our 16S sequencing data, as well as others, shows tumors have a distinct microbial profile compared to adjacent non-malignant tissue [78, 90, 185, 186]. From my data, I show how *E. coli* increases glucose uptake, lactate production, and invasive potential in LUAD cell lines. Meanwhile, others have shown *P. aeruginosa* acts as a tumor suppressor for early stages of cancers including breast, prostate, and ovarian cancer [127] by stabilizing p53 and inducing apoptosis [187]. Furthermore, previous investigators have shown the use of probiotics results in decreased progression of colorectal cancer both *in-vitro* and *in-vivo* [188-190]. While a synthetic microbiome has yet to be used to investigate cancer progression, it would be a powerful tool to characterize microbial families as either tumor associated bacteria (TAB) and tumor suppressive bacteria (TSB). The 16S sequencing data gathered from the lab can be used to develop a synthetic microbiome containing the top 12 upregulated and downregulated microbial species. The synthetic microbiome can then be inoculated into

LUAD bearing germ-free mice to determine how TAB and TSB families impact LUAD progression.

While my data has focused on the direct relationship between LUAD and the microbiome, others have shown how the microbiome can impact cancer through immunomodulatory means [77, 78]. Previous findings have shown the impact of the microbiome on $\gamma\delta$ T-cell expansion [78], which are known to have immune regulatory functions [191]. These $\gamma\delta$ T-cells can induce senescence in tumor infiltrating lymphocytes including CD4⁺ T-cells, CD8⁺ T-cells, and dendritic cells [192] through MAPK/ERK/JNK activation [193]. Interestingly, our data shows *E. coli* upregulated ERK phosphorylation in LUAD. Could the TAB also upregulate ERK in the immune cells, thus inducing senescence and facilitating in immune evasion? It has also been suggested that the immune evasion brought on by $\gamma\delta$ T-cells can be reversed through activation of TLR8 [192], which is activated by RNA such as bacterial RNA [194]. My data suggests *E. coli* secrete RNA into the media, as treating *E. coli* supplemented media resulted in phenotypic changes in LUAD by western blot. Could bacteria activate TLR8, reversing the T-cell senescence, and result in LUAD tumors becoming more sensitive to immune checkpoint inhibitors? And if so, is the activation of TLR8 more prominent when the microbiome consists of TSB? Finding the answers to these questions could have major clinical implications, as most individuals diagnosed with NSCLC are not sensitive to immune checkpoint therapies [195].

In addition to investigating the therapeutic potential of modulating the microbiome into a TSB state, we can use bacteria to deliver therapies. Early investigators have used quorum sensing, i.e. the change in microbial diversity, to activate gene

expression [196]. Currently, the use of bacteria as delivery systems has expanded and some engineered bacteria are being used in clinical trials [197]. However, one of the limitations of using engineered bacteria is the tumor microenvironment, where not all microenvironments are conducive for all bacterial species. Fortunately, our 16S sequencing, and others, can help overcome these limitations. If we know the microbial profile of different types of cancers, then we can select the engineered bacteria based on the most abundant bacteria found in the profile. For example, 16S sequencing data shows *Rhizobiales* as the most upregulated bacteria taxa in LUAD microbiome [90]. With that knowledge, I would use *Rhizobiales* as my engineered drug delivery bacteria for treating LUAD as it is suggested to thrive in the LUAD microenvironment. Finally, several lung cancer risk factors, such as smoking and COPD, have also been shown to have an impact on the diversity in the lung microbiome [198, 199]. Interestingly, previous studies have suggested using the taxonomic profile of the lung microbiome as a predictor of lung cancer [89].

Overall, the findings presented in this thesis have expanded the knowledge of how nutritional availability impacts LUAD phenotypes and the interplay between LUAD and the microbiome. Given the lethality of LUAD, there is a great demand for improved screening techniques and alternative treatment. This work represents an essential step towards using nutrition and our own microbiome as ways to combat LUAD.

REFERENCE

1. Siegel, R.L., et al., Cancer statistics, 2023. *CA Cancer J Clin*, 2023. 73(1): p. 17-48.
2. Alberg, A.J., et al., Epidemiology of lung cancer: Diagnosis and management of lung cancer, 3rd ed: American College of Chest Physicians evidence-based clinical practice guidelines. *Chest*, 2013. 143(5 Suppl): p. e1S-e29S.
3. Schabath, M.B. and M.L. Cote, Cancer Progress and Priorities: Lung Cancer. *Cancer Epidemiol Biomarkers Prev*, 2019. 28(10): p. 1563-1579.
4. Goldstraw, P., et al., The IASLC Lung Cancer Staging Project: Proposals for Revision of the TNM Stage Groupings in the Forthcoming (Eighth) Edition of the TNM Classification for Lung Cancer. *J Thorac Oncol*, 2016. 11(1): p. 39-51.
5. Jonna, S. and D.S. Subramaniam, Molecular diagnostics and targeted therapies in non-small cell lung cancer (NSCLC): an update. *Discov Med*, 2019. 27(148): p. 167-170.
6. Riihimäki, M., et al., Metastatic sites and survival in lung cancer. *Lung Cancer*, 2014. 86(1): p. 78-84.
7. Denisenko, T.V., I.N. Budkevich, and B. Zhivotovsky, Cell death-based treatment of lung adenocarcinoma. *Cell Death Dis*, 2018. 9(2): p. 117.

8. Duma, N., R. Santana-Davila, and J.R. Molina, Non-Small Cell Lung Cancer: Epidemiology, Screening, Diagnosis, and Treatment. *Mayo Clin Proc*, 2019. 94(8): p. 1623-1640.
9. Vinod, S.K. and E. Hau, Radiotherapy treatment for lung cancer: Current status and future directions. *Respirology*, 2020. 25 Suppl 2: p. 61-71.
10. Lemjabbar-Alaoui, H., et al., Lung cancer: Biology and treatment options. *Biochim Biophys Acta*, 2015. 1856(2): p. 189-210.
11. Zheng, M., Classification and Pathology of Lung Cancer. *Surg Oncol Clin N Am*, 2016. 25(3): p. 447-68.
12. Hanahan, D. and R.A. Weinberg, Hallmarks of cancer: the next generation. *Cell*, 2011. 144(5): p. 646-74.
13. Hofer, S.J., et al., The ups and downs of caloric restriction and fasting: from molecular effects to clinical application. *EMBO Mol Med*, 2022. 14(1): p. e14418.
14. Colman, R.J., et al., Caloric restriction delays disease onset and mortality in rhesus monkeys. *Science*, 2009. 325(5937): p. 201-4.
15. Lee, C., et al., Fasting cycles retard growth of tumors and sensitize a range of cancer cell types to chemotherapy. *Science translational medicine*, 2012. 4(124): p. 124ra27-124ra27.
16. Eagle, H., Nutrition needs of mammalian cells in tissue culture. *Science*, 1955. 122(3168): p. 501-14.

17. Jain, M., et al., Metabolite profiling identifies a key role for glycine in rapid cancer cell proliferation. *Science*, 2012. 336(6084): p. 1040-4.
18. Buitrago, D., et al., Impact of DNA methylation on 3D genome structure. *Nature Communications*, 2021. 12(1): p. 3243.
19. Hediger, M.A., et al., The ABCs of membrane transporters in health and disease (SLC series): introduction. *Mol Aspects Med*, 2013. 34(2-3): p. 95-107.
20. Pizzagalli, M.D., A. Bensimon, and G. Superti-Furga, A guide to plasma membrane solute carrier proteins. *FEBS J*, 2021. 288(9): p. 2784-2835.
21. Cesar-Razquin, A., et al., A Call for Systematic Research on Solute Carriers. *Cell*, 2015. 162(3): p. 478-87.
22. Huang, F., et al., SLC34A2 Up-regulation And SLC4A4 Down-regulation Correlates With Invasion, Metastasis, And The MAPK Signaling Pathway In Papillary Thyroid Carcinomas. *J Cancer*, 2021. 12(18): p. 5439-5453.
23. Kikuchi, D., et al., Upregulated solute carrier family 37 member 1 in colorectal cancer is associated with poor patient outcome and metastasis. *Oncol Lett*, 2018. 15(2): p. 2065-2072.
24. Shen, L., et al., Upregulation of the solute carrier family 7 genes is indicative of poor prognosis in papillary thyroid carcinoma. *World J Surg Oncol*, 2018. 16(1): p. 235.
25. Sweet, R., A. Paul, and J. Zastre, Hypoxia induced upregulation and function of the thiamine transporter, SLC19A3 in a breast cancer cell line. *Cancer Biol Ther*, 2010. 10(11): p. 1101-11.

26. Scalise, M., et al., The Human SLC7A5 (LAT1): The Intriguing Histidine/Large Neutral Amino Acid Transporter and Its Relevance to Human Health. *Front Chem*, 2018. 6: p. 243.
27. Fotiadis, D., Y. Kanai, and M. Palacin, The SLC3 and SLC7 families of amino acid transporters. *Mol Aspects Med*, 2013. 34(2-3): p. 139-58.
28. Kanai, Y., et al., Expression Cloning and Characterization of a Transporter for Large Neutral Amino Acids Activated by the Heavy Chain of 4F2 Antigen (CD98)*. *Journal of Biological Chemistry*, 1998. 273(37): p. 23629-23632.
29. Yan, R., et al., Structure of the human LAT1-4F2hc heteromeric amino acid transporter complex. *Nature*, 2019. 568(7750): p. 127-130.
30. Nakamura, E., et al., 4F2 (CD98) heavy chain is associated covalently with an amino acid transporter and controls intracellular trafficking and membrane topology of 4F2 heterodimer. *J Biol Chem*, 1999. 274(5): p. 3009-16.
31. Christensen, H.N., Role of amino acid transport and countertransport in nutrition and metabolism. *Physiol Rev*, 1990. 70(1): p. 43-77.
32. Wang, Q. and J. Holst, L-type amino acid transport and cancer: targeting the mTORC1 pathway to inhibit neoplasia. *Am J Cancer Res*, 2015. 5(4): p. 1281-94.
33. Horita, Y., et al., Expression of LAT1 and 4F2hc in Gastroenteropancreatic Neuroendocrine Neoplasms. *In Vivo*, 2021. 35(4): p. 2425-2432.

34. Kaira, K., et al., Clinical significance of L-type amino acid transporter 1 expression as a prognostic marker and potential of new targeting therapy in biliary tract cancer. *BMC Cancer*, 2013. 13: p. 482.
35. Muto, Y., et al., Different Response Profiles of Gastrointestinal Cancer Cells to an L-Type Amino Acid Transporter Inhibitor, JPH203. *Anticancer Res*, 2019. 39(1): p. 159-165.
36. Ohshima, Y., et al., Efficacy of system l amino acid transporter 1 inhibition as a therapeutic target in esophageal squamous cell carcinoma. *Cancer Sci*, 2016. 107(10): p. 1499-1505.
37. Yanagida, O., et al., Human L-type amino acid transporter 1 (LAT1): characterization of function and expression in tumor cell lines. *Biochimica et Biophysica Acta (BBA) - Biomembranes*, 2001. 1514(2): p. 291-302.
38. Kaira, K., et al., Prognostic significance of L-type amino acid transporter 1 expression in resectable stage I-III nonsmall cell lung cancer. *Br J Cancer*, 2008. 98(4): p. 742-8.
39. Kaira, K., et al., Prognostic significance of L-type amino-acid transporter 1 expression in surgically resected pancreatic cancer. *Br J Cancer*, 2012. 107(4): p. 632-8.
40. Hayashi, K., et al., c-Myc is crucial for the expression of LAT1 in MIA Paca-2 human pancreatic cancer cells. *Oncol Rep*, 2012. 28(3): p. 862-6.
41. Duffy, M.J., et al., MYC as a target for cancer treatment. *Cancer Treat Rev*, 2021. 94: p. 102154.

42. Dosier, L.B.M., et al., Antagonists of the system L neutral amino acid transporter (LAT) promote endothelial adhesivity of human red blood cells. *Thromb Haemost*, 2017. 117(7): p. 1402-1411.
43. Fraga, S., M.P. Serrao, and P. Soares-da-Silva, L-type amino acid transporters in two intestinal epithelial cell lines function as exchangers with neutral amino acids. *J Nutr*, 2002. 132(4): p. 733-8.
44. Kim, D.K., et al., Characterization of the system L amino acid transporter in T24 human bladder carcinoma cells. *Biochim Biophys Acta*, 2002. 1565(1): p. 112-21.
45. Kim, C.S., et al., BCH, an inhibitor of system L amino acid transporters, induces apoptosis in cancer cells. *Biol Pharm Bull*, 2008. 31(6): p. 1096-100.
46. Liang, Z., et al., Potential Biomarker of L-type Amino Acid Transporter 1 in Breast Cancer Progression. *Nucl Med Mol Imaging*, 2011. 45(2): p. 93-102.
47. Nicklin, P., et al., Bidirectional transport of amino acids regulates mTOR and autophagy. *Cell*, 2009. 136(3): p. 521-34.
48. Wang, Q., et al., Androgen receptor and nutrient signaling pathways coordinate the demand for increased amino acid transport during prostate cancer progression. *Cancer Res*, 2011. 71(24): p. 7525-36.
49. Hua, H., et al., Targeting mTOR for cancer therapy. *J Hematol Oncol*, 2019. 12(1): p. 71.
50. Wolfson, R.L., et al., Sestrin2 is a leucine sensor for the mTORC1 pathway. *Science*, 2016. 351(6268): p. 43-8.

51. Valenstein, M.L., et al., Structure of the nutrient-sensing hub GATOR2. *Nature*, 2022. 607(7919): p. 610-616.
52. Sahu, U. and I. Ben-Sahra, GATOR2 rings GATOR1 to speak to mTORC1. *Mol Cell*, 2023. 83(1): p. 6-8.
53. Kim, J. and K.L. Guan, mTOR as a central hub of nutrient signalling and cell growth. *Nat Cell Biol*, 2019. 21(1): p. 63-71.
54. Gu, X., et al., SAMTOR is an S-adenosylmethionine sensor for the mTORC1 pathway. *Science*, 2017. 358(6364): p. 813-818.
55. Altorki, N.K., et al., The lung microenvironment: an important regulator of tumour growth and metastasis. *Nat Rev Cancer*, 2019. 19(1): p. 9-31.
56. Hinshaw, D.C. and L.A. Shevde, The Tumor Microenvironment Innately Modulates Cancer Progression. *Cancer Res*, 2019. 79(18): p. 4557-4566.
57. Wu, F., et al., Single-cell profiling of tumor heterogeneity and the microenvironment in advanced non-small cell lung cancer. *Nat Commun*, 2021. 12(1): p. 2540.
58. Hao, N.B., et al., Macrophages in tumor microenvironments and the progression of tumors. *Clin Dev Immunol*, 2012. 2012: p. 948098.
59. Najafi, M., B. Farhood, and K. Mortezaee, Extracellular matrix (ECM) stiffness and degradation as cancer drivers. *J Cell Biochem*, 2019. 120(3): p. 2782-2790.
60. Bonnans, C., J. Chou, and Z. Werb, Remodelling the extracellular matrix in development and disease. *Nat Rev Mol Cell Biol*, 2014. 15(12): p. 786-801.

61. Kosibaty, Z., et al., ECT2 promotes lung adenocarcinoma progression through extracellular matrix dynamics and focal adhesion signaling. *Cancer Sci*, 2021. 112(2): p. 703-714.
62. Katara, G.K., et al., Mammary epithelium-specific inactivation of V-ATPase reduces stiffness of extracellular matrix and enhances metastasis of breast cancer. *Mol Oncol*, 2018. 12(2): p. 208-223.
63. Kim, D., et al., Identification and Characterization of Cancer-Associated Fibroblast Subpopulations in Lung Adenocarcinoma. *Cancers (Basel)*, 2022. 14(14).
64. Navab, R., et al., Prognostic gene-expression signature of carcinoma-associated fibroblasts in non-small cell lung cancer. *Proc Natl Acad Sci U S A*, 2011. 108(17): p. 7160-5.
65. Piersma, B., M.K. Hayward, and V.M. Weaver, Fibrosis and cancer: A strained relationship. *Biochim Biophys Acta Rev Cancer*, 2020. 1873(2): p. 188356.
66. Saforo, D., et al., Primary lung cancer samples cultured under microenvironment-mimetic conditions enrich for mesenchymal stem-like cells that promote metastasis. *Sci Rep*, 2019. 9(1): p. 4177.
67. Liao, Z., et al., Cancer-associated fibroblasts in tumor microenvironment - Accomplices in tumor malignancy. *Cell Immunol*, 2019. 343: p. 103729.
68. Knight, R., et al., The Microbiome and Human Biology. *Annu Rev Genomics Hum Genet*, 2017. 18: p. 65-86.

69. Sender, R., S. Fuchs, and R. Milo, Revised Estimates for the Number of Human and Bacteria Cells in the Body. *PLoS Biol*, 2016. 14(8): p. e1002533.
70. Davenport, E.R., et al., The human microbiome in evolution. *BMC Biol*, 2017. 15(1): p. 127.
71. Gomaa, E.Z., Human gut microbiota/microbiome in health and diseases: a review. *Antonie Van Leeuwenhoek*, 2020. 113(12): p. 2019-2040.
72. Hooper, L.V., et al., Molecular analysis of commensal host-microbial relationships in the intestine. *Science*, 2001. 291(5505): p. 881-4.
73. den Besten, G., et al., The role of short-chain fatty acids in the interplay between diet, gut microbiota, and host energy metabolism. *J Lipid Res*, 2013. 54(9): p. 2325-40.
74. Clemente, J.C., et al., The impact of the gut microbiota on human health: an integrative view. *Cell*, 2012. 148(6): p. 1258-70.
75. Umesaki, Y., et al., Expansion of alpha beta T-cell receptor-bearing intestinal intraepithelial lymphocytes after microbial colonization in germ-free mice and its independence from thymus. *Immunology*, 1993. 79(1): p. 32-7.
76. Hapfelmeier, S., et al., Reversible microbial colonization of germ-free mice reveals the dynamics of IgA immune responses. *Science*, 2010. 328(5986): p. 1705-9.
77. Gopalakrishnan, V., et al., The Influence of the Gut Microbiome on Cancer, Immunity, and Cancer Immunotherapy. *Cancer Cell*, 2018. 33(4): p. 570-580.
78. Jin, C., et al., Commensal Microbiota Promote Lung Cancer Development via $\gamma\delta$ T Cells. *Cell*, 2019. 176(5): p. 998-1013.e16.

79. de Martel, C., et al., Global burden of cancer attributable to infections in 2018: a worldwide incidence analysis. *Lancet Glob Health*, 2020. 8(2): p. e180-e190.
80. Sepich-Poore, G.D., et al., The microbiome and human cancer. *Science*, 2021. 371(6536).
81. Varon, C., et al., Helicobacters and cancer, not only gastric cancer? *Semin Cancer Biol*, 2022. 86(Pt 2): p. 1138-1154.
82. Cullin, N., et al., Microbiome and cancer. *Cancer Cell*, 2021. 39(10): p. 1317-1341.
83. Zella, D. and R.C. Gallo, Viruses and Bacteria Associated with Cancer: An Overview. *Viruses*, 2021. 13(6).
84. Peek, R.M., Jr. and J.E. Crabtree, Helicobacter infection and gastric neoplasia. *J Pathol*, 2006. 208(2): p. 233-48.
85. Yin, H., et al., Fusobacterium nucleatum promotes liver metastasis in colorectal cancer by regulating the hepatic immune niche and altering gut microbiota. *Aging (Albany NY)*, 2022. 14(4): p. 1941-1958.
86. Zhang, S., et al., Fusobacterium nucleatum promotes epithelial-mesenchymal transition through regulation of the lncRNA MIR4435-2HG/miR-296-5p/Akt2/SNAI1 signaling pathway. *Febs j*, 2020. 287(18): p. 4032-4047.
87. Bossuet-Greif, N., et al., The Colibactin Genotoxin Generates DNA Interstrand Cross-Links in Infected Cells. *mBio*, 2018. 9(2).

88. Pleguezuelos-Manzano, C., et al., Mutational signature in colorectal cancer caused by genotoxic pks(+) *E. coli*. *Nature*, 2020. 580(7802): p. 269-273.
89. Marshall, E.A., et al., Distinct bronchial microbiome precedes clinical diagnosis of lung cancer. *Mol Cancer*, 2022. 21(1): p. 68.
90. Vega, A.A., et al., Methionine-producing tumor micro(bi) environment fuels growth of solid tumors. *Cell Oncol (Dordr)*, 2023.
91. Simone, B.A., et al., Selectively starving cancer cells through dietary manipulation: methods and clinical implications. *Future Oncol*, 2013. 9(7): p. 959-76.
92. Malin, D., et al., Methionine restriction exposes a targetable redox vulnerability of triple-negative breast cancer cells by inducing thioredoxin reductase. *Breast Cancer Res Treat*, 2021. 190(3): p. 373-387.
93. Rajanala, S.H., R. Ringquist, and V.L. Cryns, Methionine restriction activates the integrated stress response in triple-negative breast cancer cells by a GCN2- and PERK-independent mechanism. *Am J Cancer Res*, 2019. 9(8): p. 1766-1775.
94. Strekalova, E., et al., Preclinical Breast Cancer Models to Investigate Metabolic Priming by Methionine Restriction. *Methods Mol Biol*, 2019. 1866: p. 61-73.
95. Lu, S., et al., Methionine restriction selectively targets thymidylate synthase in prostate cancer cells. *Biochem Pharmacol*, 2003. 66(5): p. 791-800.
96. Lu, S., et al., Methionine restriction induces apoptosis of prostate cancer cells via the c-Jun N-terminal kinase-mediated signaling pathway. *Cancer Lett*, 2002. 179(1): p. 51-8.

97. Poirson-Bichat, F., et al., Growth of methionine-dependent human prostate cancer (PC-3) is inhibited by ethionine combined with methionine starvation. *Br J Cancer*, 1997. 75(11): p. 1605-12.
98. Ding, L., et al., Somatic mutations affect key pathways in lung adenocarcinoma. *Nature*, 2008. 455(7216): p. 1069-1075.
99. Hanahan, D. and Robert A. Weinberg, Hallmarks of Cancer: The Next Generation. *Cell*, 2011. 144(5): p. 646-674.
100. Garcia-Bermudez, J., et al., Targeting extracellular nutrient dependencies of cancer cells. *Molecular metabolism*, 2020. 33: p. 67-82.
101. Colas, C., P.M.-U. Ung, and A. Schlessinger, SLC Transporters: Structure, Function, and Drug Discovery. *MedChemComm*, 2016. 7(6): p. 1069-1081.
102. Weiss, H.J. and S. Angiari, Metabolite Transporters as Regulators of Immunity. *Metabolites*, 2020. 10(10).
103. Fotiadis, D., Y. Kanai, and M. Palacín, The SLC3 and SLC7 families of amino acid transporters. *Molecular Aspects of Medicine*, 2013. 34(2): p. 139-158.
104. Schaller, L. and V.M. Lauschke, The genetic landscape of the human solute carrier (SLC) transporter superfamily. *Human genetics*, 2019. 138(11-12): p. 1359-1377.
105. Kaira, K., et al., Clinical significance of L-type amino acid transporter 1 expression as a prognostic marker and potential of new targeting therapy in biliary tract cancer. *BMC cancer*, 2013. 13: p. 482-482.

106. Bhutia, Y.D., et al., Amino Acid Transporters in Cancer and Their Relevance to “Glutamine Addiction”: Novel Targets for the Design of a New Class of Anticancer Drugs. *Cancer Research*, 2015. 75(9): p. 1782-1788.
107. Scalise, M., et al., The Human SLC7A5 (LAT1): The Intriguing Histidine/Large Neutral Amino Acid Transporter and Its Relevance to Human Health. *Frontiers in Chemistry*, 2018. 6(243).
108. Kaira, K., et al., l-type amino acid transporter 1 and CD98 expression in primary and metastatic sites of human neoplasms. *Cancer Science*, 2008. 99(12): p. 2380-2386.
109. Altan, B., et al., Relationship between LAT1 expression and resistance to chemotherapy in pancreatic ductal adenocarcinoma. *Cancer Chemotherapy and Pharmacology*, 2018. 81(1): p. 141-153.
110. Simner, C., et al., DNA methylation of amino acid transporter genes in the human placenta. *Placenta*, 2017. 60: p. 64-73.
111. Cha, Y.J., E.-S. Kim, and J.S. Koo, Amino Acid Transporters and Glutamine Metabolism in Breast Cancer. *International journal of molecular sciences*, 2018. 19(3): p. 907.
112. Schmidt, J.A., et al., Plasma concentrations and intakes of amino acids in male meat-eaters, fish-eaters, vegetarians and vegans: a cross-sectional analysis in the EPIC-Oxford cohort. *European Journal of Clinical Nutrition*, 2016. 70(3): p. 306-312.
113. Neuman, R.E. and T.A. McCoy, Dual requirement of Walker carcinosarcoma 256 in vitro for asparagine and glutamine. *Science*, 1956. 124(3212): p. 124-5.

114. Han, F., et al., The critical role of AMPK in driving Akt activation under stress, tumorigenesis and drug resistance. *Nat Commun*, 2018. 9(1): p. 4728.
115. Wang, X. and C.G. Proud, The mTOR pathway in the control of protein synthesis. *Physiology (Bethesda)*, 2006. 21: p. 362-9.
116. Beaumatin, F., et al., mTORC1 Activation Requires DRAM-1 by Facilitating Lysosomal Amino Acid Efflux. *Mol Cell*, 2019. 76(1): p. 163-176 e8.
117. Milkereit, R., et al., LAPT4b recruits the LAT1-4F2hc Leu transporter to lysosomes and promotes mTORC1 activation. *Nat Commun*, 2015. 6: p. 7250.
118. Kim, S.M., et al., PTEN Deficiency and AMPK Activation Promote Nutrient Scavenging and Anabolism in Prostate Cancer Cells. *Cancer Discov*, 2018. 8(7): p. 866-883.
119. Commisso, C., et al., Macropinocytosis of protein is an amino acid supply route in Ras-transformed cells. *Nature*, 2013. 497(7451): p. 633-7.
120. Roberts, T.M., et al., Identification and Characterisation of a pH-stable GFP. *Sci Rep*, 2016. 6: p. 28166.
121. Le, A.H. and L.M. Machesky, Image-based Quantification of Macropinocytosis Using Dextran Uptake into Cultured Cells. *Bio Protoc*, 2022. 12(7): p. e4367.
122. Halpern, B.C., et al., Effect of methionine replacement by homocystine in cultures containing both malignant rat breast carcinosarcoma (Walker-256) cells and normal adult rat liver fibroblasts. *In Vitro*, 1975. 11(1): p. 14-9.

123. Jeon, H., et al., Methionine deprivation suppresses triple-negative breast cancer metastasis in vitro and in vivo. *Oncotarget*, 2016. 7(41): p. 67223-67234.
124. Gao, X., et al., Dietary methionine influences therapy in mouse cancer models and alters human metabolism. *Nature*, 2019. 572(7769): p. 397-401.
125. Zhou, L., Z. Chen, and C. Liu, Identification and verification of the role of crucial genes through which methionine restriction inhibits the progression of colon cancer cells. *Oncol Lett*, 2022. 24(2): p. 274.
126. Miousse, I.R., et al., Modulation of dietary methionine intake elicits potent, yet distinct, anticancer effects on primary versus metastatic tumors. *Carcinogenesis*, 2018. 39(9): p. 1117-1126.
127. Choi, J.K., et al., Cross-talk between cancer and *Pseudomonas aeruginosa* mediates tumor suppression. *Commun Biol*, 2023. 6(1): p. 16.
128. Narunsky-Haziza, L., et al., Pan-cancer analyses reveal cancer-type-specific fungal ecologies and bacteriome interactions. *Cell*, 2022. 185(20): p. 3789-3806 e17.
129. Fu, A., et al., Tumor-resident intracellular microbiota promotes metastatic colonization in breast cancer. *Cell*, 2022. 185(8): p. 1356-1372 e26.
130. Canale, F.P., et al., Metabolic modulation of tumours with engineered bacteria for immunotherapy. *Nature*, 2021. 598(7882): p. 662-666.
131. Silhavy, T.J., D. Kahne, and S. Walker, The bacterial cell envelope. *Cold Spring Harb Perspect Biol*, 2010. 2(5): p. a000414.

132. Medzhitov, R., Toll-like receptors and innate immunity. *Nat Rev Immunol*, 2001. 1(2): p. 135-45.
133. Chen, X., et al., MiR-140-5p/TLR4 /NF-kappaB signaling pathway: Crucial role in inflammatory response in 16HBE cells induced by dust fall PM(2.5). *Ecotoxicol Environ Saf*, 2021. 208: p. 111414.
134. Ciesielska, A., M. Matyjek, and K. Kwiatkowska, TLR4 and CD14 trafficking and its influence on LPS-induced pro-inflammatory signaling. *Cell Mol Life Sci*, 2021. 78(4): p. 1233-1261.
135. Zamyatina, A. and H. Heine, Lipopolysaccharide Recognition in the Crossroads of TLR4 and Caspase-4/11 Mediated Inflammatory Pathways. *Front Immunol*, 2020. 11: p. 585146.
136. He, W., et al., TLR4 signaling promotes immune escape of human lung cancer cells by inducing immunosuppressive cytokines and apoptosis resistance. *Mol Immunol*, 2007. 44(11): p. 2850-9.
137. Dobin, A., et al., STAR: ultrafast universal RNA-seq aligner. *Bioinformatics*, 2013. 29(1): p. 15-21.
138. Trapnell, C., et al., Differential gene and transcript expression analysis of RNA-seq experiments with TopHat and Cufflinks. *Nat Protoc*, 2012. 7(3): p. 562-78.
139. Love, M.I., W. Huber, and S. Anders, Moderated estimation of fold change and dispersion for RNA-seq data with DESeq2. *Genome Biology*, 2014. 15.

140. Yu, G., et al., clusterProfiler: an R package for comparing biological themes among gene clusters. OMICS, 2012. 16(5): p. 284-7.
141. Vicent, S., et al., ERK1/2 is activated in non-small-cell lung cancer and associated with advanced tumours. Br J Cancer, 2004. 90(5): p. 1047-52.
142. Mendoza, M.C., E.E. Er, and J. Blenis, The Ras-ERK and PI3K-mTOR pathways: cross-talk and compensation. Trends Biochem Sci, 2011. 36(6): p. 320-8.
143. Ehmer, U. and J. Sage, Control of Proliferation and Cancer Growth by the Hippo Signaling Pathway. Mol Cancer Res, 2016. 14(2): p. 127-40.
144. Akrida, I., V. Bravou, and H. Papadaki, The deadly cross-talk between Hippo pathway and epithelial-mesenchymal transition (EMT) in cancer. Mol Biol Rep, 2022. 49(10): p. 10065-10076.
145. Rebe, C. and F. Ghiringhelli, Interleukin-1beta and Cancer. Cancers (Basel), 2020. 12(7).
146. Rossol, M., et al., LPS-induced cytokine production in human monocytes and macrophages. Crit Rev Immunol, 2011. 31(5): p. 379-446.
147. Wu, X., et al., Lipopolysaccharide promotes metastasis via acceleration of glycolysis by the nuclear factor-kappaB/snail/hexokinase3 signaling axis in colorectal cancer. Cancer Metab, 2021. 9(1): p. 23.
148. Szajnik, M., et al., TLR4 signaling induced by lipopolysaccharide or paclitaxel regulates tumor survival and chemoresistance in ovarian cancer. Oncogene, 2009. 28(49): p. 4353-63.

149. Zhang, D., et al., Modified apple polysaccharides suppress the migration and invasion of colorectal cancer cells induced by lipopolysaccharide. *Nutr Res*, 2013. 33(10): p. 839-48.
150. Liu, X., et al., NADPH oxidase 1-dependent ROS is crucial for TLR4 signaling to promote tumor metastasis of non-small cell lung cancer. *Tumour Biol*, 2015. 36(3): p. 1493-502.
151. Liu, W.T., et al., Toll like receptor 4 facilitates invasion and migration as a cancer stem cell marker in hepatocellular carcinoma. *Cancer Lett*, 2015. 358(2): p. 136-143.
152. Li, J., et al., TLR4 Promotes Breast Cancer Metastasis via Akt/GSK3beta/beta-Catenin Pathway upon LPS Stimulation. *Anat Rec (Hoboken)*, 2017. 300(7): p. 1219-1229.
153. Perrin-Cocon, L., et al., Toll-like Receptor 4-Induced Glycolytic Burst in Human Monocyte-Derived Dendritic Cells Results from p38-Dependent Stabilization of HIF-1alpha and Increased Hexokinase II Expression. *J Immunol*, 2018. 201(5): p. 1510-1521.
154. Yang, X., et al., TLR4 promotes the expression of HIF-1alpha by triggering reactive oxygen species in cervical cancer cells in vitro-implications for therapeutic intervention. *Mol Med Rep*, 2018. 17(2): p. 2229-2238.
155. Vallance, T.M., et al., Toll-Like Receptor 4 Signalling and Its Impact on Platelet Function, Thrombosis, and Haemostasis. *Mediators Inflamm*, 2017. 2017: p. 9605894.

156. Richard, D.E., et al., p42/p44 mitogen-activated protein kinases phosphorylate hypoxia-inducible factor 1alpha (HIF-1alpha) and enhance the transcriptional activity of HIF-1. *J Biol Chem*, 1999. 274(46): p. 32631-7.
157. Lehr, S., et al., Identification of major ERK-related phosphorylation sites in Gab1. *Biochemistry*, 2004. 43(38): p. 12133-40.
158. Kayahara, M., X. Wang, and C. Tournier, Selective regulation of c-jun gene expression by mitogen-activated protein kinases via the 12-o-tetradecanoylphorbol-13-acetate- responsive element and myocyte enhancer factor 2 binding sites. *Mol Cell Biol*, 2005. 25(9): p. 3784-92.
159. Wipf, P., et al., Synthesis of anti-inflammatory alpha-and beta-linked acetamidopyranosides as inhibitors of toll-like receptor 4 (TLR4). *Tetrahedron Lett*, 2015. 56(23): p. 3097-3100.
160. Miao, H., et al., Stearic acid induces proinflammatory cytokine production partly through activation of lactate-HIF1alpha pathway in chondrocytes. *Sci Rep*, 2015. 5: p. 13092.
161. Hu, X., et al., Toll-like receptor 4 is a master regulator for colorectal cancer growth under high-fat diet by programming cancer metabolism. *Cell Death Dis*, 2021. 12(8): p. 791.
162. Rodriguez, B.V. and M.J. Kuehn, *Staphylococcus aureus* secretes immunomodulatory RNA and DNA via membrane vesicles. *Sci Rep*, 2020. 10(1): p. 18293.

163. Pandey, S., T. Kawai, and S. Akira, Microbial sensing by Toll-like receptors and intracellular nucleic acid sensors. *Cold Spring Harb Perspect Biol*, 2014. 7(1): p. a016246.
164. Flemer, B., et al., Tumour-associated and non-tumour-associated microbiota in colorectal cancer. *Gut*, 2017. 66(4): p. 633-643.
165. Vaupel, P., H. Schmidberger, and A. Mayer, The Warburg effect: essential part of metabolic reprogramming and central contributor to cancer progression. *Int J Radiat Biol*, 2019. 95(7): p. 912-919.
166. Sonveaux, P., et al., Targeting lactate-fueled respiration selectively kills hypoxic tumor cells in mice. *J Clin Invest*, 2008. 118(12): p. 3930-42.
167. Canale, F.P., et al., Metabolic modulation of tumours with engineered bacteria for immunotherapy. *Nature*, 2021.
168. Gong, W.J., et al., Resistin facilitates metastasis of lung adenocarcinoma through the TLR4/Src/EGFR/PI3K/NF-kappaB pathway. *Cancer Sci*, 2018. 109(8): p. 2391-2400.
169. Nyati, K.K., et al., TLR4-induced NF-kappaB and MAPK signaling regulate the IL-6 mRNA stabilizing protein Arid5a. *Nucleic Acids Res*, 2017. 45(5): p. 2687-2703.
170. Lee, G.L., et al., TLR4-Activated MAPK-IL-6 Axis Regulates Vascular Smooth Muscle Cell Function. *Int J Mol Sci*, 2016. 17(9).
171. Wang, W., et al., Role of TLR4-p38 MAPK-Hsp27 signal pathway in LPS-induced pulmonary epithelial hyperpermeability. *BMC Pulm Med*, 2018. 18(1): p. 178.

172. Weiss, A.S., et al., In vitro interaction network of a synthetic gut bacterial community. *ISME J*, 2022. 16(4): p. 1095-1109.
173. Tessema, M., et al., Common cancer-driver mutations and their association with abnormally methylated genes in lung adenocarcinoma from never-smokers. *Lung Cancer*, 2018. 123: p. 99-106.
174. Blaha, C.S., et al., A non-catalytic scaffolding activity of hexokinase 2 contributes to EMT and metastasis. *Nat Commun*, 2022. 13(1): p. 899.
175. Zhang, C., et al., GSK3 β inhibits epithelial-mesenchymal transition via the Wnt/ β -catenin and PI3K/Akt pathways. *Int J Ophthalmol*, 2018. 11(7): p. 1120-1128.
176. Zhou, B.P., et al., Dual regulation of Snail by GSK-3 β -mediated phosphorylation in control of epithelial-mesenchymal transition. *Nat Cell Biol*, 2004. 6(10): p. 931-40.
177. Park, S.Y., et al., Snail1 is stabilized by O-GlcNAc modification in hyperglycaemic condition. *EMBO J*, 2010. 29(22): p. 3787-96.
178. Blount, B.C., et al., Folate deficiency causes uracil misincorporation into human DNA and chromosome breakage: implications for cancer and neuronal damage. *Proc Natl Acad Sci U S A*, 1997. 94(7): p. 3290-5.
179. Heydt, C., et al., Novel approaches against epidermal growth factor receptor tyrosine kinase inhibitor resistance. *Oncotarget*, 2018. 9(20): p. 15418-15434.
180. Kapalczynska, M., et al., 2D and 3D cell cultures - a comparison of different types of cancer cell cultures. *Arch Med Sci*, 2018. 14(4): p. 910-919.

181. Kaczmarczyk, J.A., et al., Comparative microsomal proteomics of a model lung cancer cell line NCI-H23 reveals distinct differences between molecular profiles of 3D and 2D cultured cells. *Oncotarget*, 2021. 12(20): p. 2022-2038.
182. Duval, K., et al., Modeling Physiological Events in 2D vs. 3D Cell Culture. *Physiology (Bethesda)*, 2017. 32(4): p. 266-277.
183. Eberl, C., et al., Reproducible Colonization of Germ-Free Mice With the Oligo-Mouse-Microbiota in Different Animal Facilities. *Front Microbiol*, 2019. 10: p. 2999.
184. Brugiroux, S., et al., Genome-guided design of a defined mouse microbiota that confers colonization resistance against *Salmonella enterica* serovar Typhimurium. *Nat Microbiol*, 2016. 2: p. 16215.
185. Nejman, D., et al., The human tumor microbiome is composed of tumor type-specific intracellular bacteria. *Science*, 2020. 368(6494): p. 973-980.
186. Urbaniak, C., et al., The Microbiota of Breast Tissue and Its Association with Breast Cancer. *Appl Environ Microbiol*, 2016. 82(16): p. 5039-48.
187. Xu, C., Y. Zhao, and B. Zhao, The interaction of azurin and C-terminal domain of p53 is mediated by nucleic acids. *Arch Biochem Biophys*, 2010. 503(2): p. 223-9.
188. Jacouton, E., et al., Probiotic Strain *Lactobacillus casei* BL23 Prevents Colitis-Associated Colorectal Cancer. *Front Immunol*, 2017. 8: p. 1553.
189. Tiptiri-Kourpeti, A., et al., *Lactobacillus casei* Exerts Anti-Proliferative Effects Accompanied by Apoptotic Cell Death and Up-Regulation of TRAIL in Colon Carcinoma Cells. *PLoS One*, 2016. 11(2): p. e0147960.

190. Ghanavati, R., et al., Inhibitory effects of Lactobacilli cocktail on HT-29 colon carcinoma cells growth and modulation of the Notch and Wnt/beta-catenin signaling pathways. *Microb Pathog*, 2020. 139: p. 103829.
191. Peters, C., D. Kabelitz, and D. Wesch, Regulatory functions of gammadelta T cells. *Cell Mol Life Sci*, 2018. 75(12): p. 2125-2135.
192. Ye, J., et al., Tumor-derived gammadelta regulatory T cells suppress innate and adaptive immunity through the induction of immunosenescence. *J Immunol*, 2013. 190(5): p. 2403-14.
193. Ye, J., et al., Human regulatory T cells induce T-lymphocyte senescence. *Blood*, 2012. 120(10): p. 2021-31.
194. Cervantes, J.L., et al., TLR8: the forgotten relative revindicated. *Cell Mol Immunol*, 2012. 9(6): p. 434-8.
195. Carbognin, L., et al., Differential Activity of Nivolumab, Pembrolizumab and MPDL3280A according to the Tumor Expression of Programmed Death-Ligand-1 (PD-L1): Sensitivity Analysis of Trials in Melanoma, Lung and Genitourinary Cancers. *PLoS One*, 2015. 10(6): p. e0130142.
196. Danino, T., et al., A synchronized quorum of genetic clocks. *Nature*, 2010. 463(7279): p. 326-30.
197. Wu, L., et al., Bacterially mediated drug delivery and therapeutics: Strategies and advancements. *Adv Drug Deliv Rev*, 2022. 187: p. 114363.

198. Campos, M., et al., Lower respiratory tract microbiome composition and community interactions in smokers. *Access Microbiol*, 2023. 5(3).
199. Mammen, M.J. and S. Sethi, COPD and the microbiome. *Respirology*, 2016. 21(4): p. 590-9.

CURRICULUM VITAE

Alexis Avidan Vega

744 East Madison Street. APT 744A

Louisville, KY 40202

Alexis.vega@louisville.edu

EDUCATION

- 2012-2014 B.S. in Biotechnology, Florida Gulf Coast University, Fort Myers, FL
- 2016-2018 M.S. in Biochemistry and Molecular Genetics, University of Louisville
School of Medicine, Louisville, KY
- 2018-2023 Ph.D. in Biochemistry and Molecular Genetics, University of Louisville
School of Medicine, Louisville, KY

PROFESSIONAL EXPERIENCE

- 2016-2018 Laboratory Technician I, University of Louisville School of Medicine,
Louisville, KY

ADDITIONAL TRAINING

- June 2021 Mentoring Academy, University of Louisville School of Medicine
- Jan 2023 UCSC Genome Browser Workshop

RESEARCH EXPERIENCE

- 2013-2014 Undergraduate Research Assistant – Investigating the relevance of sex on acquisition of MRSA strains, Mentor: Jan DeJarnette, Ph.D.
- 2016-2018 Graduate Research Assistant – Functional consequences of PSAT1 association on PKM2’s inherent enzymatic activity, Mentor: Brian F. Clem Ph.D.
- Fall 2018 Lab Rotation I – Investigating the effects of DZA on acute myeloid leukemia and hematopoietic cell differentiation.
- Spring 2019 Lab Rotation II – Investigating ceramide metabolism in nCDase KO mouse kidneys, Mentor: Leah J. Siskind, Ph.D.
- 2019-2023 Graduate Student – Understanding the crosstalk between LUAD, nutrient availability, and the microbiome, Mentor: Levi J. Beverly, Ph.D.

MEMBERSHIPS AND ACTIVITIES

- 2017 Louisville Regional Science Fair Judge, Louisville, KY
- 2018 Louisville Regional Science Fair Judge, Louisville, KY
- 2020-2023 Big Brothers and Big Sisters of Kentuckiana
- 2021-2023 American Society for Biochemistry and Molecular Biology (ASBMB)

HONORS AND AWARDS

- 2017 Graduate Student Council Research Award
- 2018 Graduate Student Council Travel Award
- 2018 IPIBS Fellowship, University of Louisville School of Medicine

PEER REVIEWED RESEARCH PUBLICATIONS

1. **Vega, A.A.**, Marshall, E.A., Noonan, A.J.C., Filho., F.S.L., Yang, J., Stewart, G.L., Johnson, F.D., Vucic, E.A., Pewarchuk, M.E., Shah, P.P., Clem, B.F., Nislow, C., Lam, S., Lockwood, W.W., Hallam, S.J., Leung, J.M., Beverly, L.J., Lam, W.L. Methionine-producing tumor micro(be) environment fuels growth of solid tumors. *Cellular Oncology* (2023).
2. Sears, S.M., **Vega, A.A.**, Kurlawala, Z., Oropilla, G.B., Krueger, A., Shah, P.P., Doll, M.A., Miller, R., Beverly, L.J., Siskind, L.J. F4/80^{hi} Resident Macrophages Contribute to Cisplatin-Induced Renal Fibrosis. *Kidney360* (2022).
3. Sears, S.M., Dupre, T.V., Shah, P.P., Davis, D.L., Doll, M.A., Sharp, C.N., **Vega, A.A.**, Megyesi, J., Beverly, L.J., Snider, A.J., Obeid, L.M., Hannun, Y.A., Siskind, L.J. Neutral Ceramidase Deficiency Protects Against Cisplatin-Induced Acute Kidney Injury. *J Lipid Res.* (2022).
4. Sears, S.M., Feng, J.L., Orwick, A., **Vega, A.A.**, Krueger, A.M., Shah, P.P., Doll, M.A., Beverly, L.J., Siskind, L.J. Pharmacological Inhibitors of Autophagy Have Opposite Effects in Acute and Chronic Cisplatin-Induced Kidney Injury. *Am J Physiol Renal Physiol* (2022).
5. Doll, M.A., Ray, A.R., Salazar-Gonzalez, R.A., Shah, P.P., **Vega, A.A.**, Sears, S.M., Krueger, A.M., Hong, K.U., Beverly, L.J., Hein, D.W. Deletion of Arylamine N-acetyltransferase 1 in MDA-MB-231 Human Breast Cancer Cells

Reduces Primary and Secondary Tumor Growth in vivo with No Significant Effects on Metastasis. *Mol Carcinog* (2022).

6. Shah, P.P., Saurabh, K., Kurlawala, Z., **Vega, A.A.**, Siskind, L.J., Beverly, L.J. Towards a Molecular Understanding of the Overlapping and Distinct Roles of UBQLN1 and UBQLN2 in Lung Cancer Progression and Metastasis. *Neoplasia* (2022).
7. Barve, A., **Vega, A.**, Shah, P.P., Ghare, S., Casson, L., Wundelrich, M., Siskind, L.J., Beverly, L.J. Perturbation of Methionine/S-adenosylmethionine Metabolism as a Novel Vulnerability in MLL Rearranged Leukemia. *Cells* (2019).

POSTER

Barve, A., Ghare, S., Shah, C., Wunderlich, M., Mulloy, J., Shah P., **Vega, A.**, Beverly, L. Alterations to methionine/S-adenosylmethionine metabolism regulate DOT1L expression and function; a novel vulnerability in MLL fusion leukemia. April 2019. 14th Midwest Blood Club Meeting, St. Jude Children's Research Hospital, Memphis, TN.

Vega, A.A., Shah, P.P., Beverly, L.J. The benefits of methionine restriction on lung cancer. August 2019. Biochemistry and Molecular Genetics Retreat, Louisville Zoo, Louisville, KY.

Vega, A.A., Shah, P.P., Beverly, L.J. The benefits of methionine restriction on lung cancer. September 2021. Research!Louisville, University of Louisville School of Medicine, Louisville, KY.

Eckert, R.L., **Vega, A.A.**, Shah, P.P., Beverly, L.J. The role of UBQLN in survival under nutrient deprivation. September 2021. Research!Louisville, University of Louisville School of Medicine, Louisville, KY.

Sears, S., **Vega, A.**, Doll, M., Beverly, L., Siskind, L. F4/80^{hi} resident macrophages contribute to cisplatin-induced kidney fibrosis and M2 polarization in C57BL/6 Mice. September 2021. Research!Louisville, University of Louisville School of Medicine, Louisville, KY.

Shah P.P., **Vega, A.**, Barve, A., Sears, S., Casson, L., Thomas S., Beverly, L.J. Classification of a new gene that blocks breast cancer metastasis. September 2021. Research!Louisville, University of Louisville School of Medicine, Louisville, KY.

Sears S., Feng, J., Orwick, A., **Vega, A.**, Krueger, A., Shah, P., Doll, M., Beverly L., Siskind, L. Paradoxical roles of autophagy highlight biological differences between acute and chronic cisplatin-induced kidney injury.

Vega, A.A., Shah, P.P., Casson, L., Beverly, L.J. Nutrient Transport Inhibition Leads to Induction of Macropinocytosis in Lung Adenocarcinoma Cells. September 2021. Research!Louisville, University of Louisville School of Medicine, Louisville, KY.

Vega, A.A., Shah, P.P., Casson, L., Beverly, L.J. Nutrient Transport Inhibition Leads to Induction of Macropinocytosis in Lung Adenocarcinoma Cells. August 2022. Biochemistry and Molecular Genetics Retreat, Captain's Quarters, Louisville, KY.

ORAL PRESENTATIONS

Research Conference: BMG University of Louisville, 2018 “Functional consequence of association of PKM2 and PSAT1 on their inherent enzymatic activity.”

Rotation Report I: BMG University of Louisville, 2018 “Investigating the effects of DZA on acute myeloid leukemia and hematopoietic cell differentiation.”

Rotation Report II: BMG University of Louisville, 2019 “Investigating ceramide metabolism in nCDase KO mouse kidneys.”

Seminar II: BMG University of Louisville, 2019 “Extracellular vesicles and breast cancer: you’ve got mail.”

Research Conference: BMG University of Louisville, 2020 “Lung adenocarcinoma (LUAD) and the lung microbiome: The shady deal happening in you.”

Research Conference: BMG University of Louisville, 2021 “Methionine Wars: Episode V BCH Strikes Back”

Research Conference: BMG University of Louisville, 2023 “The interplay between lung adenocarcinoma cells, nutrition, and the microbiome.”